AD-759 403

Development of a Concept for a High Capacity Pneumatic Conveying System Employing a Fluid Attachment Device for Use in Underground Excavation

Battelle Memorial Institute

prepared for

Bureau of Mines
Advanced Research Projects Agency

FEBRUARY 1973

Distributed By:

NTIS
National Technical Information Service
U. S. DEPARTMENT OF COMMERCE

Development of a Concept for a High Capacity Pneumatic Conveying System Employing a Fluid Attachment Device for Use in Underground Excavation

A. K. Postma
J. D. Smith
D. S. Trent

Final Technical Report
February 28, 1973

U.S. Bureau of Mines
Contract Number H0220027

Sponsored by
Advanced Research Products Agency
ARPA Order 1579, Amendment 3
Program Code 62701D

Battelle
Pacific Northwest Laboratories
Richland, Washington 99352

AD 759 403

Security Classification

DOCUMENT CONTROL DATA - R & D

(Security classification of title, body of abstract and indexing annotation must be entered when the overall report is classified)

1 ORIGINATING ACTIVITY (Corporate author) Pacific Northwest Laboratories a Division of Battelle Memorial Institute	2a. REPORT SECURITY CLASSIFICATION Unclassified 2b GROUP

3 REPORT TITLE

Development of a concept for a High Capacity Pneumatic Conveying System Employing a Fluid Attachment Device for Use in Underground Excavation

4 DESCRIPTIVE NOTES (Type of report and inclusive dates)

Final Report

5 AUTHOR(S) (First name, middle initial, last name)

6 REPORT DATE February 28, 1973	7 NO OF PAGES	7b NO OF REFS 3
8a CONTRACT OR GRANT NO b. PROJECT NO c d	9a ORIGINATOR'S REPORT NUMBER(S) None 9b OTHER REPORT NO(S) (Any other numbers that may be assigned this report) None	

10 DISTRIBUTION STATEMENT

Distribution of this document is unlimited.

11 SUPPLEMENTARY NOTES	12 SPONSORING MILITARY ACTIVITY Advanced Research Projects Agency Washington, D.C. 20301

13 ABSTRACT

A 1 year study of the fluid flow in Coanda eductors has been completed. The objective of this study was to develop a mathematical model to predict the performance of such eductors. The model would serve as a tool in the design of Coanda eductors to be used for pneumatic conveying of excavated rock materials. The work completed included both theoretical studies and experimental measurements. The theoretical approaches considered included dimensional analysis, similarity theory, and a vorticity transport method for solving the differential equations of fluid flow in geometries which have axial symmetry. The latter theoretical approach was selected as the most promising, and was developed to the point where a computer code was used to predict stream lines, velocities, and developed pressures within the flow field. Comparison of model predictions with experimental data demonstrated the qualitative correctness of the predicted flow field. However, satisfactory quantitative agreement between theory and experiment were not achieved because the model did not fully account for spatial variations in eddy viscosity. It was concluded that incorporation of a turbulence model into the calculational routine would eliminate this problem. A conveying capacity of 4 tons per hour was achieved using an eductor having a throat diameter of 2 inches, a value high enough to make the concept worth pursing.

DD FORM 1 NOV 65 1473 (PAGE 1)

0102-014-6600

UNCLASSIFIED

Security Classification

14 KEY WORDS	LINK A		LINK B		LINK C	
	ROLE	WT	ROLE	WT	ROLE	WT
Coanda Effect						
Wall Jet						
Eductor						
Pneumatic Conveying						
Fluid Mechanics						
Numerical Computer Code						
Navier-Stokes Equations						
Underground Excavation						

ia

FINAL TECHNICAL REPORT

COVERING TECHNICAL WORK FROM

FEBRUARY 10, 1972 TO FEBRUARY 10, 1973

ARPA Order Number: 1579, Amendment 3

Program Code Number: 62701D

Name of Contractor:

Pacific Northwest Laboratories
a division of Battelle Memorial
Institute

Effective Date of Contract:

February 10, 1972

Contract Expiration Date:

April 10, 1973

Amount of Contract:

$74,820

Contract Number:
H0220027

Program Director*

D. E. Rasmussen

Telephone Number: (509) 946-2407

Short Title of Work:

Development of a Concept for a High Capacity Pneumatic Conveying System Employing a Fluid Attachment Device for Use in Underground Excavation

This research was supported by the Advanced Research Projects Agency of the Department of Defense and was monitored by Bureau of Mines under Contract Number H0220027.

---

* For project functional organization, see Appendix A.

FOREWORD

This report summarizes the work completed by Battelle-Northwest for the U.S. Bureau of Mines under Contract Number H0220027. The program director is D. E. Rasmussen and principal investigators are A. K. Postma, J. D. Smith and D. S. Trent.

TABLE OF CONTENTS

LIST OF FIGURES

DEVELOPMENT OF A CONCEPT FOR A HIGH CAPACITY PNEUMATIC CONVEYING SYSTEM EMPLOYING A FLUID ATTACHMENT DEVICE FOR USE IN UNDERGROUND EXCAVATION

to

U.S. BUREAU OF MINES

CONTRACT NUMBER H0220027

INTRODUCTION

This report describes the work completed during the course of a program carried out by Battelle-Northwest for the U.S. Bureau of Mines. The objective of this research program was to develop a mathematical model to describe the fluid mechanics of a Coanda eductor. A satisfactory model will serve as a tool in design of Coanda eductors for pneumatic conveying of excavated rock materials.

The possible use of a Coanda eductor for pneumatic transport was suggested by preliminary experiments carried out at Battelle-Northwest. A small model was found to be highly effective in entraining granular materials and discussions with personnel from the U.S. Bureau of Mines led to the current interest in assessing the potential use of such an eductor in transporting rock in underground excavations.

The term "Coanda" derives from the Romanian-born engineer named Henri Coanda. Henri Coanda nearly suffered an early demise as a result of unexpected flow along exhaust deflector plates he had installed on a wooden airplane powered by a type of jet engine. Instead of deflecting the exhaust gas away from the wooden fuselage, installed deflector plates were actually sucking the flames toward it. Coanda survived this mishap, and spent much of the remainder of his life studying the curious attachment phenomena which accompany flow along solid surfaces. Most of the scientific effort devoted to attached or "Coanda" flow has been directed to the use of the phenomenon in vehicle propulsion.

Use of the fluid attachment principle in an eductor is attractive because of very simple mechanical designs which are possible, and more importantly, because of the possibility of designing eductors with large

throat openings free from obstructions. These advantages are of potentially great importance in pneumatic conveying of solids. This problem had not been studied previously to an appreciable extent. The approach taken in the present study is to develop a mathematical model which adequately describes fluid flow in Coanda eductors. The merits for using a Coanda eductor in a specific case can then be judged from eductors designed to meet specific requirements of flow rate and pressure drop.

SUMMARY

A 12-month program with the objective to develop a mathematical model of fluid flow in Coanda eductors is complete. Tasks which were completed include writing a detailed program plan, reviewing available technical literature, making a comparison of performance of Coanda eductors with other momentum transfer methods, adaptation of a numerical computer program for solving the differential equation of fluid flow for axial symmetric flow, and experimental measurements of flow fields in model eductors.

Many studies of wall jet flow have been performed for two-dimensional flow over flat and curved surfaces. The experimental and theoretical data that were available, however, did not apply directly to flow in cylindrical, axisymmetric geometries of interest for the Coanda eductor.

Comparison of the Coanda eductor with other types of momentum transfer devices indicated that the chief advantages offered by this eductor lie in its extreme mechanical simplicity, and in its large open throat. Energy requirements for the Coanda eductor are expected to be higher than for mechanical systems such as conveyers or pneumatic conveyors with airlock feeders. Energy requirements are expected to be equivalent to those for presently available ejectors.

Three approaches to building a mathematical model for the flow field were considered. These included model theory based on dimensional analysis, similarity theory, and numerical solution of the time-smoothed Navier-Stokes equations. A decision was made to pursue the latter approach because it can provide the most detailed description of the flow field with

the least amount of experimental data. An existing computer code which solves the Navier-Stokes equations for flows having axial symmetry was modified to calculate the flow field for a Coanda eductor. This computer code has provided theoretical predictions of velocity profiles and centerline pressures for air flow through Coanda eductors. While the theoretical profiles have shown qualitative similarity to those obtained experimentally, it is apparent that the detailed flow structure is not correctly described by the model. An improved model will require addition of a calculational scheme for evaluating the turbulent eddy viscosity at each nodal point.

An experimental apparatus was designed and fabricated to provide data on pressure drop, entrained flow, and velocity profiles for several geometries. The experimental data was used to test the validity of the mathematical model and to provide input regarding numerical values of eddy viscosity.

CONCLUSIONS AND RECOMMENDATIONS

The following conclusions are supported by the work completed.

- Coanda eductors possess potential advantages compared to alternate ejectors and other momentum transfer devices. The advantages are primarily related to the simplicity of the mechanical design, and the flow characteristics. These allow for passage of large aggregate particles without plugging, lead to automatic termination of feed input when pressure drop increases in the transport pipe (automatic clearing of incipient blockage situation), and result in highly reliable operation in underground applications.
- Experimental studies, designed primarily to support a theoretical modelling effort, have demonstrated that crushed rock can be conveyed at high rates by means of a Coanda eductor (detailed results shown on page 73).

- A fully satisfactory theoretical model was not achieved. The weak element in the theoretical model developed was the lack of a calculational scheme to predict turbulent eddy viscosities at each nodal point. Development of a computational scheme to do this was beyond the scope of the present contract.
- It is recommended that the development effort to apply Coanda eductors underground be continued. The next step appears to be the development of an eddy viscosity model (such models have become state-of-the-art during the past year, see page 37) which would eliminate the weak element in the present mathematical model. Subsequent effort would be the underground demonstration of optimum-designed devices.

LITERATURE REVIEW

Literature on the Coanda effect was reviewed with the purpose of gathering information which would support the present Coanda eductor study. A bibliography of the literature reviewed is included as Appendix B. The review revealed that very little information is available concerning wall jet behavior in geometries with cylindrical symmetry. A number of studies, both theoretical and experimental, have dealt with two-dimensional flow over flat and curved surfaces. In addition, a relatively large body of information has been developed for ejectors (or jet pumps) which entrain fluid by flowing primary air through a tube centered in a larger mixing tube. For the Coanda eductor, the primary air is introduced through an annular slit, and becomes attached to the inlet surface prior to entry into a mixing zone. Geometries for the two eductors are similar downstream from the entry to mixing section, hence information developed for this region in ejectors should apply to the Coanda eductor. The following paragraphs briefly describe the information obtained from the literature search.

Studies of ejectors have included both theoretical and experimental approaches. Theoretical studies consist of the one-dimensional approach, with details of the fluid mechanics typically being neglected. Reversible

thermodynamics have been assumed along with equations of state for the fluids. Thus, the theoretical analyses establish an upper limit to performance, but shed little light on how to design Coanda eductors to achieve the maximum performance. Experimental studies with air ejectors have shown optimum designs. The length-to-diameter ratio for the mixing section is found to be near 7. The optimum angle of divergence in the outlet diffuser is found to be in the 7° to 10° range. Because of the similarity in geometry, these optimum parameters would be expected to apply to the Coanda eductor.

Attachment of air jets to surfaces has been the subject of a number of experimental studies. Applications have been directed primarily toward fluidic amplifiers and to aircraft propulsion. Jet attachment has been studied as a function of jet width, step height, and angle of inclination of attachment surface compared to the slit. From the results one can predict the distance of attachment as a function of these conditions. Several studies have focused on the effect of curvature on detachment and fluid entrainment. Entrainment increases with increasing curvature where curvature is defined as the reciprocal of the radius of curvature (1/R). From these results, one would expect that the greatest entrainment ratios could be obtained by using large curvature upstream from the constant area mixing section of the Coanda eductor. On the other hand, the largest pressures could likely be developed using inlet surfaces which employed less curvature.

To date, the most realistic theoretical approaches have relied on similarity theory to simplify the flow equations, thus permitting solution. This similarity approach appears to be quite successful in predicting the flow field for flat and curved two-dimensional flows. Similarity has not been applied to the axisymmetric case of interest in the Coanda eductor.

Several examples of reported results are briefly discussed here. Figure 1 shows the results of Bourque and Newman[1] for reattachment of a jet to an inclined plane. The minimum length of plate required to cause spontaneous attachment is shown as the upper curve. The maximum angle at

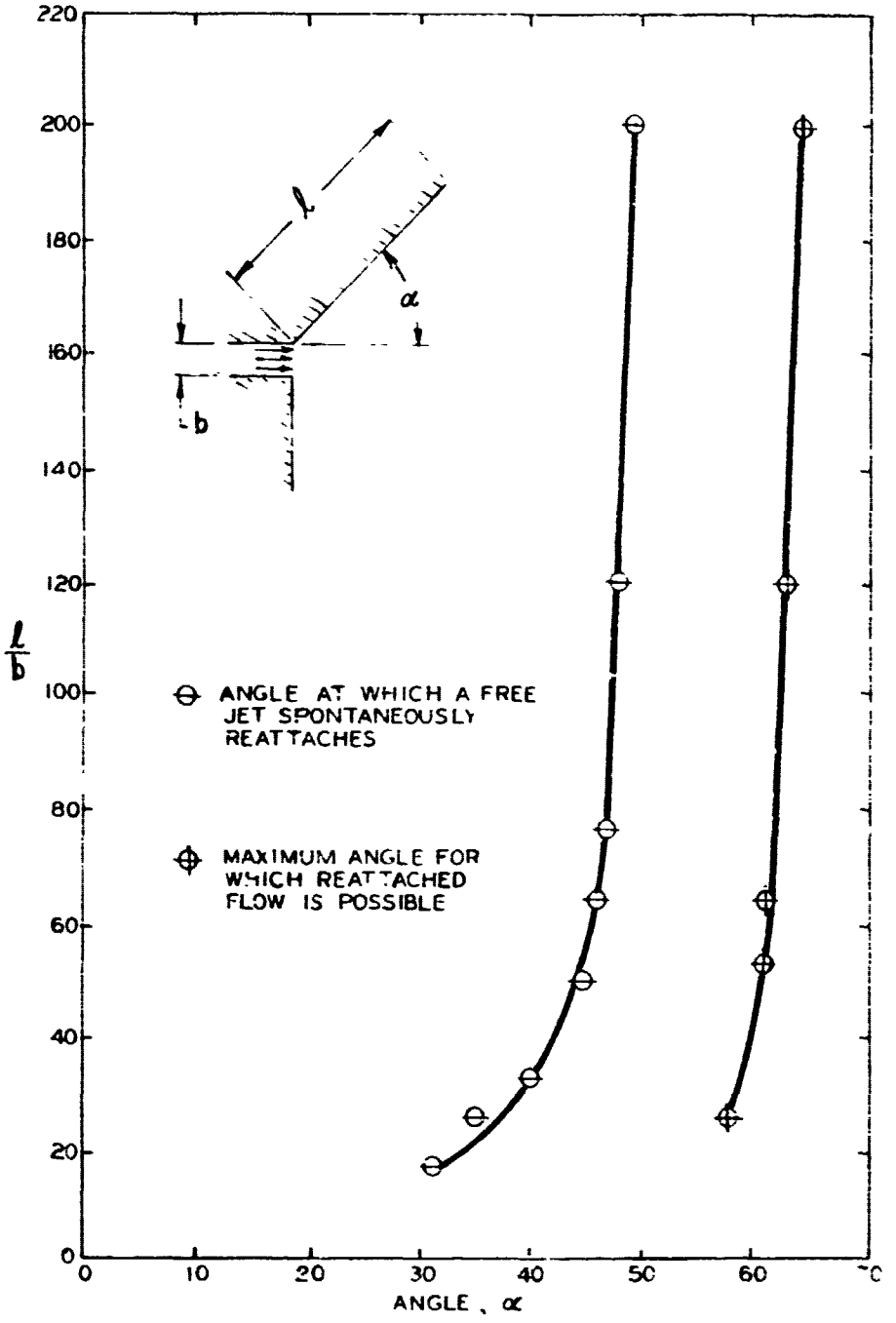

FIGURE 1. Results of Bourque and Newman[1] for Attachment of Plane Jet to Inclined Plane

which spontaneous attachment occurs is approximately 50°. Once the jet becomes attached, however, a hysteresis effect becomes evident since attachment can be maintained up to about 65°.

Experimental data on entrainment for jet flow along the surface of a cylinder were reported by Sridhar and Tu.[2] Their results are shown in Figure 2, in which the dimensionless entrainment velocity is shown as a function of curvature of the cylindrical surface. For convex surfaces, entrainment per unit length increases as the radius of curvature decreases. For convex surfaces, just the opposite occurs.

The literature review was primarily concerned with studies conducted on the "Coanda effect" and on "wall jets". Some of the material was useful in our effort to develop a reliable analytical method for the design of eductors incorporating the fluid attachment principle.

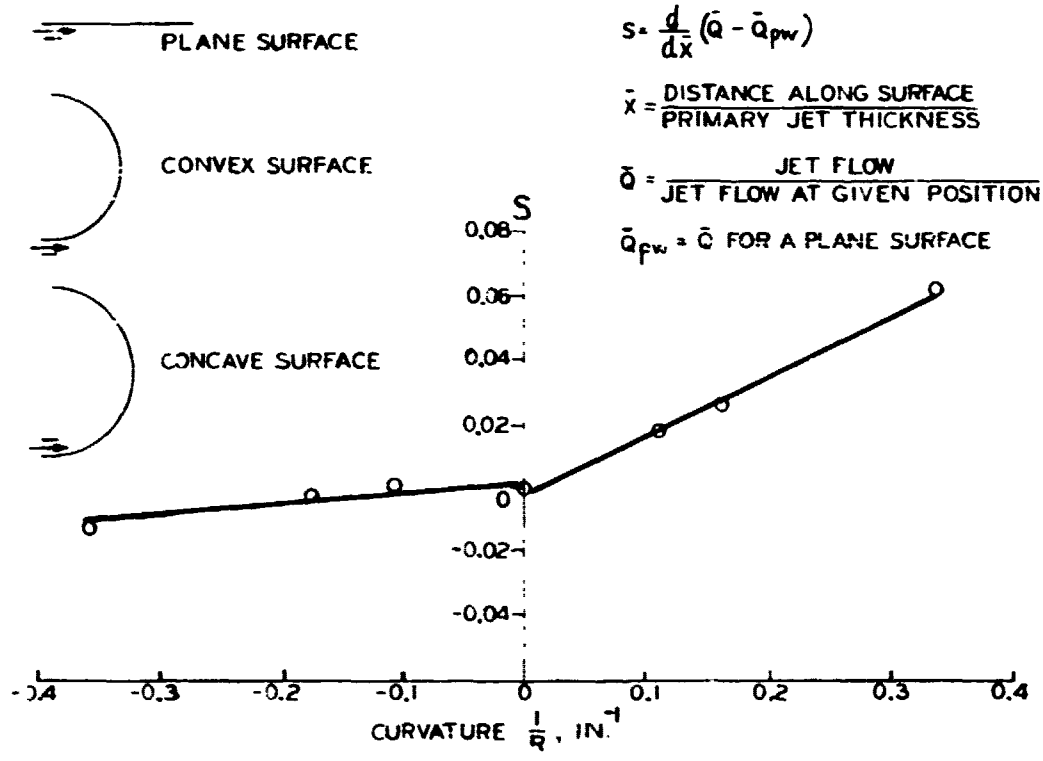

FIGURE 2. Results of Sridhar and Tu[2] for Dimensionless Entrainment as a Function of Surface Curvature

However, little was revealed that would provide the basis for a reliable comparison of a Coanda eductor to other momentum transfer methods. It is, however, reasonable to assume that the performance of a Coanda eductor will be similar to that of an air ejector since both incorporate inlet entrainment regions for a high velocity motive jet to entrain ambient air, a constant cross-sectional area mixing region, and a diffusor section to increase the discharge pressure (see Figure 3). If this assumption is valid, then from air ejector technology we can predict the performance for Coanda eductors. Figure 4 shows anticipated performance for a family of motive air supply pressures in terms of entrainment (R_W) and discharge pressure.

MATHEMATICAL MODEL DEVELOPMENT

The ultimate use of the mathematical model will be to predict material transport rates for eductors employing the Coanda effect. The material transport capabilities of the eductor are expected to be related closely to the air flow rate and the pressure drop developed across the eductors. Thus, the mathematical model should permit prediction of these two parameters as a function of design elements including fluid properties, primary jet velocity, and geometric design of a specific eductor.

To develop a theoretical model within the time allotted, we identified three possible approaches. The first approach was to use model theory which relies on dimensional analysis to permit scaling of data from model to prototype. The second approach was to use similarity theory. This involves simplifying assumptions to convert boundary layer partial differential equations to total differential equations which are easily solved. Similarity theory has been used successfully in modeling wall jet flows.[3] The third potential theoretical approach involved adapting an existing fluid flow computer code capable of numerically solving the Navier-Stokes equations for axial symmetric flow fields.

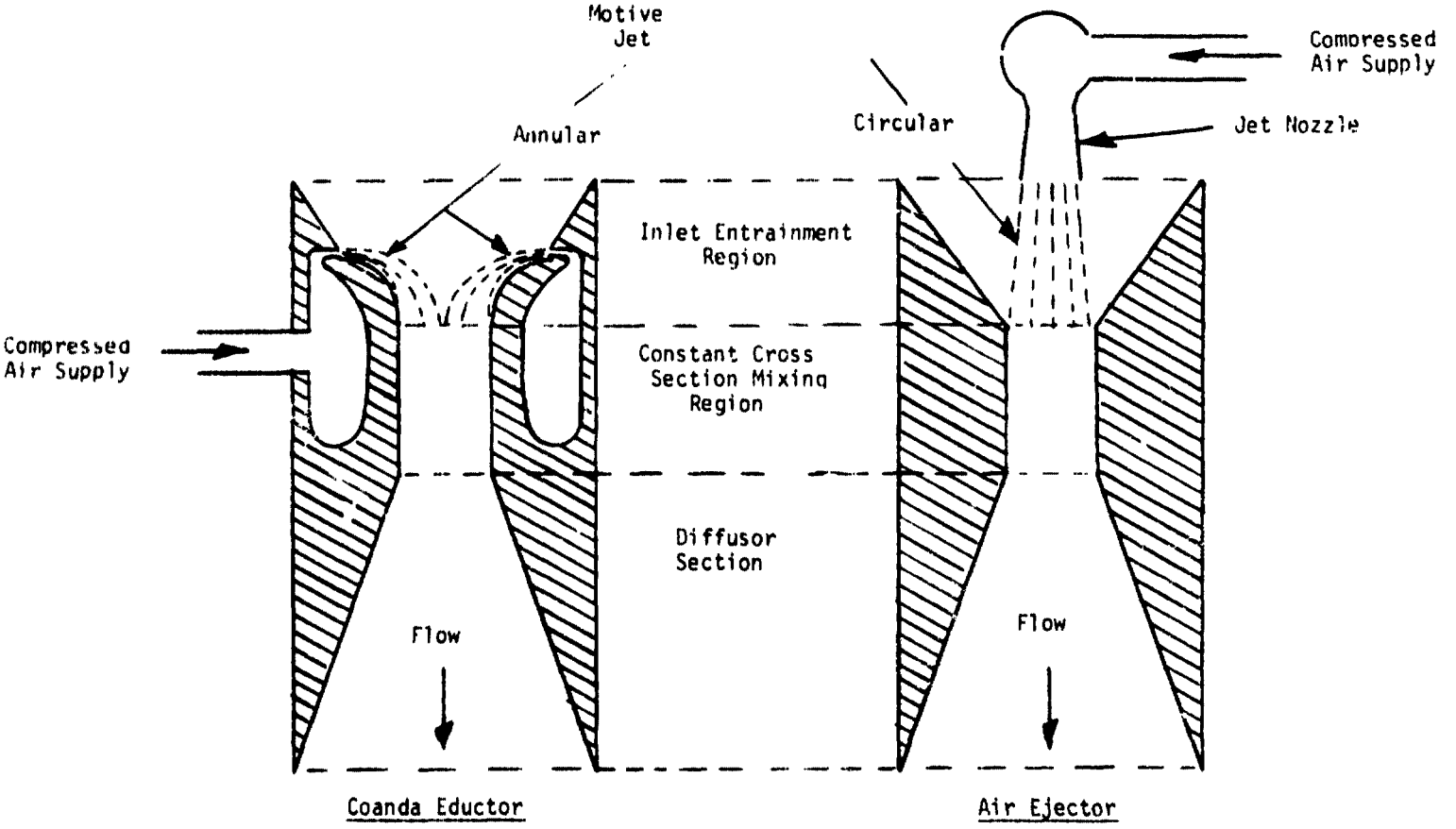

FIGURE 3. Cross Section of Cylindrical Eductors

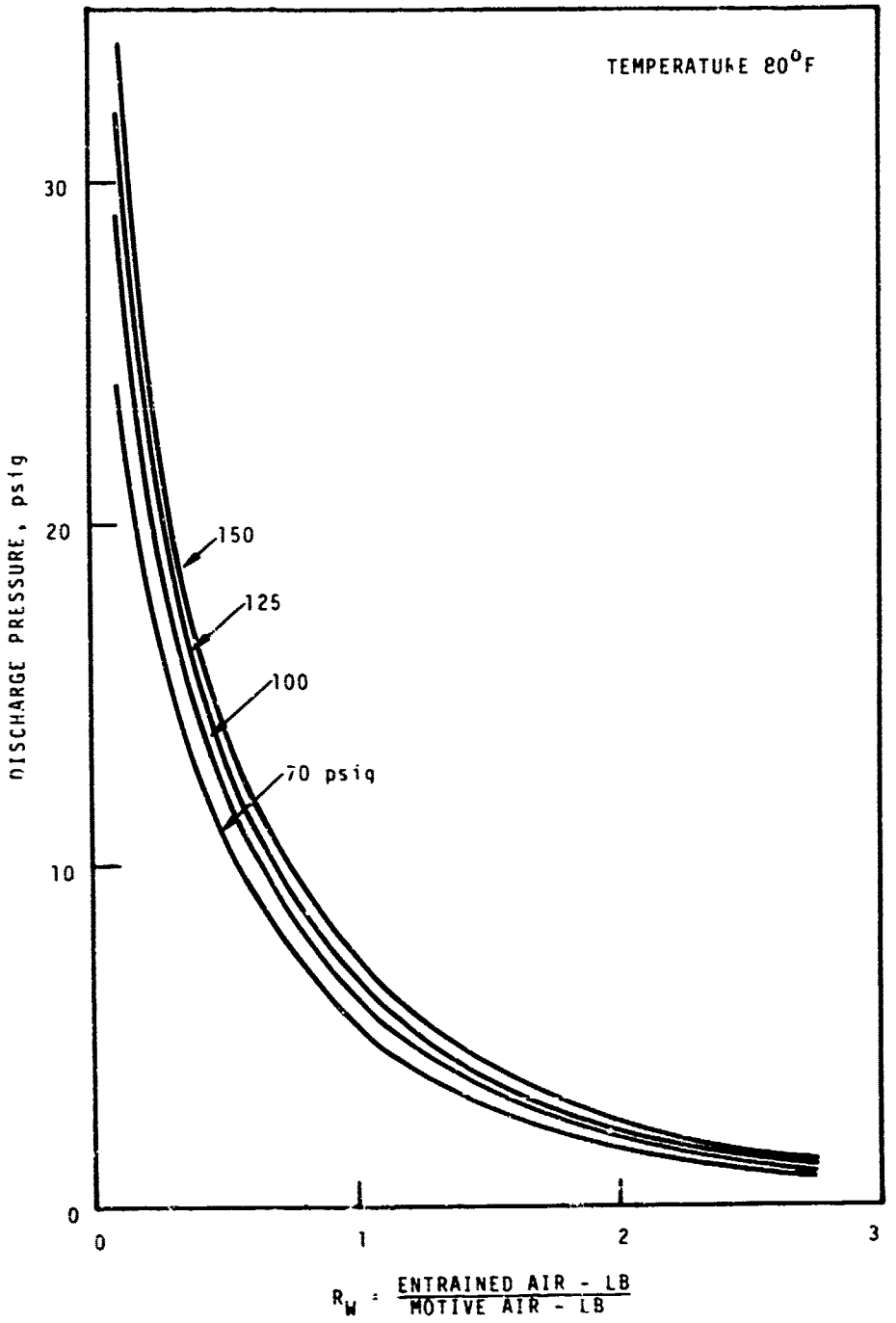

FIGURE 4. Air Ejector Performance for Motive Air Supply Pressures

Our first efforts were to briefly survey these theoretical approaches to verify the plausibility of each for application to the present problem. As a result of this survey, the decision was made to focus on the use of an existing numerical computer code since it promised the most complete prediction of the flow field and at the same time required the least amount of experimental data as input. Each of the three alternative mathematical approaches is described further in the following sections of this report.

DIFFERENTIAL EQUATIONS OF FLUID FLOW

The mathematical formulation of the differential equations for fluid flow are obtained by making mass, force, and energy balances on a small fluid element in space. These basic equations form the basis for theoretical attacks on the fluid flow problem. Although the full set of equations is too complicated to solve generally, they were listed to establish the following:

- Simplifying assumptions used in various theoretical approaches
- Identification of important physical parameters
- Description of important boundary conditions
- Basis for dimensional analysis.

The continuity equation results from a statement that mass is conserved. For cylindrical coordinates, the continuity equation is

$$\frac{\partial \rho}{\partial t} + \frac{1}{r}\frac{\partial}{\partial r}\left(\rho r v_r\right) + \frac{1}{r}\frac{\partial}{\partial \theta}\left(\rho v_\theta\right) + \frac{\partial}{\partial z}\left(\rho v_z\right) = 0 \qquad (1)$$

where

ρ = fluid density,

t = time

r = distance measured in radial direction,

v_r = fluid velocity in radial direction,
v_θ = fluid velocity in θ direction,
v_z = fluid velocity in z direction,
θ = angular position measured around z axis,
z = distance measured in axial direction.

As written, Equation (1) applies to the three-dimensional flow of a compressible fluid. For special cases, this equation may be appreciably simplified.

The momentum equations are derived by balancing the forces on a fluid element. Statically unbalanced forces are equated to the fluid mass times its acceleration. Thus, it amounts to application of Newton's second law of motion to a small fluid element. However, deformation of the fluid element by tangential forces must also be accounted for, and this greatly complicates the equations of motion as compared to those for nondeformable bodies. For three-dimensional flow, three separate momentum equations result. Written in cylindrical coordinates, in terms of stress components, the momentum equations are as follows:

r-component

$$\rho\left(\frac{\partial v_r}{\partial t} + v_r \frac{\partial v_r}{\partial r} + \frac{v_\theta}{r}\frac{\partial v_r}{\partial \theta} - \frac{v_\theta^2}{r} + v_z \frac{\partial v_r}{\partial z}\right) = -\frac{\partial p}{\partial r}$$

$$-\left[\frac{1}{r}\frac{\partial}{\partial r}\left(r\tau_{rr}\right) + \frac{1}{r}\frac{\partial \tau_{r\theta}}{\partial \theta} - \frac{\tau_{\theta\theta}}{r} + \frac{\partial \tau_{rz}}{\partial z}\right] + \rho g_r \qquad (2)$$

θ-component

$$\rho\left(\frac{\partial v_\theta}{\partial t} + v_r \frac{\partial v_\theta}{\partial r} + \frac{v_\theta}{r}\frac{\partial v_\theta}{\partial \theta} + \frac{v_r v_\theta}{r} + v_z \frac{\partial v_\theta}{\partial z}\right) = -\frac{1}{r}\frac{\partial p}{\partial \theta}$$

$$-\left[\frac{1}{r^2}\frac{\partial}{\partial r}\left(r^2\tau_{r\theta}\right) + \frac{1}{r}\frac{\partial \tau_{\theta\theta}}{\partial \theta} + \frac{\partial \tau_{\theta z}}{\partial z}\right] + \rho g_\theta \qquad (3)$$

z-component $$\rho\left(\frac{\partial v_z}{\partial t} + v_r \frac{\partial v_z}{\partial r} + \frac{v_\theta}{r}\frac{\partial v_z}{\partial \theta} + v_z \frac{\partial v_z}{\partial z}\right) = -\frac{\partial p}{\partial z}$$

$$-\left[\frac{1}{r}\frac{\partial}{\partial r}\left(r\tau_{rz}\right) + \frac{1}{r}\frac{\partial \tau_{\theta z}}{\partial \theta} + \frac{\partial \tau_{zz}}{\partial z}\right] + \rho g_z \qquad (4)$$

These momentum equations apply quite generally because simplifying assumptions have not yet been made.

The energy equation is obtained from an energy balance written on a small fluid element. In cylindrical coordinates it may be written in terms of stress components as

$$\rho\hat{C}_v\left(\frac{\partial T}{\partial t} + v_r \frac{\partial T}{\partial r} + \frac{v_\theta}{r}\frac{\partial T}{\partial \theta} + v_z \frac{\partial T}{\partial z}\right) = -\left[\frac{1}{r}\frac{\partial}{\partial r}\left(rq_r\right) + \frac{1}{r}\frac{\partial q_\theta}{\partial \theta} + \frac{\partial q_z}{\partial z}\right]$$

$$- T\left(\frac{\partial P}{\partial T}\right)_\rho\left[\frac{1}{r}\frac{\partial}{\partial r}\left(rv_r\right) + \frac{1}{r}\frac{\partial v_\theta}{\partial \theta} + \frac{\partial v_z}{\partial z}\right] - \left[\tau_{rr}\frac{\partial v_r}{\partial r}\right.$$

$$\left. + \tau_{\theta\theta}\frac{1}{r}\left(\frac{\partial v_\theta}{\partial \theta} + v_r\right) + \tau_{zz}\frac{\partial v_z}{\partial z}\right] - \left\{\tau_{r\theta}\left[r\frac{\partial}{\partial r}\left(\frac{v_\theta}{r}\right) + \frac{1}{r}\frac{\partial v_r}{\partial \theta}\right]\right.$$

$$\left. + \tau_{rz}\left(\frac{\partial v_z}{\partial r} + \frac{\partial v_r}{\partial z}\right) + \tau_{\theta z}\left(\frac{1}{r}\frac{\partial v_z}{\partial \theta} + \frac{\partial v_\theta}{\partial z}\right)\right\} \qquad (5)$$

where

$\hat{C}_v$ = heat capacity at constant volume,

T = temperature,

$q_r = k\frac{\partial T}{\partial r}$,

$q_\theta = -k\frac{1}{r}\frac{\partial T}{\partial \theta}$,

$$q_z = -k \frac{\partial T}{\partial z} ,$$

k = thermal conductivity.

The stress components which are included in Equations (2) through (5) are defined as follows for a newtonian fluid.

$$\tau_{rr} = -\mu \left[2 \frac{\partial v_r}{\partial r} - \frac{2}{3} \left(\nabla \cdot v \right) \right]$$

$$\tau_{\theta\theta} = -\mu \left[2 \left(\frac{1}{r} \frac{\partial v_\theta}{\partial \theta} + \frac{v_r}{r} \right) - \frac{2}{3} \left(\nabla \cdot v \right) \right]$$

$$\tau_{zz} = -\mu \left[2 \frac{\partial v_z}{\partial z} - \frac{2}{3} \left(\nabla \cdot v \right) \right]$$

$$\tau_{r\theta} = \tau_{\theta r} = -\mu \left[r \frac{\partial}{\partial r} \left(\frac{v_\theta}{r} \right) + \frac{1}{r} \frac{\partial v_r}{\partial \theta} \right]$$

$$\tau_{\theta z} = \tau_{z\theta} = -\mu \left[\frac{\partial v_\theta}{\partial z} + \frac{1}{r} \frac{\partial v_z}{\partial \theta} \right]$$

$$\tau_{zr} = \tau_{rz} = -\mu \left[\frac{\partial v_z}{\partial r} + \frac{\partial v_r}{\partial z} \right]$$

$$\left(\nabla \cdot v \right) = \frac{1}{r} \frac{\partial}{\partial r} \left(r v_r \right) + \frac{1}{r} \frac{\partial v_\theta}{\partial \theta} + \frac{\partial v_z}{\partial z}$$

Equations (1) through (5) fully describe the flow of fluids in three-space dimension. In practice, some degree of simplification is required before these equations can be solved.

DIMENSIONAL ANALYSIS

Any mathematical relationship which is dimensionally consistent may be written as a relationship between dimensionless groups. The various techniques of dimensional analysis identify the dimensionless groups for a given physical problem. The utility of this approach is that it can greatly reduce the number of independent variables which must be considered in experiments. Once a relationship between dimensionless groups is defined by means of model experiments, predictions can be made for prototypes provided the numerical values taken by the various dimensionless groups fall within the range investigated in model tests.

One way of deriving the important dimensionless groups for a problem is based on simple mathematical operations on the basic differential equations. This method is well described by Klinkenberg and Mooy.[4] We have used this approach with the momentum and energy equations, Equations (2) through (5). The following dimensionless groups shown in Table 1 appeared from this analysis.

TABLE 1. Dimensionless Groups Obtained from Momentum and Energy Equations

Name of Dimensionless Group	Definition
Reynolds No., Re	$\rho dv/\mu$
Prandtl No., Pr	$C_p\mu/k$
Eckert No., Ec	$v^2/C_v t$
Euler No., Eu	$p/\rho v^2$
Brinkman No., Br	$\mu v^2/kT$
Specific Heat Ratio, γ	C_p/C_v
Froude No., Fr	gd/V^2

where

ρ = fluid density,

V = velocity,

μ = viscosity,

C_p = heat capacity at constant pressure,

k = thermal conductivity,

C_v = heat capacity at constant volume,

T = temperature,

P = pressure,

g = acceleration due to gravity,

d = diameter.

A second approach to deriving important dimensionless groups is to list all important parameters for a given physical situation. The parameters can then be grouped as dimensionless ratios using standard techniques. A hypothetical Coanda eductor is shown schematically in Figure 5. In addition to the 12 geometric dimensions, flow properties expected to be important include: fluid density, fluid viscosity, specific heat, specific heat ratio, thermal conductivity, temperature, velocity of primary air, velocity of entrained air, and pressure drop across nozzle. Using the Buckingham method[5] for forming the dimensionless group, we obtain the following expression for the entrained air flow.

$$\frac{\text{Entrained Flow}}{\text{Primary Flow}} = \text{function (Re, Ma, Br, Eu, } \gamma\text{, geometric length ratios)} \quad (6)$$

where

Re = Reynolds No.

Ma = Mach No.

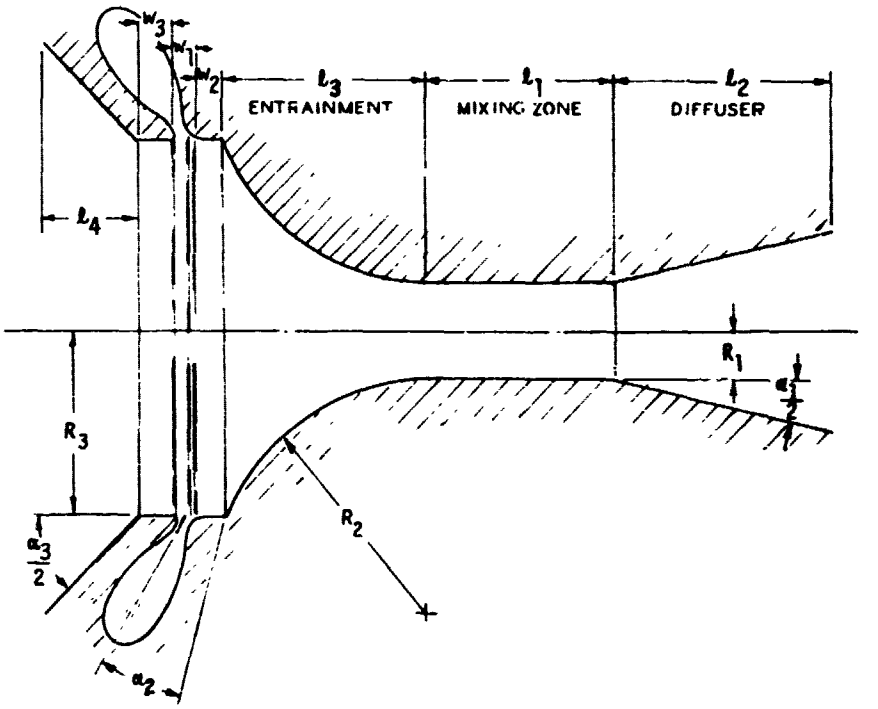

w_1 = width of primary air inlet slit

w_2 = height of step separating jet and Coanda wall

w_3 = length of inlet cylinder upstream from primary air slit

α_1 = angle of divergence of outlet diffuser

α_2 = angle of inclination of primary jet

α_3 = angle of convergence of inlet

ℓ_1 = length of mixing section (constant area)

ℓ_2 = length of outlet diffuser

ℓ_3 = length of Coanda entrainment section

ℓ_4 = length of inlet transition

R_1 = radius of throat of nozzle

R_2 = radius of curvature of Coanda entrainment section

FIGURE 5. Schematic View of Hypothetical Coanda Eductor Showing Geometric Parameters

Br = Brinkman No.

Eu = Euler No.

γ = specific heat ratio.

The Mach No. is closely related to the Eckert No. which appeared earlier. From Equation (6), one could, in theory, perform experiments that would provide the functional relationship between the groups. In practice, too many experiments would be required to evaluate the relationship among the five flow related groups and the 12 geometric ratios. The next step in using the dimensional analysis approach would be to eliminate the groups of minor importance, and key on the several controlling groups. This step was not accomplished in the present work.

SIMILARITY THEORY

Similarity theory is a method for simplifying the equations of motion to a point where they can be solved. The term "similarity" derives from the assumed shape of the velocity profile, which is assumed to have a prescribed similarity at each downstream position, x. A classical example of similarity theory is that used by Glauert[3] in his analysis of the wall jet. Glauert's beginning point is the simplified, two-dimensional boundary layer momentum equation written as

$$u \frac{\partial u}{\partial x} + v \frac{\partial u}{\partial y} = \nu \frac{\partial^2 u}{\partial y^2} \tag{7}$$

where

u = velocity in x direction,

v = velocity in y direction,

ν = kinematic viscosity.

A stream function, ψ, is defined satisfy the continuity equation:

$$-\frac{\partial \psi}{\partial x} = xv \tag{8}$$

and

$$\frac{\partial \psi}{\partial y} = xu \tag{9}$$

where

ψ = stream function.

The continuity equation may be written as

$$\frac{\partial}{\partial x}(xu) + \frac{\partial}{\partial y}(xv) = 0 \tag{10}$$

By defining a new variable, $\eta = yx^n$, the two partial differential equations, Equation (7) and Equation (10) are transformed to a total differential equation:

$$f''' + ff'' + \alpha f'^2 = 0 \tag{11}$$

In Equation (11) the argument of the function, f, is η; α is a numerical parameter related to n.

Glauert's[3] solution to Equation (11) provides velocity profiles which agree well with experimental measurements, showing that the mathematical assumptions made were justified. It is possible that similar approaches could be made for axisymmetric flows encountered in the Coanda eductor. No attempt was made to pursue the similarity theory approach in this study.

NUMERICAL MODEL BASED ON VORTICITY TRANSPORT THEORY

The following discusses the mathematical basis and the finite difference method of solution used in the vorticity transport method.

Mathematical Basis

The differential equations governing Coanda eductor fluid flow are derived from the two conservation laws:

- conservation of mass (continuity)
- conservation of momentum (Newton's second law).

These equations written for incompressible, turbulent flow in cartesian tensor form are:

Continuity:

$$\frac{\partial u_i}{\partial x_i} = 0 \ , \tag{12}$$

Momentum:

$$\frac{Du_i}{Dt} = -\frac{1}{\rho}\frac{\partial p}{\partial x_i} + \frac{\partial}{\partial x_j}\left(\varepsilon_{ij}\frac{\partial u_i}{\partial x_j}\right) . \tag{13}$$

In the above equations, time and spatial changes of the fluid density, ρ, have been ignored (incompressibility condition).

Notation used in Equations (12) and (13) is as follows:

u_i = velocity along i^{th} coordinate

x_i = i^{th} space coordinate

P = pressure

t = time

ε_{ij} = Eddy diffusivity tensor for momentum.

The operator D/Dt is the substantial derivative defined as

$$\frac{D}{Dt} = \frac{\partial}{\partial t} + u_j \frac{\partial}{\partial x_j}$$

The tensor index i (or j) for three-space takes values i = 1, 2 and 3. Einsteinian notation is used where a repeated index implies summation over the possible values i (or j) = 1, 2 and 3.

In the momentum Equation (13), we have neglected gravitational effects and have assumed that the effects of Reynolds stresses (turbulent stresses) may be approximated through the use of an eddy diffusivity, ε_{ij}.

For the Coanda eductor study, it is possible to express the equations of continuity and momentum in terms of axisymmetric coordinates, thus using only the two-space coordinates z (axial) and r (radial). This assumption ignores mean azimuthal variation of the dependent variables such as mean azimuthal velocity (swirl). Also, the Coanda study is directed to steady-flow operation of the eductor, hence time dependence may also be eliminated in the equations of motion.

Thus, the equations which are used for analysis of the Coanda eductor are the following steady-flow, axisymmetric equations of continuity and motion:

Continuity:

$$\frac{1}{r} \frac{\partial ur}{\partial r} + \frac{\partial v}{\partial z} = 0 \, . \tag{14}$$

Momentum:

r-direction,

$$u \frac{\partial u}{\partial r} + v \frac{\partial u}{\partial r} = - \frac{1}{\rho} \frac{\partial p}{\partial r} + \frac{\partial}{\partial r} \left(\frac{\varepsilon_r}{r} \frac{\partial ur}{\partial r} \right) + \frac{\partial}{\partial z} \left(\varepsilon_z \frac{\partial u}{\partial z} \right) , \tag{15}$$

z-direction,

$$u \frac{\partial v}{\partial r} + v \frac{\partial v}{\partial z} = - \frac{1}{\rho} \frac{\partial p}{\partial z} + \frac{1}{r} \frac{\partial}{\partial r} \left(r \varepsilon_r \frac{\partial v}{\partial r} \right) + \frac{\partial}{\partial z} \left(\varepsilon_z \frac{\partial v}{\partial z} \right) \quad . \tag{16}$$

In the above equations, u and v are velocity in the r and z directions, respectively, and the eddy diffusivity tensor is assumed to have components ε_r and ε_z only.

Use of only the ε_r and ε_z components of momentum diffusion is to assume that the diffusion coefficient for v-velocity and u-velocity are the same in a given direction.

Vorticity Transport

In the application of numerical analysis we consider solving Equations (14), (15) and (16) by finite-difference techniques without further simplification. However, we must devise some method to solve for pressure, P. This may be done by taking the divergence of Equations (14) and (15) and adding the results to obtain

$$\nabla^2 p = - \left\{ \left(\frac{u}{r} \right)^2 + \left(\frac{\partial u}{\partial r} \right)^2 + \left(\frac{\partial v}{\partial z} \right)^2 + 2 \frac{\partial u}{\partial z} \cdot \frac{\partial v}{\partial r} \right\} \tag{17}$$

where the operator

$$\nabla^2 = \frac{\partial^2}{\partial r^2} + \frac{1}{r} \frac{\partial}{\partial r} + \frac{\partial^2}{\partial z^2}$$

In Equation (17), terms involving derivatives of ε_r and ε_z have been ignored for the sake of this discussion. To obtain a solution to the Coanda dynamics, Equations (15), (16) and (17) would be solved simultaneously. However, experience has shown that Equation (17) is difficult to solve numerically because of required boundary conditions.

To circumvent simultaneous solutions to the pressure equation and associated difficulty with the boundary condition, one may choose to solve an equivalent set of equations which eliminates pressure as an explicit part of the analysis. This approach is called the vorticity transport method.

We define vorticity, ω, as

$$\omega = \frac{\partial u}{\partial z} - \frac{\partial v}{\partial r} \quad . \tag{18}$$

A stream function, ψ, is defined by

$$u = -\frac{1}{r}\frac{\partial \psi}{\partial r} \text{ and} \tag{19}$$

$$v = \frac{1}{r}\frac{\partial \psi}{\partial z} \tag{20}$$

which identically satisfies the continuity Equation (14). An elliptic partial differential equation is obtained for ψ by substituting Equations (19) and (20) into (18) which yields

$$\frac{\partial^2 \psi}{\partial r^2} - \frac{1}{r}\frac{\partial \psi}{\partial r} + \frac{\partial^2 \psi}{\partial z^2} = -r\omega \quad . \tag{21}$$

Velocities u and v may be obtained by solving Equation (21) for ψ and then solving the auxiliary Equations (19) and (20).

However, to obtain solution to Equation (21), the flow field vorticity, $\omega(r,z)$, must be known. A vorticity transport equation may be derived by cross-differentiating Equations (15) and (16) and subtracting the latter result from the former to obtain

$$\frac{\partial u\omega}{\partial r} + \frac{\partial v\omega}{\partial z} = \varepsilon_r \frac{\partial}{\partial r}\left(\frac{1}{r}\frac{\partial \omega r}{\partial r}\right) + \varepsilon_z \frac{\partial^2 \omega}{\partial z^2} + \frac{\partial}{\partial z}\left(\frac{1}{r}\frac{\partial ur}{\partial r}\cdot\frac{\partial \varepsilon_r}{\partial r} + \frac{\partial u}{\partial z}\cdot\frac{\partial \varepsilon_z}{\partial z}\right)$$

$$+ \frac{\partial \varepsilon_r}{\partial z}\cdot\frac{\partial}{\partial r}\left(\frac{1}{r}\frac{\partial ur}{\partial r}\right) + \frac{\partial \varepsilon_z}{\partial z}\cdot\frac{\partial^2 u}{\partial z^2} - \frac{\partial}{\partial r}\left(\frac{\partial v}{\partial r}\cdot\frac{\partial \varepsilon_r}{\partial r} + \frac{\partial v}{\partial z}\cdot\frac{\partial \varepsilon_z}{\partial z}\right)$$

$$- \frac{\partial \varepsilon_r}{\partial r}\cdot\left(\frac{\partial^2 v}{\partial r^2} + \frac{1}{r}\frac{\partial v}{\partial r}\right) - \frac{\partial \varepsilon_z}{\partial r}\cdot\frac{\partial^2 v}{\partial z^2} \quad . \tag{22}$$

If the turbulent structure of the flow field is homogeneous and isotropic, derivatives of ε_r and ε_z vanish and the vorticity transport equation becomes

$$\frac{\partial u\omega}{\partial r} + \frac{\partial v\omega}{\partial z} + \varepsilon_o \frac{\partial}{\partial r}\left(\frac{1}{r}\frac{\partial \omega r}{\partial r}\right) + \varepsilon_o \frac{\partial^2 \omega}{\partial z^2} \quad . \tag{23}$$

Note that pressure, P, does not explicitly appear in Equations (22) and (23). Once the vorticity solution is obtained (and hence, the velocity solution), one may back-calculate pressure from Equation (17). Alternatively, pressure may also be calculated using either Equation (15) or (16).

Description of the SYMJET Code (Coanda Version)

The Coanda version of the SYMJET code solves Equations (21) and (22) along with the auxiliary relationships Equations (19) and (20), by finite-difference techniques. However, these equations are first scaled with the dimensionless variables and parameters defined as follows:

$$R = r/r_o$$

$$Z = z/r_o \ , \ \bar{Z} = z/D$$

$$U = u/v_o$$

$$V = v/v_0$$

$$\psi = \psi/\left(r_0^2\, v_0\right)$$

$$\Omega = \omega\, r_0/v_0$$

$$RE_r = \frac{r_0 v_0}{\varepsilon_r} \quad , \text{(radial, turbulent Reynolds No.)}$$

$$RE_z = \frac{r_0 v_0}{\varepsilon_z} \quad , \text{(vertical, turbulent Reynolds No.)}$$

In the above, r_c is the characteristic radius of the Coanda eductor and v_0 is a characteristic reference velocity which may be taken as the Coanda slot velocity.

In their scaled form the governing equations become:

Stream Function:

$$\frac{\partial^2 \Psi}{\partial R^2} - \frac{1}{R}\frac{\partial \Psi}{\partial R} + \frac{\partial^2 \Psi}{\partial Z^2} = - R\Omega \tag{24}$$

Vorticity Transport:

$$\frac{\partial U\Omega}{\partial R} + \frac{\partial V\Omega}{\partial Z} = \frac{1}{RE_r}\left(\frac{\partial^2 \Omega}{\partial R^2} + \frac{1}{R}\frac{\partial \Omega}{\partial R} - \frac{\Omega}{R^2}\right) + \frac{1}{RE_z}\frac{\partial^2 \Omega}{\partial Z^2} \quad , \tag{25}$$

along with the auxiliary relationships for velocity:

$$U = - \frac{1}{R}\frac{\partial \Psi}{\partial Z} \tag{26}$$

$$V = \frac{1}{R}\frac{\partial \Psi}{\partial R} \tag{27}$$

Terms involving derivatives of RE_r and RE_z are not included in Equation (25) but are accounted for in the SYMJET code.

Finite Difference Grid System

The finite difference grid layout consists of two grid systems. One grid is used to calculate the stream function, Ψ, which provides information to compute velocity components, U and V. This system coincides with the physical boundaries and is illustrated by the wider lines on Figure 6. The stream function is calculated at the system interior intersection points designated by the solid round symbols. The U components of the velocity field are computed at vertical midpoints which are designated by open circle symbols; whereas, the V components are computed at horizontal midpoints (K coordinate) and designated by open box symbols. In this manner, the stream function grid layout defines a system of cells with the stream function, Ψ, computed at each corner point (or set by boundary conditions, as the case may be) and velocities defined at the center of the cell face.

The second grid system is used to calculate vorticity, Ω, and is illustrated in Figure 6 by the narrow lines. This layout completely overlaps the Ψ grid (and physical system) with interior intersection points centered in the cells which are defined by the Ψ grid system. These interior grid points are indicated by crosses.

This staggered grid system is used for computational convenience in treating boundary conditions and to permit direct evaluation of convective transport terms at cell faces.

The Ψ grid system is sized by NJ and NK grid points in the R direction and vertical direction, respectively. The Ω system has size NJ + 1 and NK + 1 in the respective directions. Points on the Ψ grid are indicated by (j, k), whereas points on the Ω grid are specified by (p, q). Vertical spacing for the system is defined by ΔZ_k which may be variable. Grid spacing along the R coordinate is designated by ΔR.

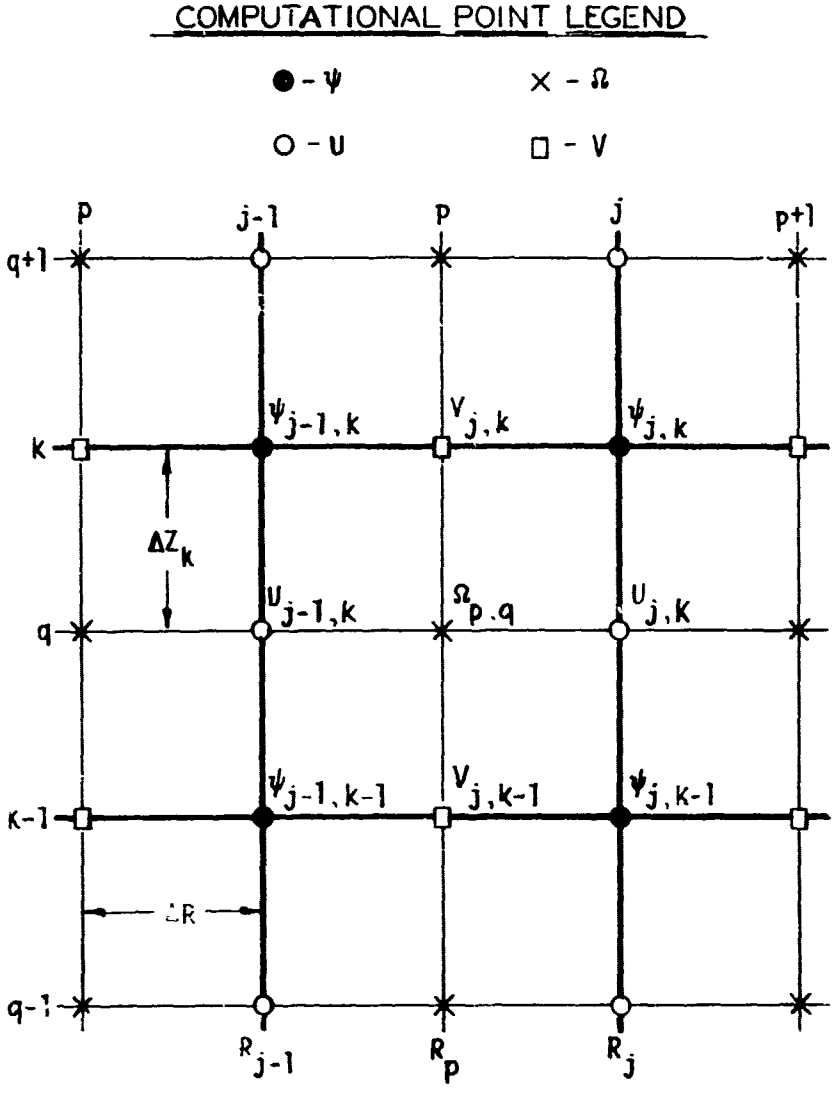

FIGURE 6. Typical Finite Difference Cell Illustrating Indices for ψ, Ω, and V

Difference Equations

Standard difference representation is used wherever possible in this discussion. Central differences are used for both first and second partial derivatives except for convective terms where special upstream methods are used. These methods are similar to those used by Torrance and Rockett[6] and Runchal and Wolfshtein,[7] and details of the application here are explained by Trent.[8] Techniques for uneven spacing are used for the vertical differences.

Stream Function and Velocity

Consider the stream function grid system illustrated in Figure 6. The finite difference representation of Equation (24) based on central differences for both first and second partial derivatives is as follows:

$$2\left(\frac{1}{\Delta R^2}+\frac{1}{\Delta Z_k \Delta Z_{k+1}}\right)\Psi_{j,k}=\frac{1}{\Delta R^2}\left(1-\frac{\Delta R}{2R}\right)\Psi_{j+1,k}+\frac{1}{\Delta R^2}\left(1+\frac{\Delta R}{2R}\right)\Psi_{j-1,k}$$

$$+\frac{2}{\Delta Z_{k+1}\left(\Delta Z_{k+1}+\Delta Z_k\right)}\cdot\Psi_{j,k+1}$$

$$+\frac{2}{\Delta Z_k\left(\Delta Z_{k+1}+\Delta Z_k\right)}\cdot\Psi_{j,k-1}+\bar{\Omega}_{j,k}R_j \quad . \qquad (28)$$

In the above difference equation, the quantity $\bar{\Omega}_{j,k}$ is the average value vorticity at point (j,k), hence the over ar. This average value is used since $\Omega_{p,q}$ does not lie on the Ψ computational grid.

Velocity is calculated at cell faces by

$$U_{j,k}=\frac{-1}{R_j\,\Delta Z_k}\cdot\left(\Psi_{j,k}-\Psi_{j,k-1}\right) \qquad (29)$$

and

$$V_{j,k} = \frac{1}{R_j\ \Delta R} \cdot \left(\Psi_{j,k} - \Psi_{j-1,k}\right) \quad . \tag{30}$$

Transport Equations

Referring to the p,q grid system illustrated in Figure 6, the difference representation of the steady flow vorticity transport Equation (25) is written as (after collecting terms).

$$\left[\frac{2}{RE_z\Delta Z_k} \cdot \left(\frac{1}{\Delta Z_k+\Delta Z_{k+1}} + \frac{1}{\Delta Z_k+\Delta Z_{k-1}}\right) + \frac{1}{RE_r\Delta R^2} \cdot \left(2+\frac{\Delta R^2}{R_p^2}\right) + \frac{1}{2\Delta R} \cdot \left(|U_{j,k}|\right.\right.$$

$$\left. + U_{j,k} + |U_{j-1,k}| - U_{j-1,k}\right) + \frac{1}{2\Delta Z_k} \cdot \left(|V_{j,k}| + V_{j,k} + |V_{j,k-1}|\right.$$

$$\left.\left. - V_{j,k-1}\right)\right]\Omega_{p,q} = \left[\frac{1}{2\Delta R} \cdot \left(|U_{j-1,k}| + U_{j-1,k}\right) + \frac{1}{RE_r\Delta R^2}\right.$$

$$\left. \cdot \left(1 - \frac{\Delta R}{2R_p}\right)\right]\Omega_{p-1,q} + \left[\frac{1}{2\Delta R} \cdot \left(|U_{j,k}| - U_{j,k}\right) + \frac{1}{RE_r\Delta R^2}\right.$$

$$\left. \cdot \left(1 + \frac{\Delta R}{2R_p}\right)\right]\Omega_{p+1,q} + \left[\frac{1}{2\Delta Z_k} \cdot \left(|V_{j,k-1}| + V_{j,k-1}\right) + \frac{2}{RE_z\Delta Z_k}\right.$$

$$\left. \cdot \left(\frac{1}{\Delta Z_k+\Delta Z_{k-1}}\right)\right]\Omega_{p,q-1} + \left[\frac{1}{2\Delta Z_k} \cdot \left(|V_{j,k}| - V_{j,k}\right) + \frac{2}{RE_z\Delta Z_k}\right.$$

$$\left. \cdot \left(\frac{1}{\Delta Z_k+\Delta Z_{k+1}}\right)\right]\Omega_{p,q+1} \quad . \tag{31}$$

The SYMJET code solves the two difference Equations (28) and (31) by Gauss-Siedel iteration. Iteration is continued until the computed velocity meets a particular convergence criterion. Although this criterion is left to the discretion of the user, computation in the present work was carried out until the maximum relative change in velocity for the entire flow field was less than 10^{-3} for one iteration.

Pressure Calculation

The pressure developed by the Coanda nozzle was predicted from the computed velocity profiles using the z-direction momentum equation. For steady state, axisymmetric flows, the z-direction momentum equation is

$$u \frac{\partial v}{\partial r} + v \frac{\partial v}{\partial z} = - \frac{1}{\rho} \frac{\partial P}{\partial z} + \frac{1}{r} \frac{\partial}{\partial r} \left(r \varepsilon_r \frac{\partial v}{\partial r} \right) + \frac{\partial}{\partial z} \left(\varepsilon_z \frac{\partial v}{\partial z} \right). \qquad (16)$$

Along the center-line, r=o, this equation may be simplified. By symmetry u=o, and $\frac{\partial v}{\partial r} = o$. Equation (16) may be written as

$$\frac{1}{\rho} \frac{\partial P}{\partial z} = \frac{\partial v}{\partial z} \left(\frac{\partial Ez}{\partial z} - v \right) + \partial E_r \frac{\partial^2 v}{\partial r^2} + Ez \frac{\partial^2 v}{\partial z^2}. \qquad (32)$$

This equation may be integrated with respect to z. When the integration is carried out using the dimensionless quantities used in the SYMJET code, the result may be written as

$$P - P_o = \rho V_o \int_{Z=o}^{Z=2} \left[-v \frac{\partial v}{\partial z} + \frac{\partial E_r}{R_o V_o} \frac{\partial^2 V}{\partial R^2} + \frac{E_z}{R_o V_o} \frac{\partial^2 V}{\partial z^2} \right] dz. \qquad (33)$$

Equation (33) was solved numerically, using the velocity data generated by the SYMJET code. Integration was performed using the trapezoidal rule. The grid system used for the pressure calculation was identical to that used for solution of the vorticity transport equations. The pressure calculation was performed by a subroutine termed (PRESS) which was appended to the SYMJET code.

This method of calculating the developed pressure is only as correct as the velocity profile data, and the coefficients of eddy viscosity which are used to compute the integrand. The relative values of the three terms in the integrand have been examined for several cases, and it appears that the first term, $\frac{-v\partial v}{\partial z}$, which accounts for fluid acceleration, is dominant. Thus the accuracy of the pressure calculation depends primarily on the accuracy of the axial velocity profile.

Application of the SYMJET Code to the Coanda Eductor

A first step in application of the computer code was to develop a computational routine which would permit definition of solid boundaries from input. This routine is essential because the calculational grid system used is different for each physically unique eductor. The routine developed has proven highly satisfactory. All boundary conditions may be specified from an input card, and the search routine maps the specified boundary conditions onto the overal grid system.

Initial flow calculations were carried out for an eductor geometry which duplicated a small Coanda eductor which was available prior to the beginning of this study. The grid system used for this eductor is shown in Figure 7.

At the center of the nozzle, the boundary condition requires that the velocity gradient in the radial direction be zero. Along the outer walls of the eductor, the no-slip criteria (velocity zero at solid wall) was used. At the outlet, velocity profiles were specified; at the inlet (top) of Figure 7), the free-flow boundary condition was used. This condition requires only that the streamlines remain straight as they enter. At the primary jet opening, the velocity was specified.

The unequal grid spacing evident in Figure 7 was required to adequately handle flow issuing from the primary jet. Initial attempts to use an equal spacing, with only a single-mesh node being within the primary jet, failed to converge.

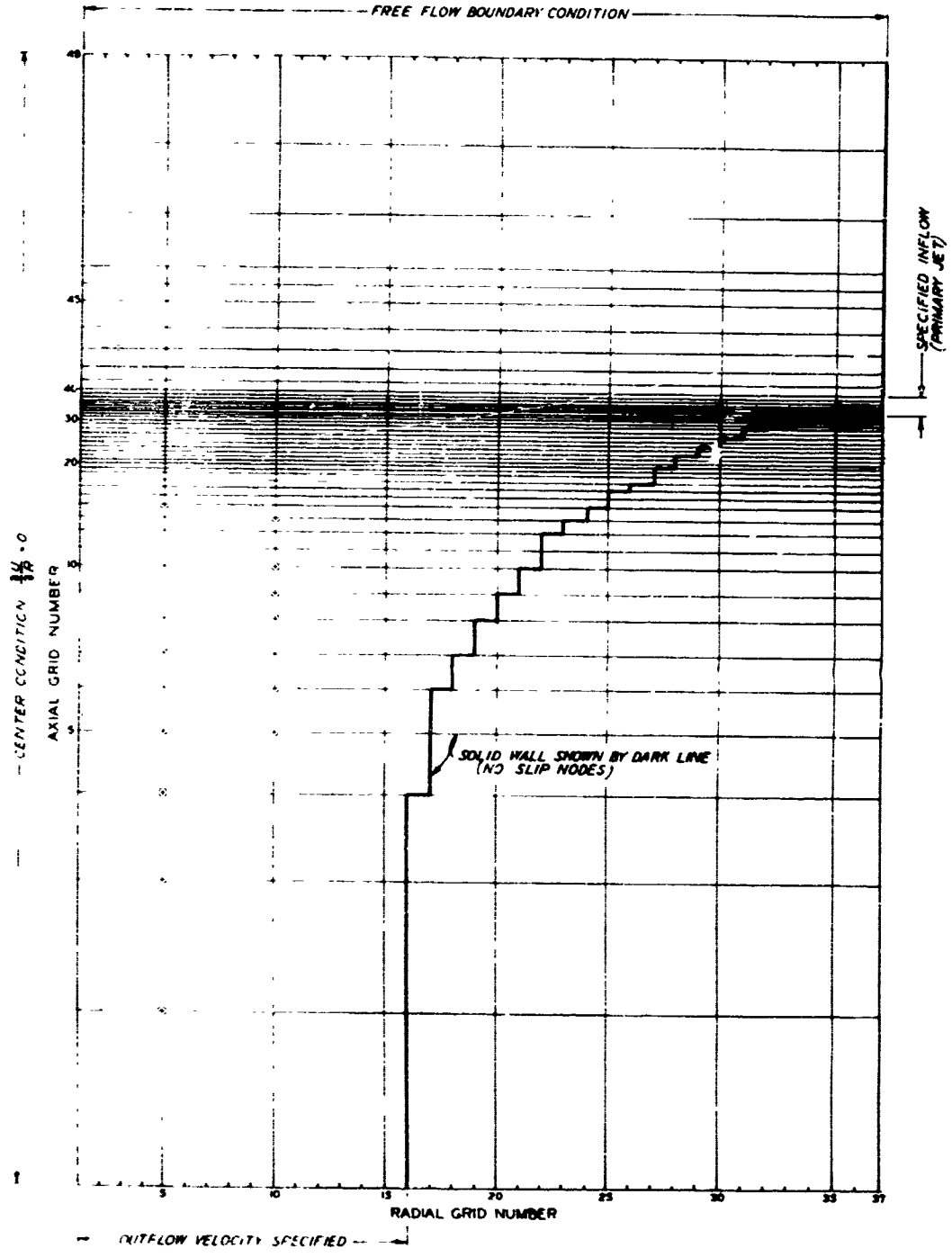

FIGURE 7. Calculational Grid System Showing Boundary Conditions and Grid Spacing

Only the inlet section of the Coanda eductor was included in the calculational grid system. Although it is possible to include downstream regions, this would substantially increase the number of calculational nodes and the computer time. This was considered unnecessary for initial runs.

Results for a typical case in which the total air flow was five times the flow of the primary air are presented in Figure 8. The shape of the streamlines demonstrates that the primary jet becomes attached to the outer wall of the eductor, and entrains additional air.

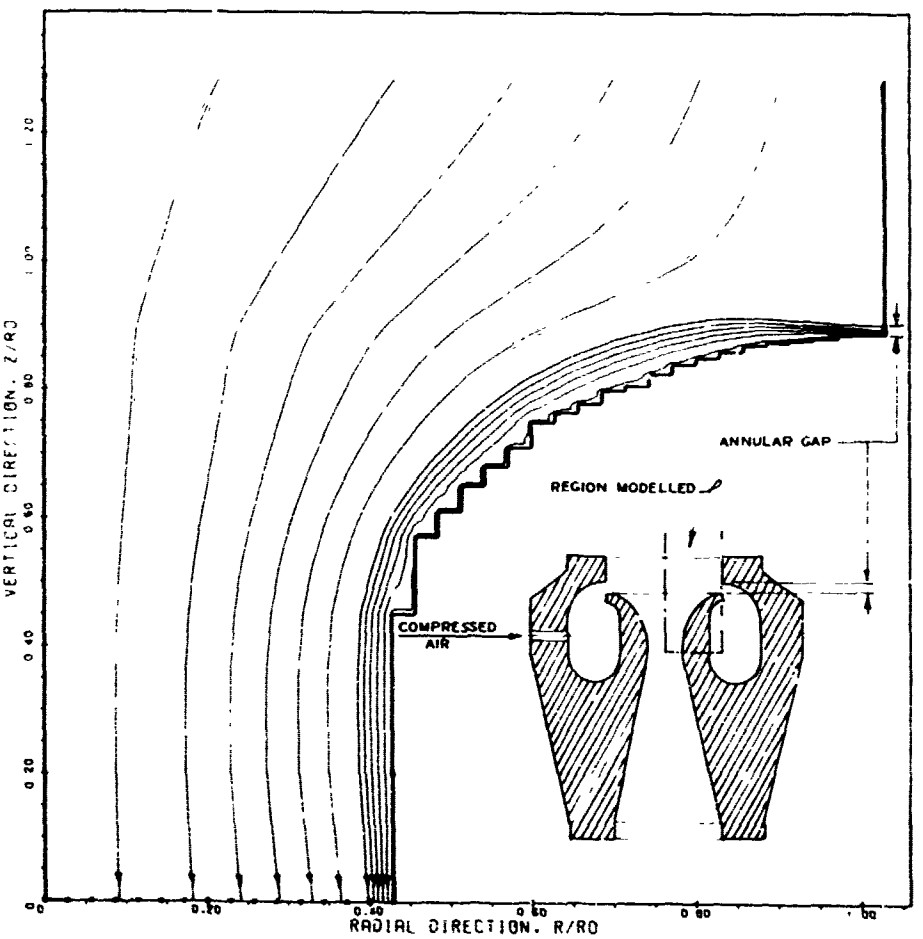

FIGURE 8. Streamlines Predicted for an Entrainment Ratio of 5

Figure 9 shows results obtained for a lower entrainment ratio. The total air flow was reduced by lowering the specified outlet velocity. The total flow leaving through the outlet (bottom of Figure 9) was slightly lower than that entering through the primary air slit. Flow separation occurred near the center of the nozzle, with a part of the primary air exiting through the normal inlet. It is worth noting that this type of behavior could not be predicted using similarity theory because the velocity profiles are not similar at the various downstream positions.

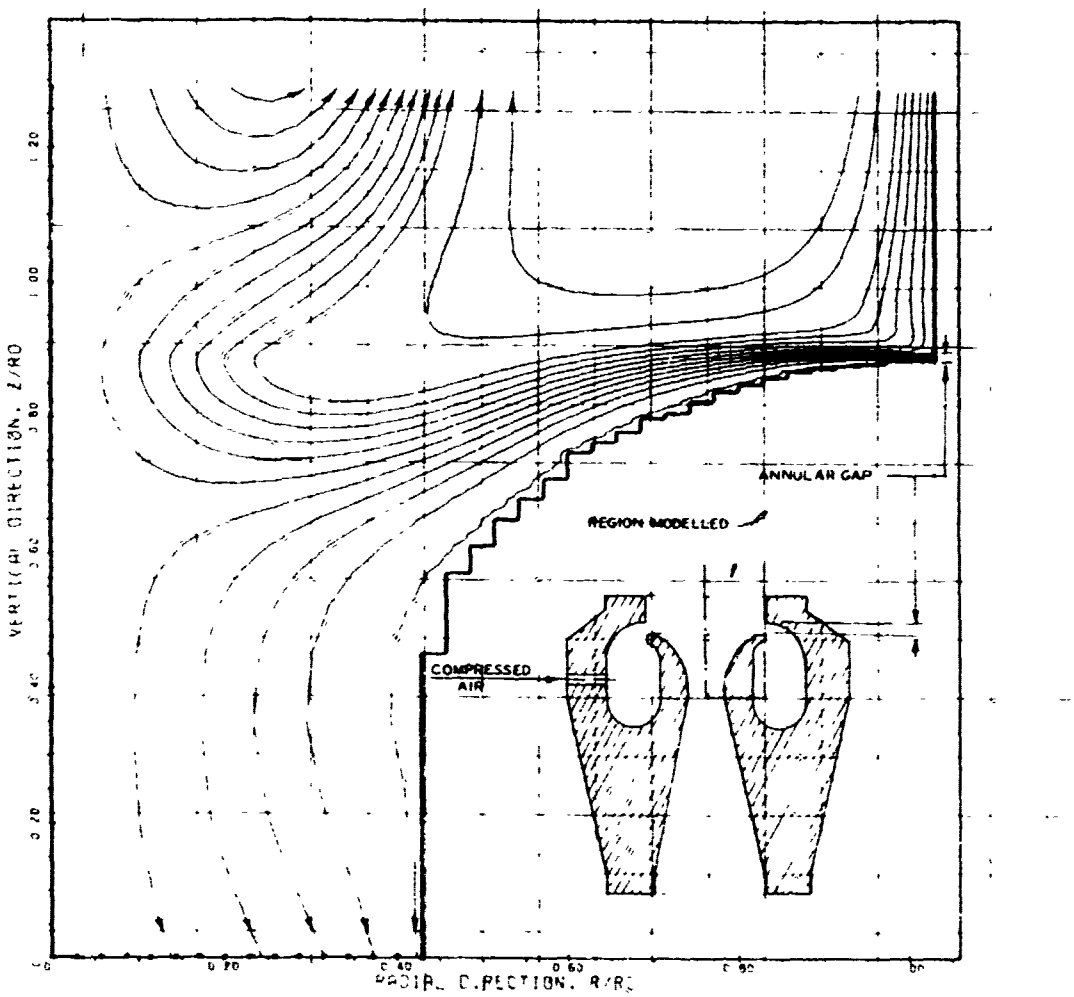

FIGURE 9. Streamlines Predicted for an Entrainment Ratio of 0.8

For the cases shown in Figures 8 and 9, the eddy viscosity was taken as constant throughout the flow field. This is a recognized oversimplification which was subsequently shown to be a serious limitation of the calculational code.

In addition to the streamline output shown in Figures 8 and 9, the SYMJET program prints velocity components, stream functions, and vorticity at each flow node.

Application of the SYMJET code to the eductor geometries considered in the present study led to discovery of problem areas not evident from the results shown in Figures 8 and 9. These problem areas and their solutions are discussed below.

Problem Area 1. Arbitrary Specification of Outlet Velocity

As is evident from Figure 7, initial predictions were done using a velocity profile specified at the outflow boundary of the eductor. It was recognized that arbitrary specification of a velocity profile was not strictly correct, but the degree of error resulting from this procedure was not thought to be controlling. When experimental data became available, however, it became obvious that the model was not yielding accurate velocity profiles.

The lack of quantitative agreement between measured and predicted velocity profiles prompted a modification in the specification of the boundary conditions at the outlet of the eductor. In place of specifying the velocity profile, the free-flow boundary condition was used. The total flow leaving the eductor was determined by specifying the numerical values of the center-line and wall streamlines. This free flow boundary condition is physically equivalent to allowing the eductor to discharge into an infinite volume.

This change in the outlet boundary condition did not appreciably change the character of the flow field. It was concluded that the change represented a theoretical improvement, but that use of a specified outlet velocity profile was not the primary cause for the discrepancy between measured and predicted flow fields.

Problem Area 2. Inclusion of Mixing Section in Computational Field

Use of the free flow boundary condition at the outlet of the entrainment section of the eductor was recognized as unreal. Physically this boundary condition is equivalent to operation of the eductor without the mixing tube. In order to assess the degree to which use of this boundary condition would influence the results, an experimental eductor was operated without the mixing section. It was determined experimentally that the pressure distribution and velocity profiles were significantly affected by the absence of the mixing section and it was concluded that the calculational model must include the mixing tube as well as the entrainment section.

The computational grid system was expanded to include the mixing tube. The most obvious effect of this change was a marked improvement in the rate of convergence of the model. Although the flow field and pressure drop changed to a limited extent, inclusion of the mixing section did not eliminate the tendency of the model to predict a flow separation where none was observed experimentally. Also, inclusion of the mixing section did little to improve the capability of the model to predict the thin, high velocity wall jet which was observed to flow along the wall of the entrainment section. Typically the model predicted a wider, more diffuse wall jet than was observed experimentally.

Problem Area 3. Constancy of Radial and Axial Components of Eddy Viscosity

At present, the SYMJET code allows for variations in eddy viscosity only with the axial and radial directions. E_r and E_z may be different, but they must be constant for the entire flow field. Although this was recognized as a limitation, past experience with the SYMJET code did not indicate that this limitation would severely affect the validity of the predicted flow fields.

The numerical values of E_r and E_z were systematically varied to determine how sensitive the predicted flow fields depended on the input viscosities. It was found that the value of E_z was critically important in determining whether the flow would attach or separate from the curved surface in

the entrainment region. For E_z smaller than 0.012 ft^2/sec, the high velocity primary jet would detach from the curved surface. For larger values, the flow would remain attached, in agreement with experimental measurements.

The numerical value of E_r was relatively unimportant, and little change in the flow field was observed when E_r was varied between 0.02 and 0.0002 ft^2/sec.

The minimum usable value of E_z of 0.0012 ft^2/sec noted above corresponds to a relatively high viscosity. Use of a highly viscous fluid in a Coanda eductor would be expected to alter the flow pattern compared to that for air. The major anticipated effect would be to cause rapid thickening and dissipation of the primary jet. For a highly viscous fluid, one would expect greater viscous dissipation of kinetic energy and therefore a lower pressure gain than could be achieved with a low viscosity fluid.

This problem area can apparently be resolved only if a method is developed for predicting the eddy viscosity at each point of the grid. Suitably low viscosities (axial component) cannot be used in the SYMJET code because the primary jet will not remain attached to the curved surface when realistic viscosities are used. Thus, in order to achieve an attached flow, high viscosities must be used, and this leads to rapid dissipation of the primary jet. In reality, the effective viscosity of the flowing fluid varies greatly with position. Within the high velocity jet, turbulent viscosities would be high, but for most of the volume, the viscosity would be close to the molecular value.

Although development of a calculational code for predicting eddy viscosities at each node was beyond the scope of this project, work published by others very recently indicates that such a calculational scheme can be considered to be "state-of-the-art" today. Important publications which would serve as a base for incorporating a turbulence model include those of Gibson and Spalding,[9] of Ng and Spalding,[10] of Rotta,[11,12] and of Bradshaw and Ferriss.

EXPERIMENTAL PROGRAM

EXPERIMENTAL TECHNIQUE

The apparatus used in the Experimental Program is shown in Figure 10. The system comprised: A rotometer to measure the motive air flow, an eductor nozzle with features for changing the inlet geometry, a constant area mixing section, a diffuser, an orifice meter to measure the mixed flow and a valve to regulate the back pressure on the system. The apparatus was further instrumented to provide pressure and temperature data of the motive air flow and the mixed motive and entrained air flow.

Velocity Profiles

Flow field data was gathered by pitot tube which was mounted on a precision x-y table with features for adjusting the angle of the pitot tube with respect to the axis or the eductor, (Figure 11). The flow field data in the eductor inlet region was taken on a horizontal radial plane.

Pressure Developed

The back pressure or pressure gain across the eductor was measured at the outlet of the diffuser section. The data was taken by liquid manometer and pressure gauge.

Calibration of temperature and pressure instrumentation was by conventional means. Pressure and differential pressure were measured by liquid manometer where practical. Both the pitot tubes and the orifice meter (Figure 12 and 13) were calibrated with a Dresser-Industrial flow meter, Model 7M 125. For each condition of motive air pressure used, the rotometers were calibrated against the orifice meter. Calibration of the 0.036 in. O.D. - 0.020 in. I.D. pitot tubes found them both to have a velocity coefficient of unity.

For most of the experiments, motive air was supplied by a portable-diesel powered 250 scfm - 120 psig rotary compressor.

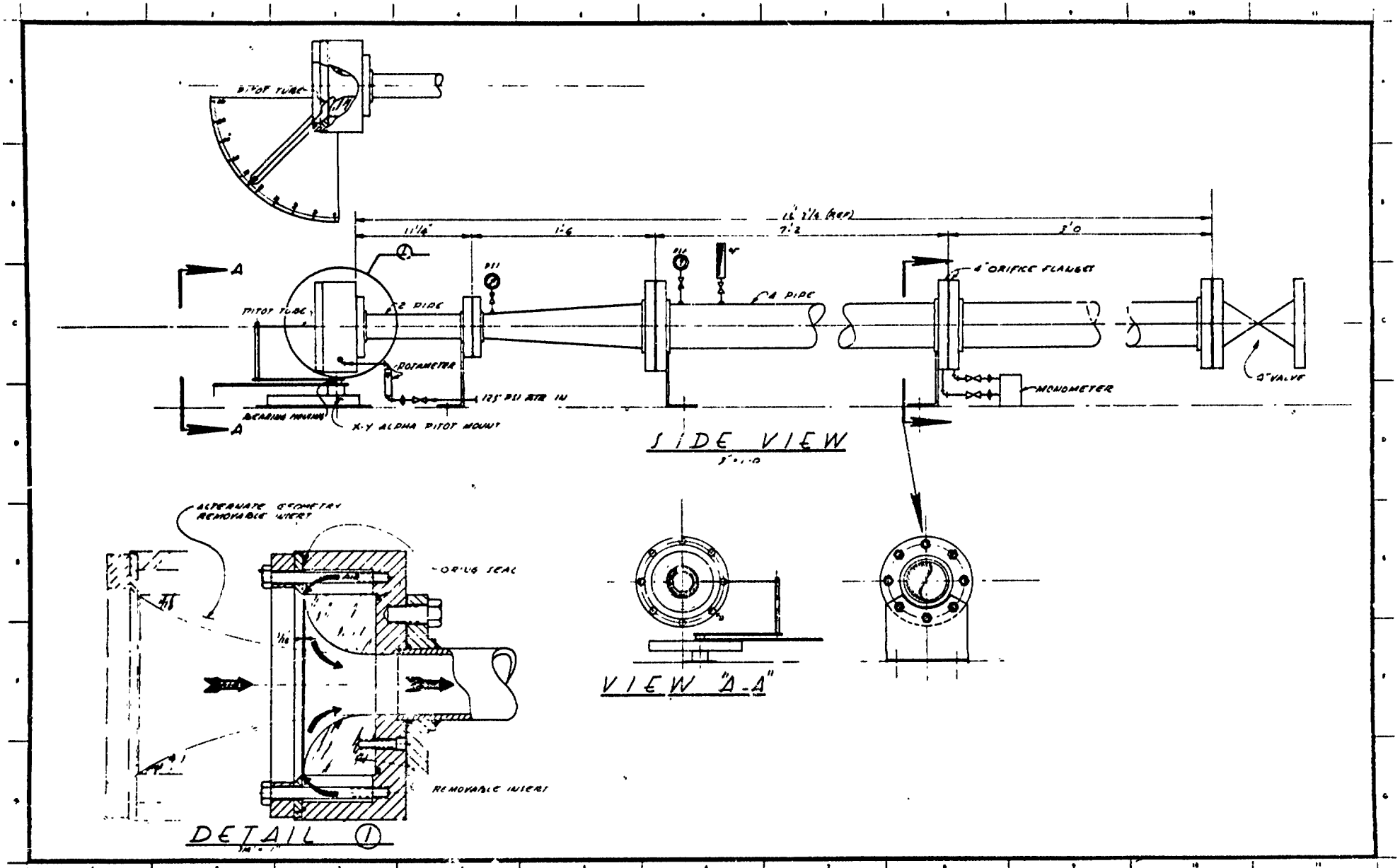

FIGURE 10. Schematic View of Experimental Equipment

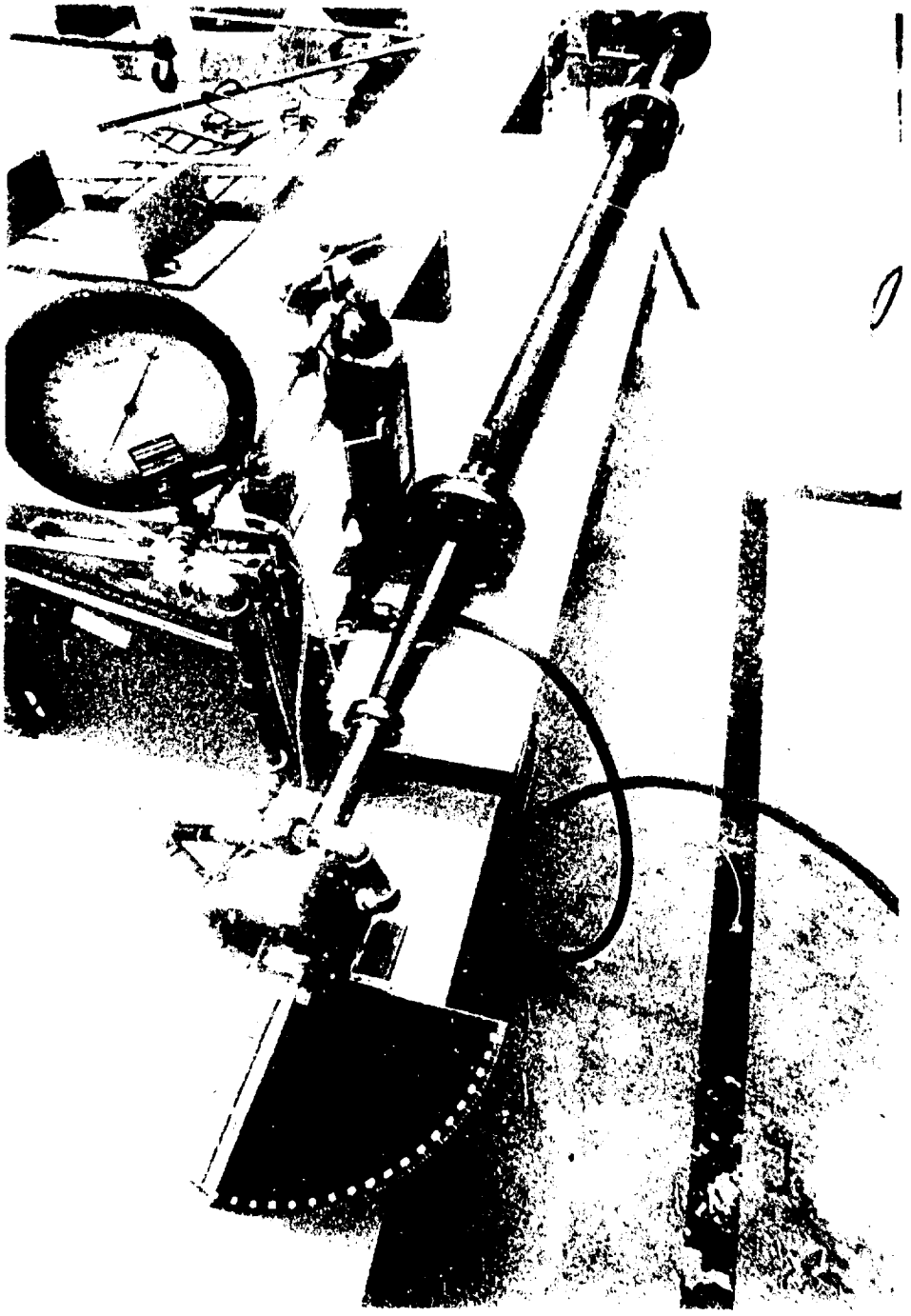

Neg. 731122-3

FIGURE 11. Experimental Apparatus Showing x-y Pitot Mount

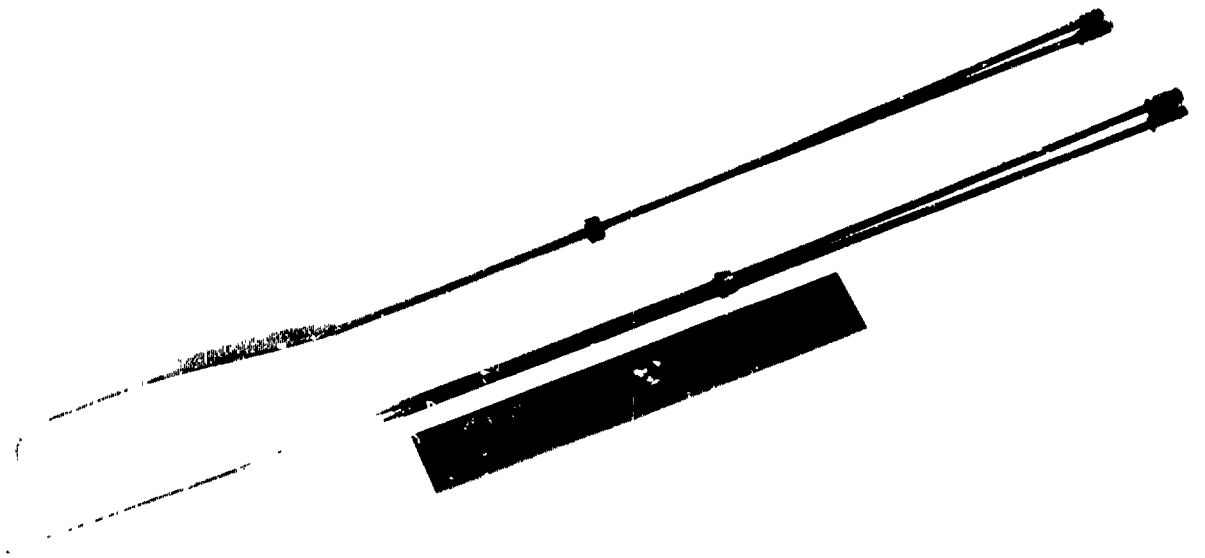

Neg. 731018-1

FIGURE 12. Pitot Tube Used to Measure Flow Fields

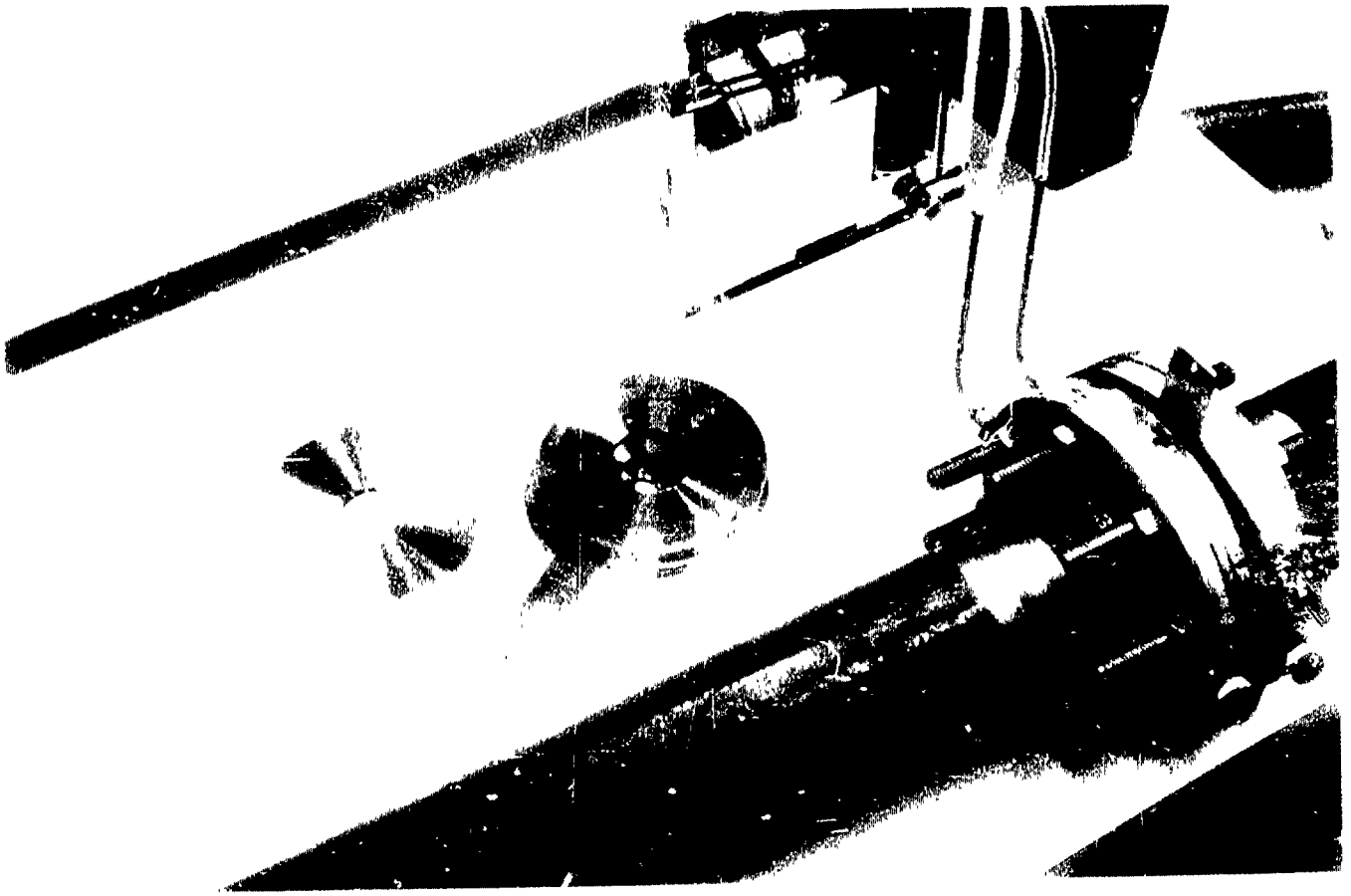

Neg. 731122-2

FIGURE 13. Orifice Meter Used to Measure Mixed Motive and Entrained Flow

Entrainment

The motive air flow was measured by rotometers. The mixed motive and entrained flow was measured by an orifice meter. The entrainment ratio was calculated from the measured primary flow and total flow.

Geometries Studied

Eductor inlet geometry was modified by the use of machined inserts. Figure 14 shows three inserts which provided eductors with: 0.5 $in.^{-1}$ curvature - 6.0 in. diameter motive air annulus, 0.5 $in.^{-1}$ curvature - 4.0 in. diameter motive air annulus, and 0.33 $in.^{-1}$ curvature - 6.0 in. diameter motive air annulus. The motive air annulus gap was adjusted by the addition or removal of shim material.

In all, some 7500 individual experimental measurements were made. During the study, Table 2 lists the combinations of inlet geometry and annulus dimensions that were experimentally examined.

TABLE 2. Experimental Eductor Geometries

Eductor Curvature $-in.^{-1}$	Annulus Diameter -in.	Annulus Gap -in.
0.5	6.0	0.006
0.5	6.0	0.011
0.33	6.0	0.006
0.5	4.0	0.006
0.5	4.0	0.009
0.5	4.0	0.010
0.5	4.0	0.014
0.5	4.0	0.015
0.5	4.0	0.020

Neg. 731018-2

FIGURE 14. Machined Inserts Used to Vary Eductor Inlet Geometry

Material Transport

The experimental apparatus was modified (Figure 15) for material transport experiments. The modification included an inclined feed chute and a gas tight collection box which allowed orifice meter measurement of the mixed motive and entrained air during the conveying tests. Material transport rates were determined by material balance as a function of time.

EXPERIMENTAL RESULTS

The information of interest that was ga hered experimentally during this study included; the static pressure dis:ribution within the inlet region of the eductors, the velocity and direction of the flowing gases, the downstream developed pressure and the ratio of the entrained air to the motive air supplied to the eductors.

Velocity and Pressure Profiles

Effect of Geometry

Of particular interest was the effect of inlet eductor geometry and the motive air annulus gap on the flow fields and pressure profiles.

Flow fields and pressure profiles were measured on the eductor nozzle with a curvature of 0.50 $in.^{-1}$. The eductor had a two inch throat diameter, a six inch annular orifice diameter and a 0.006 in. annular gap. Figure 16 shows the flow field for an entrainment of 2.15. For this condition there is a flow reversal causing a discharge of air from the center region of the eductor. The back pressure regulating valve was then further opened to allow an entrainment of 2.62. Figure 17 presents similar data for this condition. Comparing these data shows that with the increase in entrainment, the flow reversal collapsed and that a stationary eddy circulation now exists in the inlet region of the eductor. An eductor nozzle with a curvature of 0.33 $in.^{-1}$ was installed in the e.perimental apparatus. As in the previous geometry above, the eductor had a two inch throat diameter, a six inch annular orifice and a 0.006 in. annular gap. Flow fields and pressure profiles were measured for entrainment conditions of 2.62 and 0.0 in Figures 18 and 19. As in the case for the eductor with a curvature

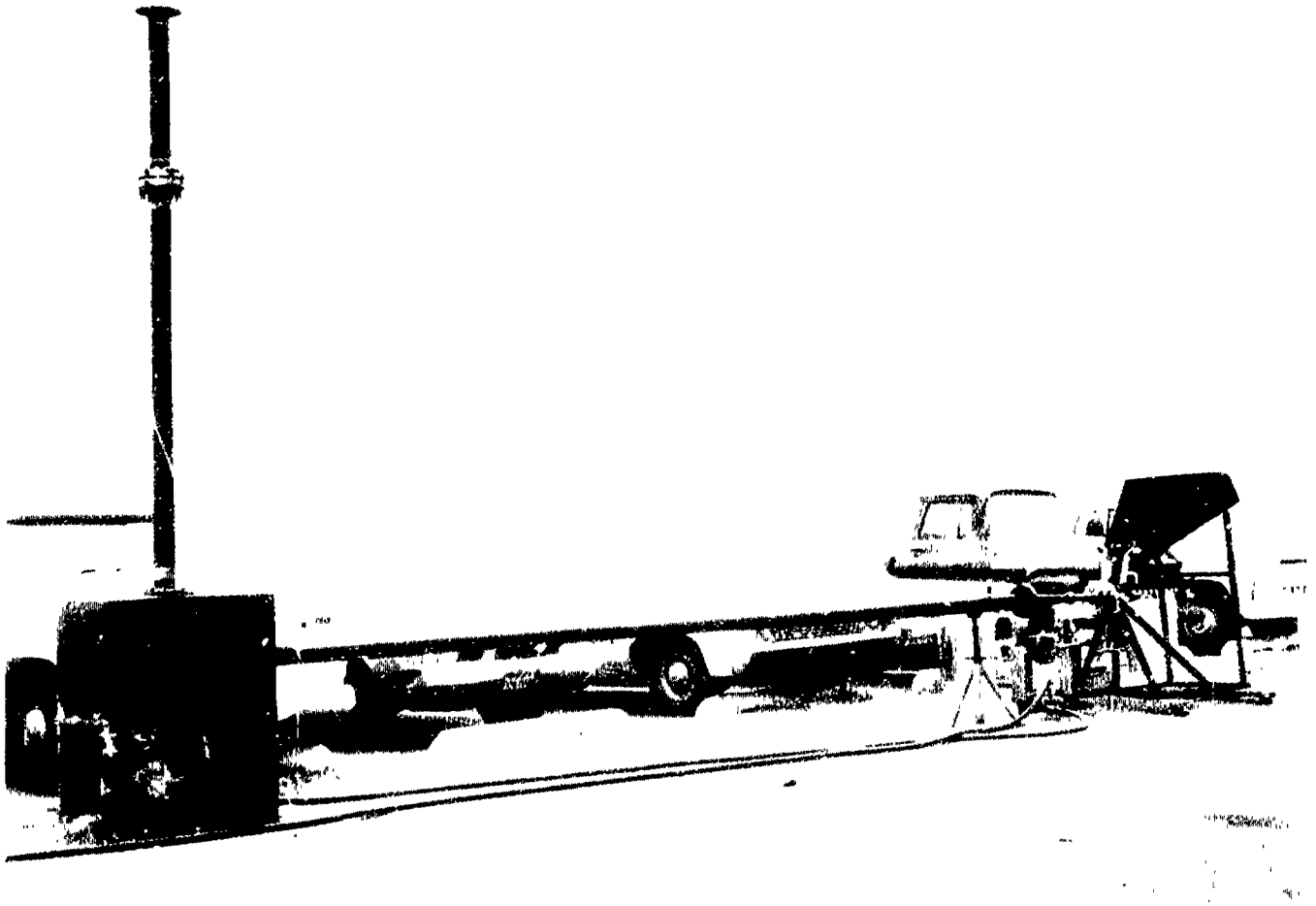

FIGURE 15. Experimental Appartus for Material Transport Experiments

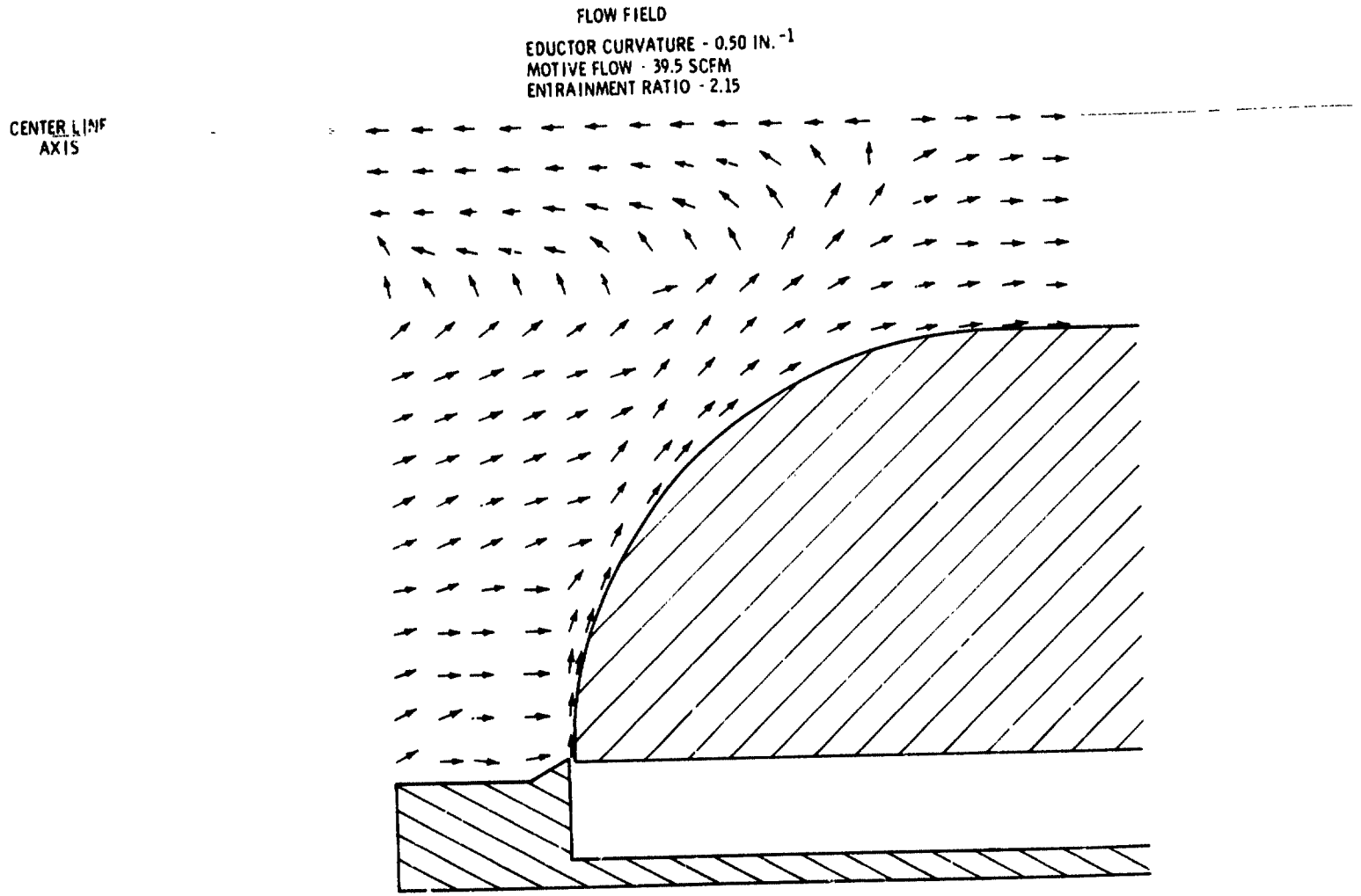

FIGURE 16. Flow Field Case No. 1

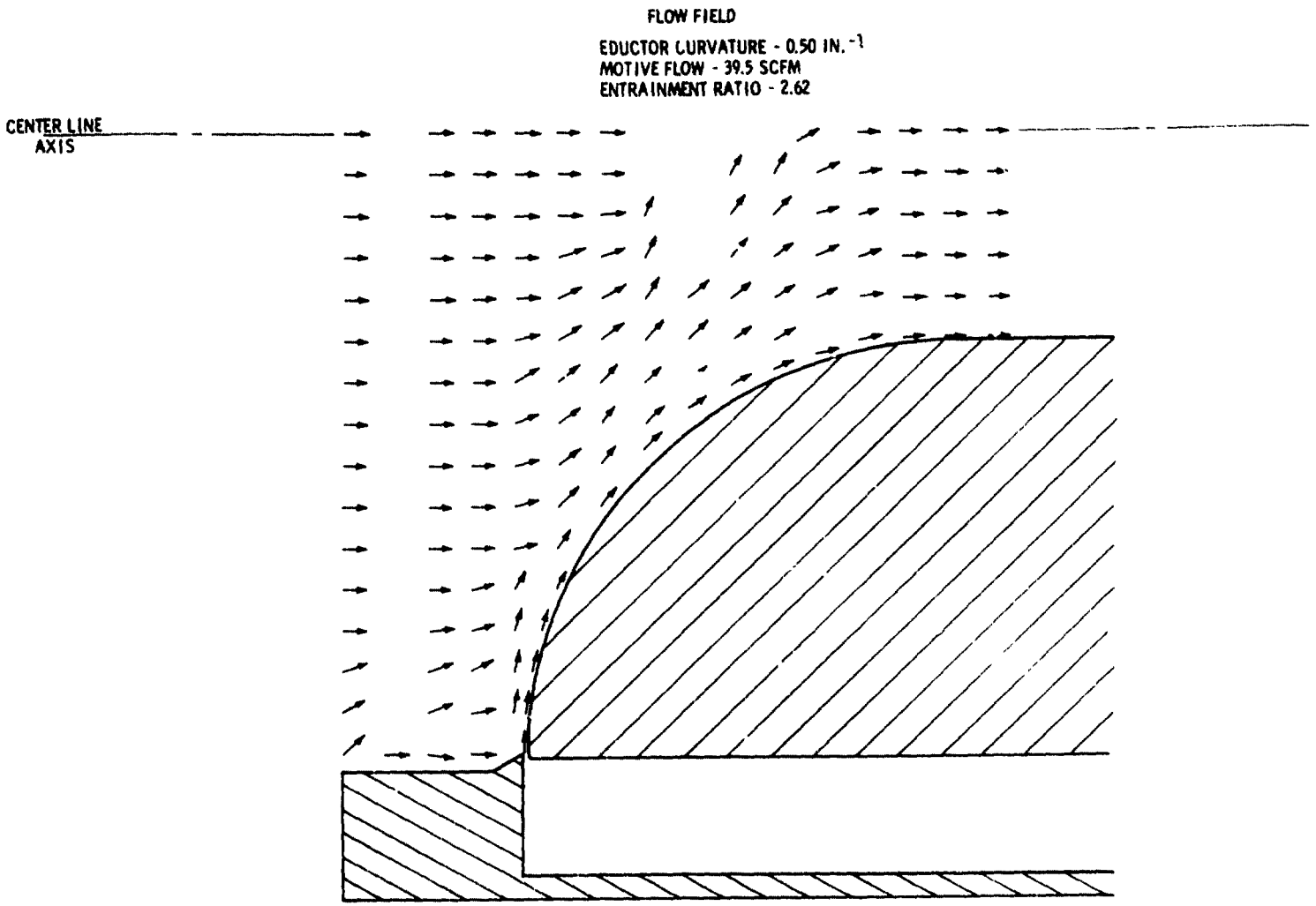

FIGURE 17. Flow Field Case No. 2

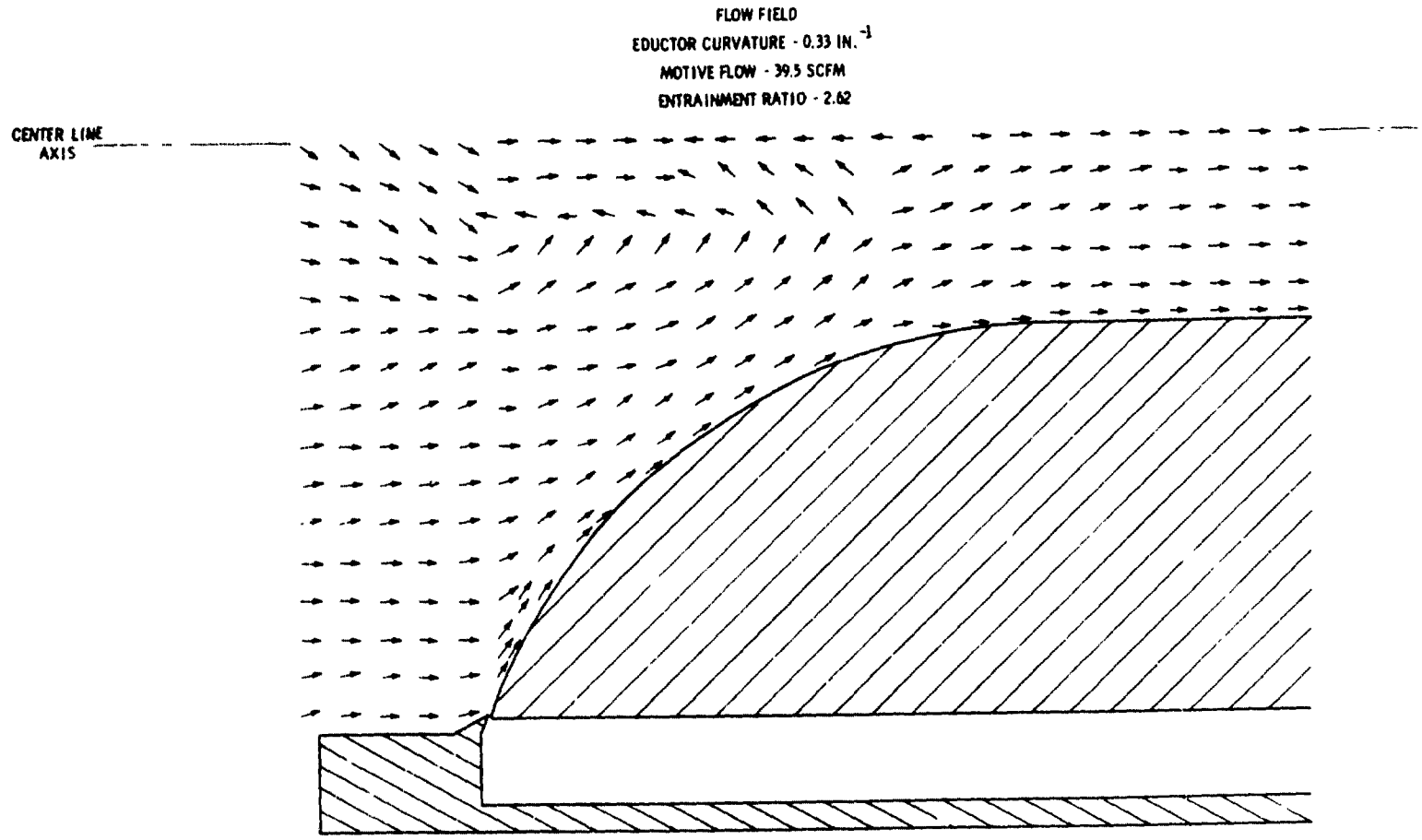

FIGURE 18. Flow Field Case No. 4

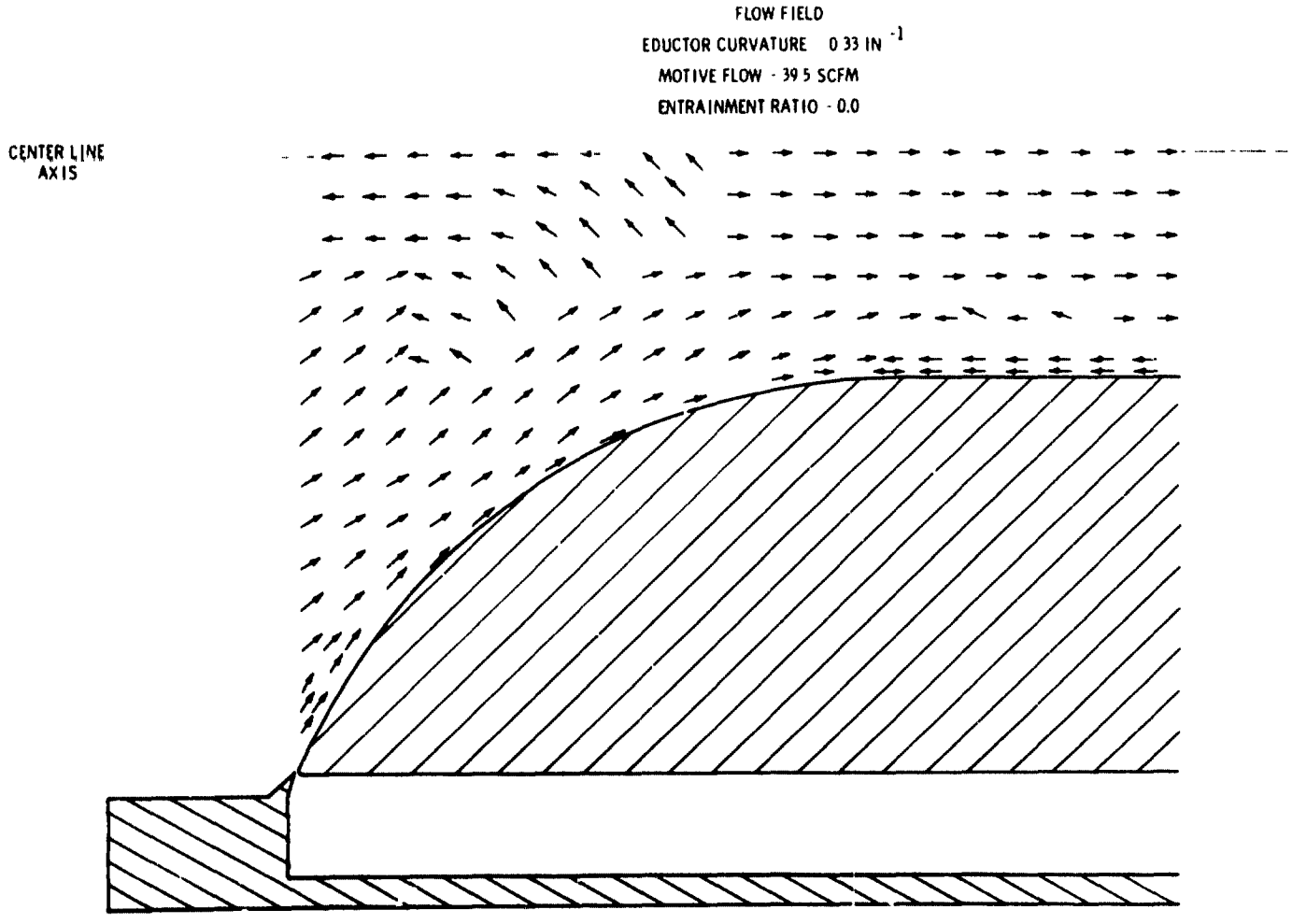

FIGURE 19. Flow Field Case No. 3

of 0.5 $in.^{-1}$, the flow reversal experienced in low entrainment ratios disappears and a stationary eddy circulation in the inlet region is established. For both the case of the 0.5 $in.^{-1}$ curvature and the 0.33 $in.^{-1}$ curvature a mo ive air supply of 40 scfm was used.

Effect of Cylindrical Mixing Section

Reasonable agreement was not achieved between values measured experimentally and those predicted by the analytical model. It was postulated that the analytical treatment of the eductor outlet as a free flow boundary might be the cause of this disagreement in that the experimental apparatus included a two inch diameter, twelve inch long cylindrical mixing section attached to the eductor outlet. Experiments were performed to determine the effects of the mixing section on the flow field of an eductor with a curvature of 0.50 $in.^{-1}$, an annulus diameter of 6.0 in. and an annular gap of 0.011 in. Data was gathered on the eductor with the two inch diameter mixing section attached to the outlet. The apparatus was then modified to effectively provide a free flow boundary at the eductor outlet (Figure 20). For both configurations, the motive air supplied to the eductor was 40 scfm. The results of these experiments showed that a significant effect on the flow field and performance was experienced by the inclusion of the two inch diameter mixing section. For the eductor with the two inch diameter mixing section, the maximum entrainment was 2.0. In the case of the eductor with the free flow boundary at the outlet, the maximum entrainment achieved was only 1.0. Figures 21 and 22 show the flow fields for the two conditions. Evaluation of these data led to the conclusion that the cylindrical mixing section must be incorporated into the mathematical model.

Performance

Effect of Geometry

Of particular interest to this study was the effect on eductor performance from variations in geometry of the inlet region. The performance factors most important to the end usage of these eductors are the ratio of the entrained air to the motive air and the developed pressure capabilities. Data were gathered to investigate the effect on these performance factors.

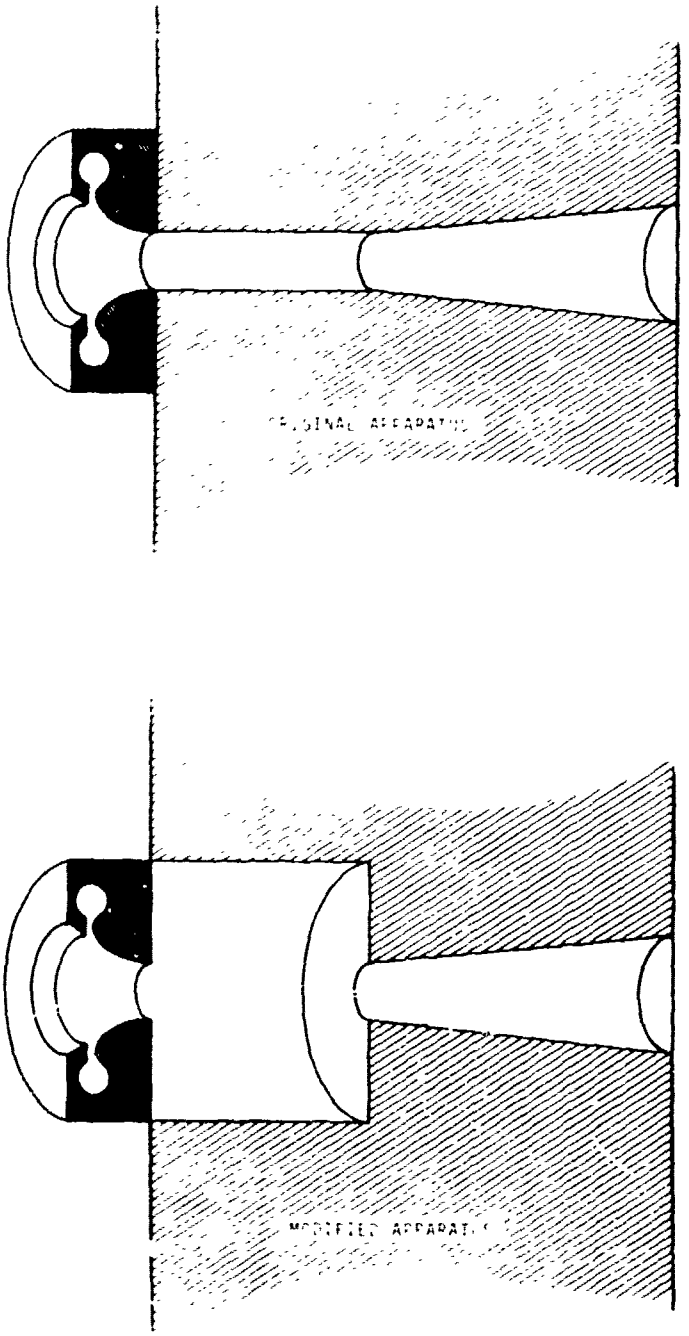

FIGURE 20. Apparatus to Examine the Effects of a Mixing Section (Cross Section)

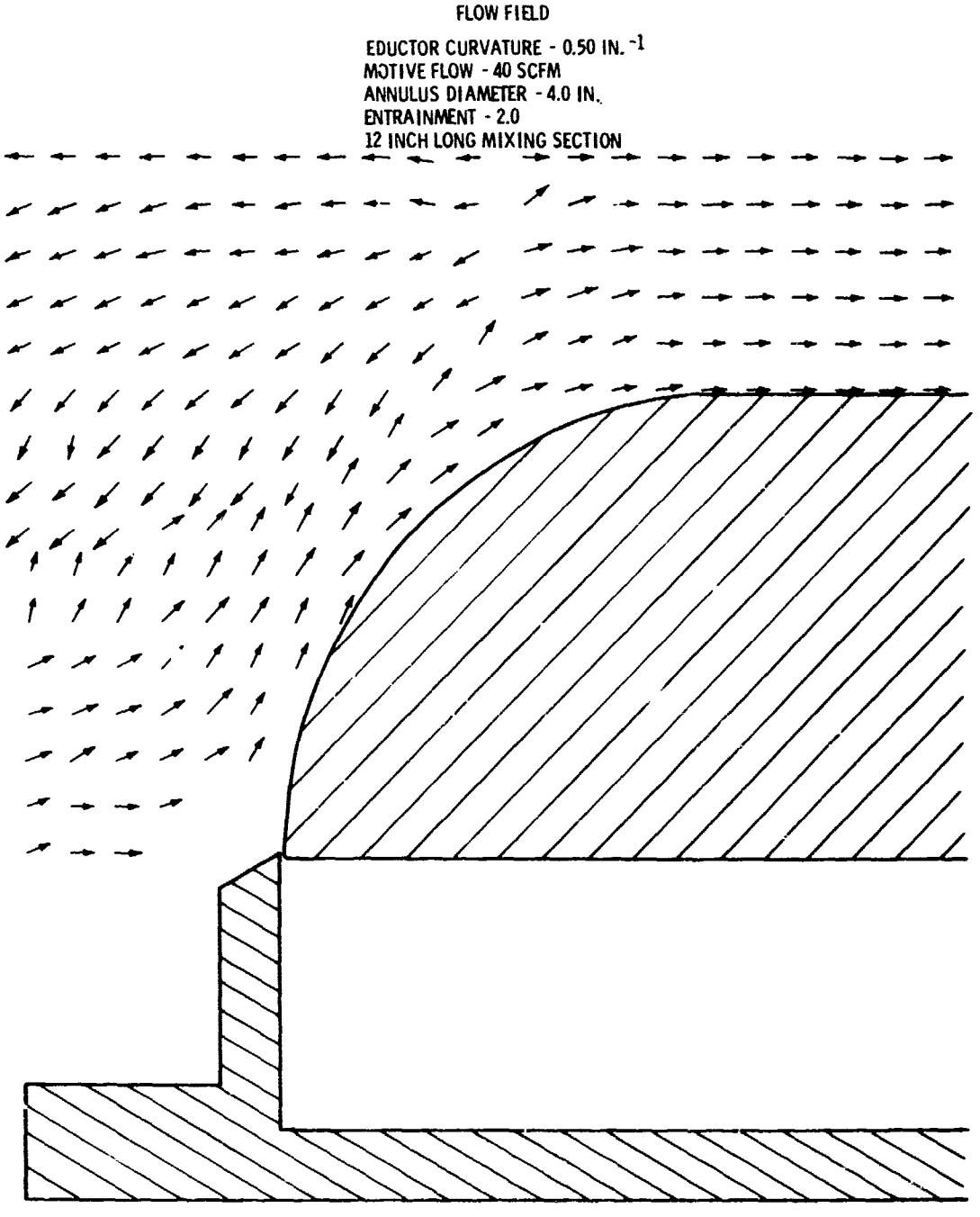

FIGURE 21. Flow Field Case No. 8

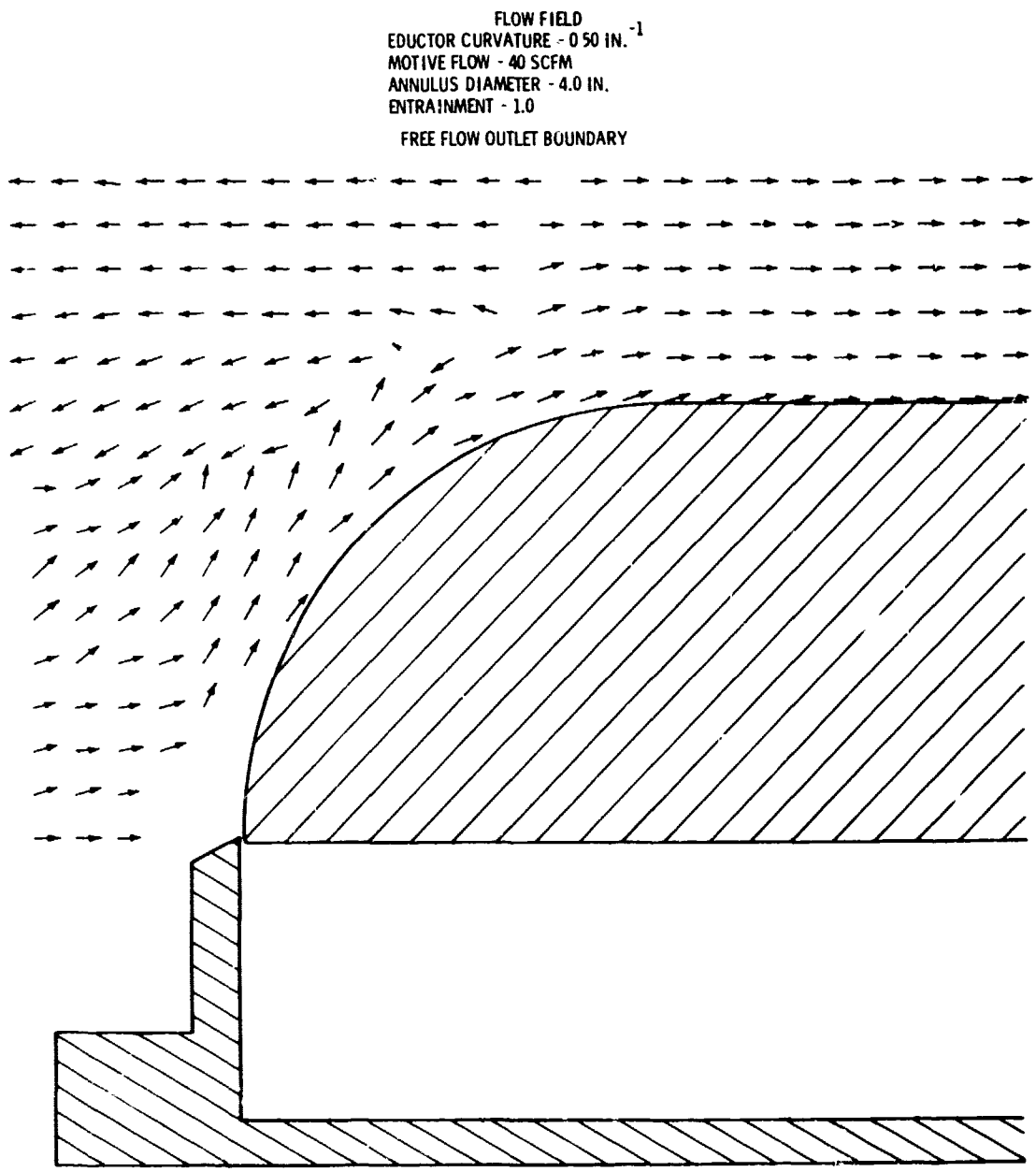

FIGURE 22. Flow Field Case No. 7

Figures 23, 24, and 25 show the developed pressure or pressure gain across the eductor as a function of motive flow. Each plot shows two values, representing the maximum pressure developed against a blockage and the minimum pressure developed when the valve on the discharge piping of the experimental apparatus was fully opened. In each of the three cases the dimension of the annular gap was 0.006 in. The three geometries were: 0.33 $in.^{-1}$ curvature - 6.0 in. diameter annulus, 0.50 $in.^{-1}$ curvature - 6.0 in. diameter annulus and 0.50 $in.^{-1}$ curvature - 4.0 in. diameter annulus. Comparison of the data shows that an increase in curvature produces higher pressure capabilities and that a decrease in annulus diameter also produces higher pressure capabilities. The eductor with the 0.50 $in.^{-1}$ curvature and 4.0 in. diameter annulus was evaluated for the effect of variations in the motive air annular gap. Figures 26, 27, 28, and 29 similarly present data as before for gap dimensions of 0.006 in., 0.009 in., 0.014 in., and 0.020 in. Analysis of these data indicates that the system capability to produce pressure against a blockage optimizes with the eductor having a motive air annulus gap of approximately 0.009 in.

Of equal importance to eductor usage for pneumatic conveying is ratio of entrained to motive air. The experimental data showed that the highest entrainment ratios were achieved for low motive air inputs with eductors having a large motive air annulus diameter and a low curvature (Figure 30). For the higher motive air inputs, the difference in the entrainment from one eductor geometry to another was not as significant. Figures 31 through 35 present the entrainment versus motive flow for eductor geometries of 0.50 $in.^{-1}$ curvature - 6.0 in. diameter annulus - 0.010 in. gap and 0.50 $in.^{-1}$ curvature - 4.0 in. diameter annulus with annulus gaps of 0.006 in., 0.009 in., 0.014 in., and 0.020 in. These data show that as the dimension of the motive air annulus gap is increased, the entrainment is decreased for all motive flow conditions.

Effect of Back Pressure

In that the entrainment of atmospheric air will be reduced during material transport operations, the developed pressure as a function of the

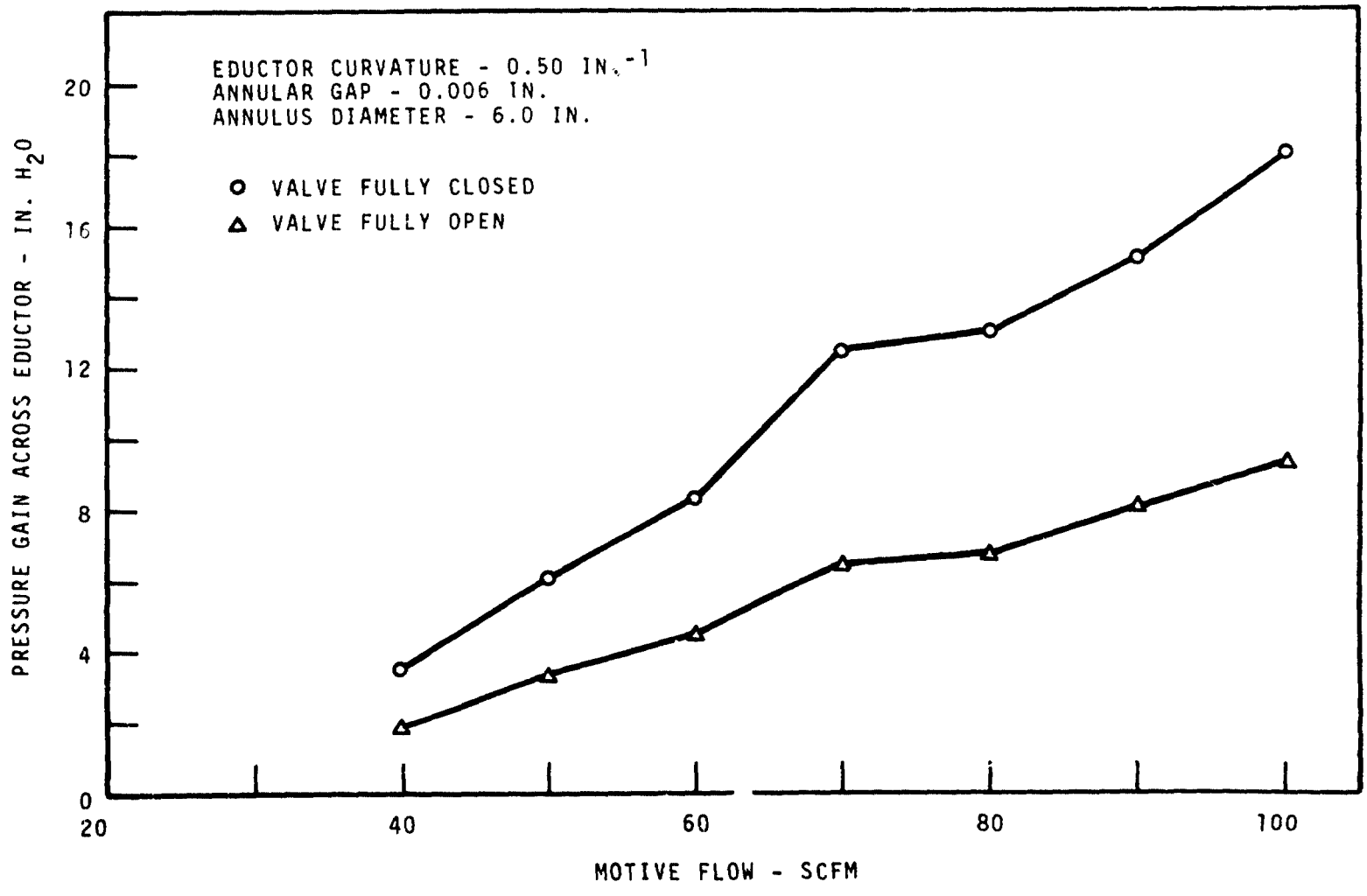

FIGURE 23. Pressure Gain Across Eductor Versus Motive Flow, Run P-1

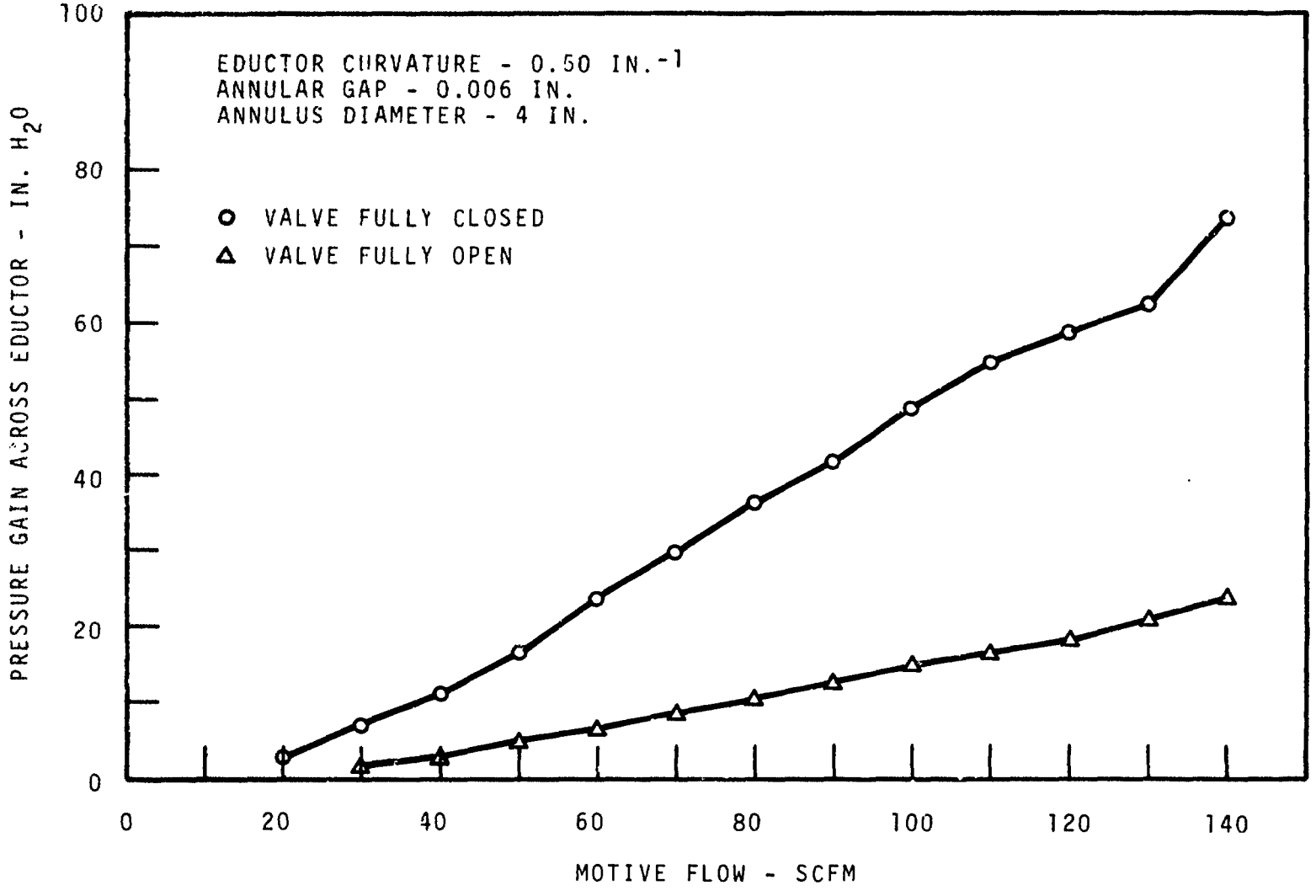

FIGURE 24. Pressure Gain Across Eductor Versus Motive Flow, Run P-2

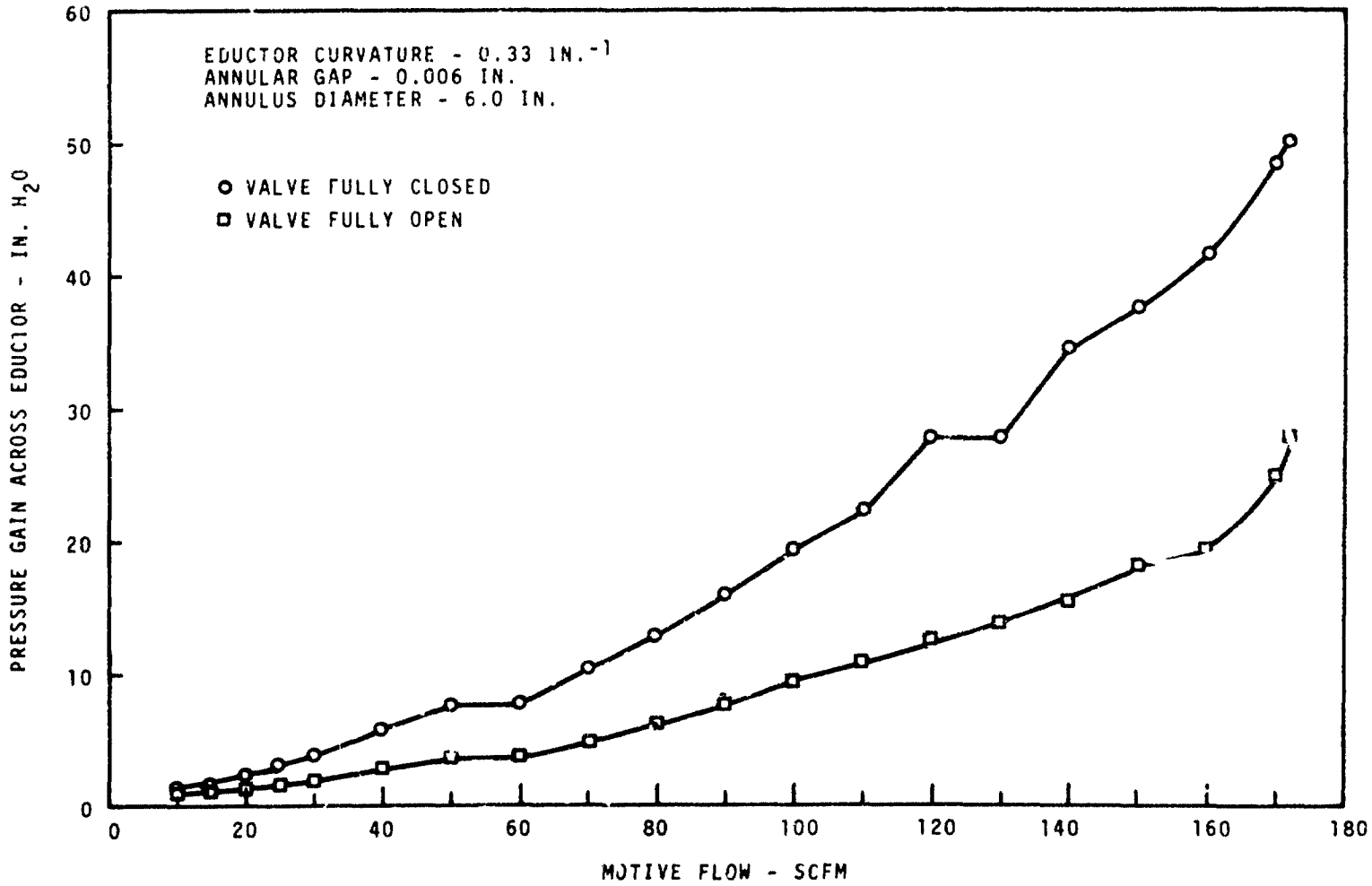

FIGURE 25. Pressure Gain Across Eductor Versus Motive Flow, Run P-3

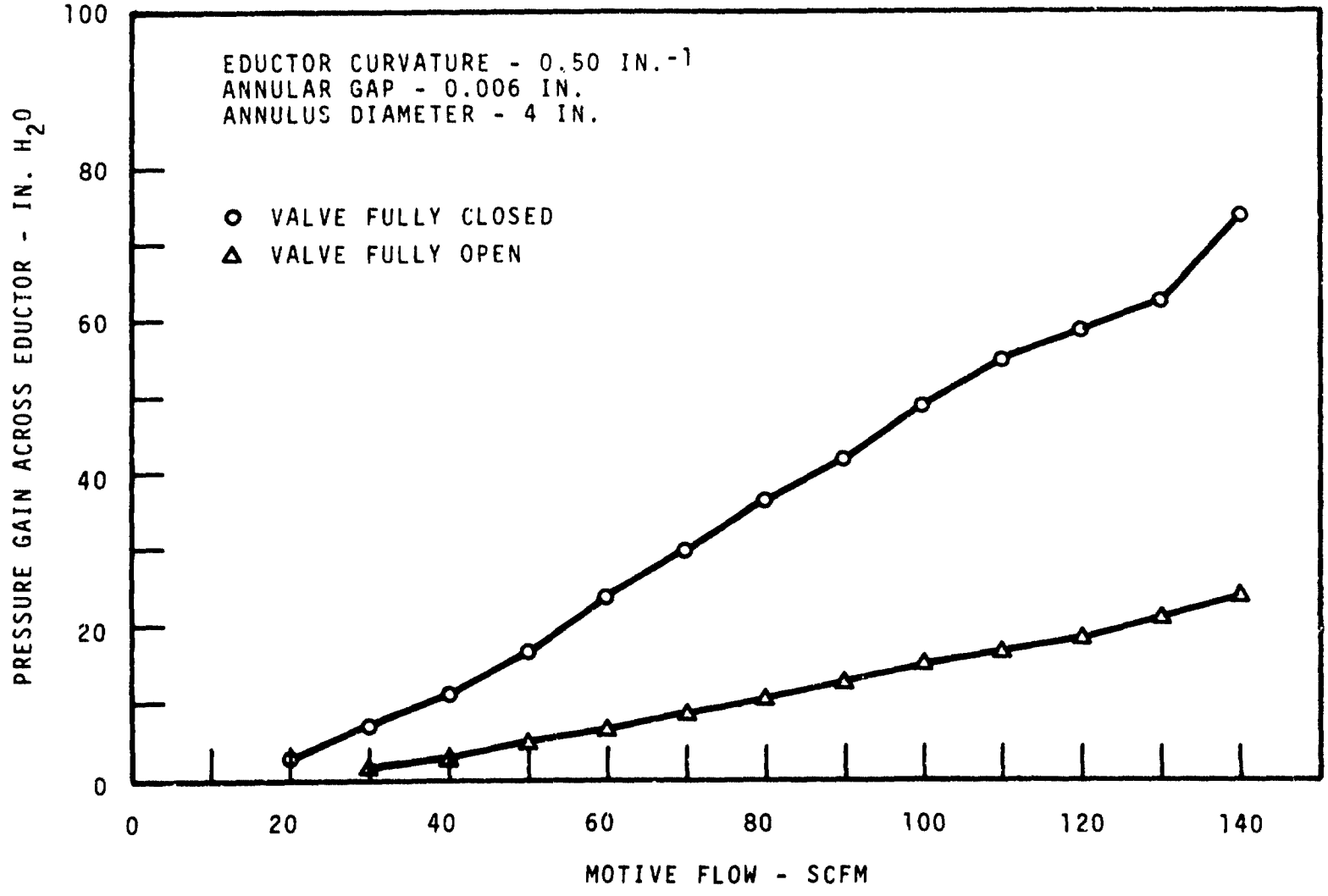

FIGURE 26. Pressure Gain Across Eductor Versus Motive Flow, Run P-4

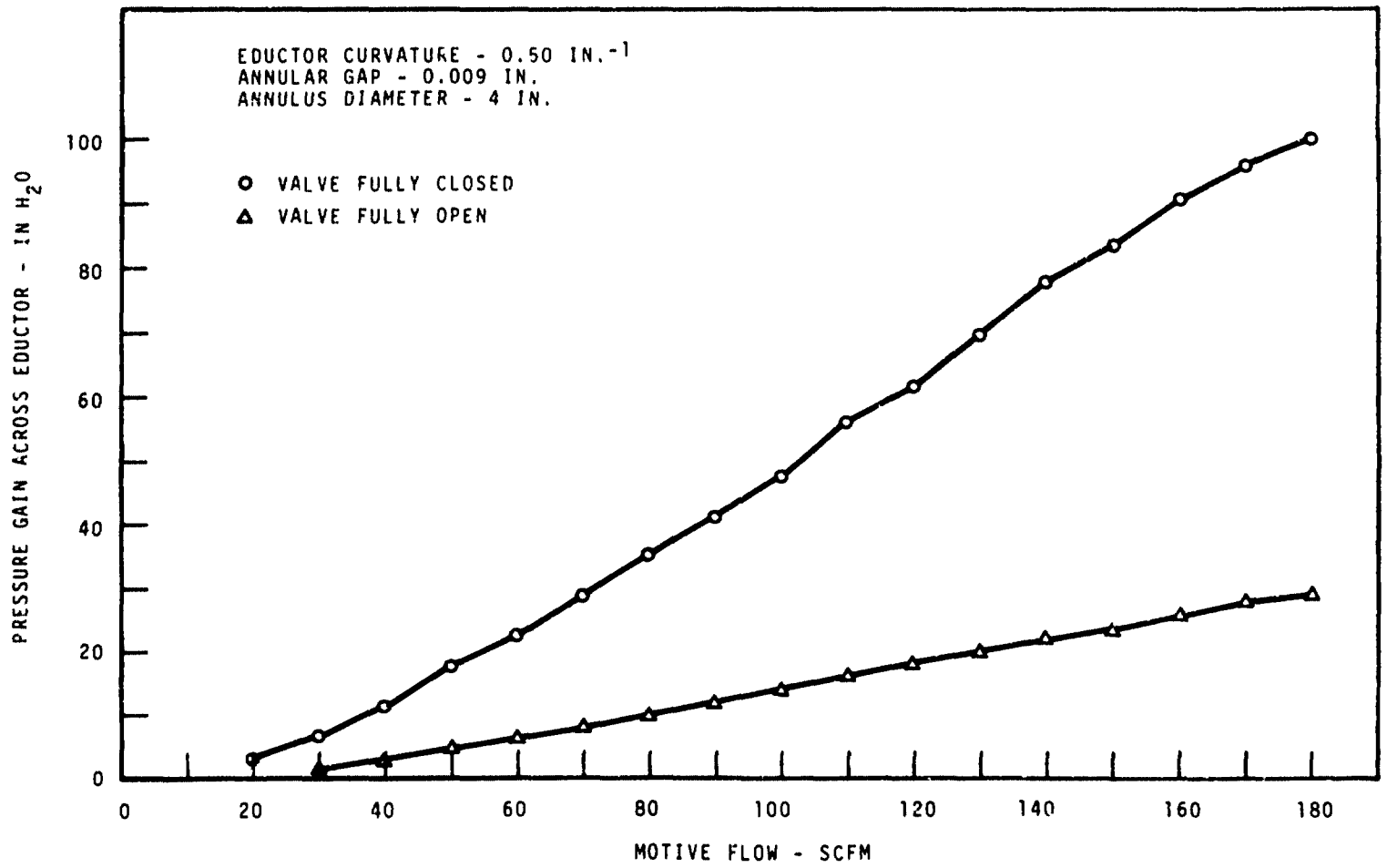

FIGURE 27. Pressure Gain Across Eductor Versus Motive Flow, Run P-5

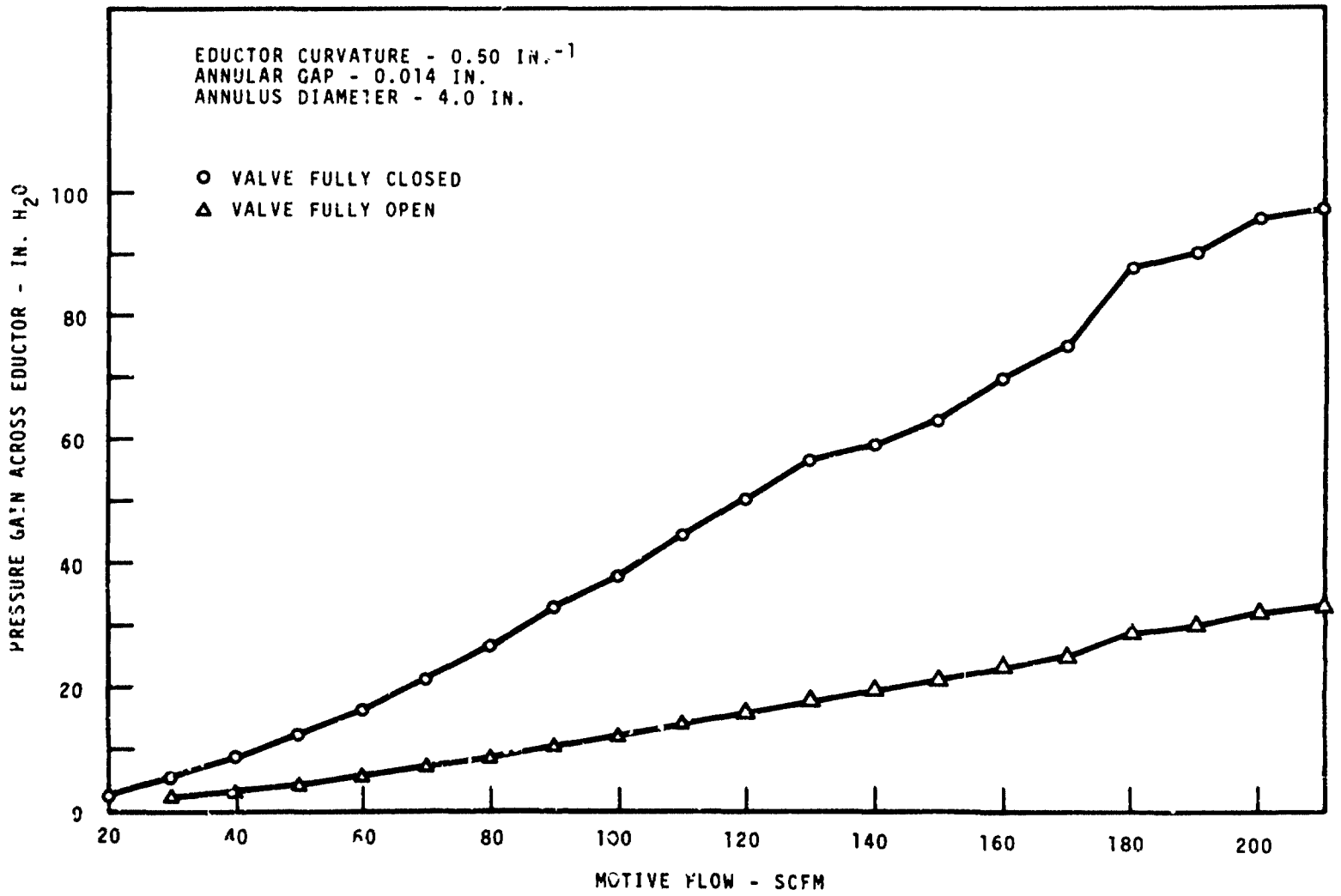

FIGURE 28. Pressure Gain Across Eductor Versus Motive Flow, Run P-6

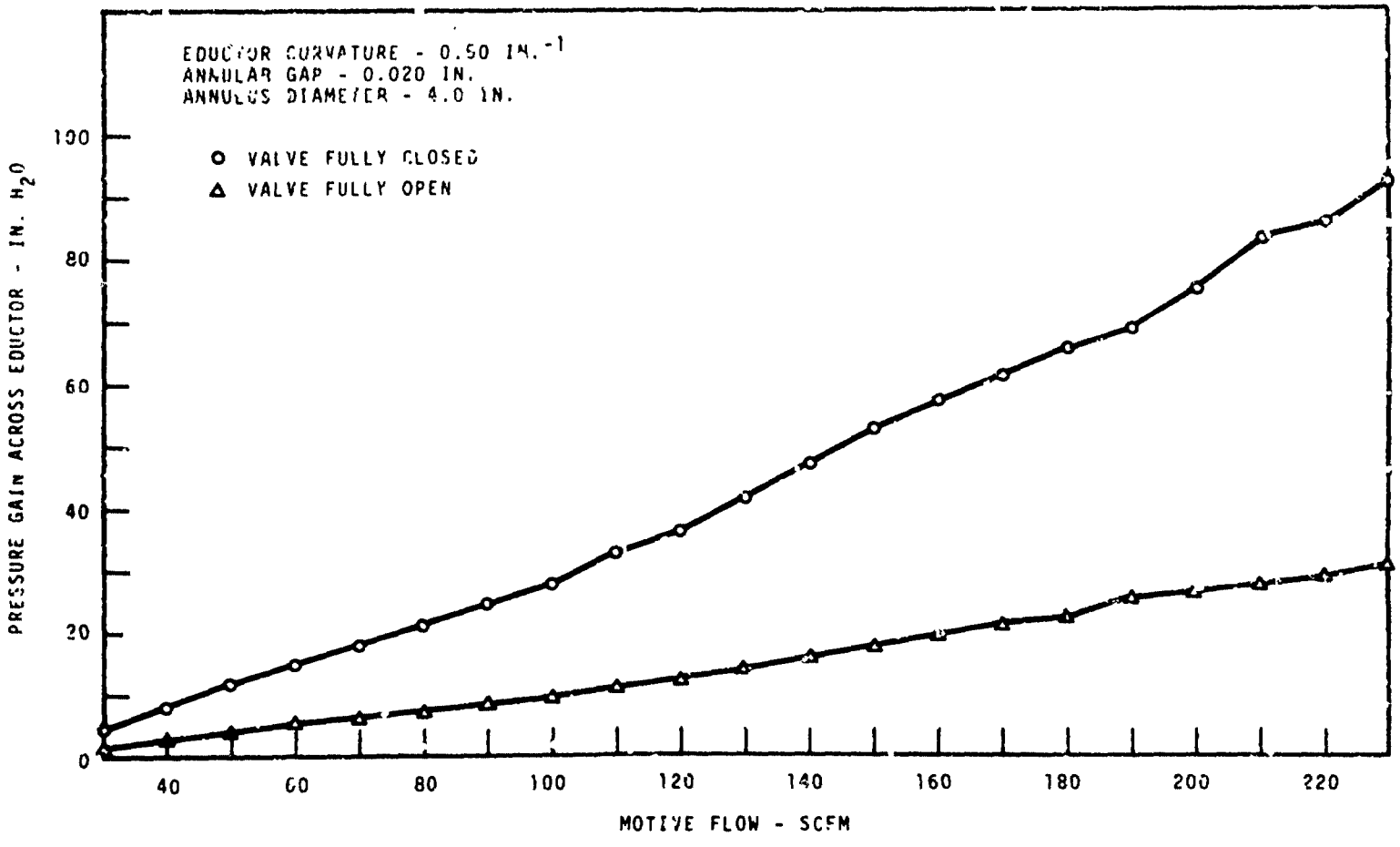

FIGURE 29. Pressure Gain Across Eductor Versus Motive Flow, Run P-7

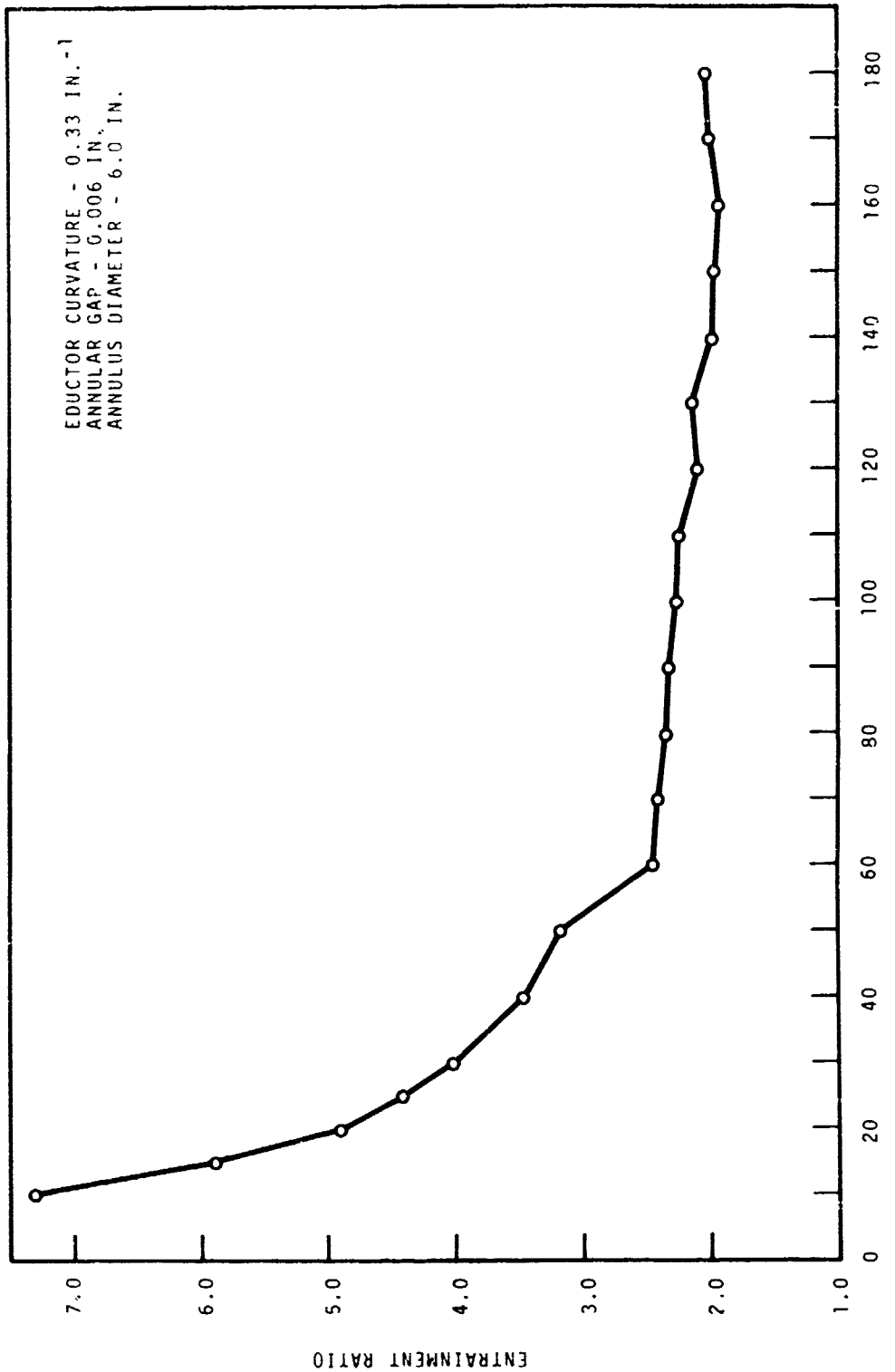

FIGURE 30. Entrainment Ratio Versus Motive Flow, Run E-1

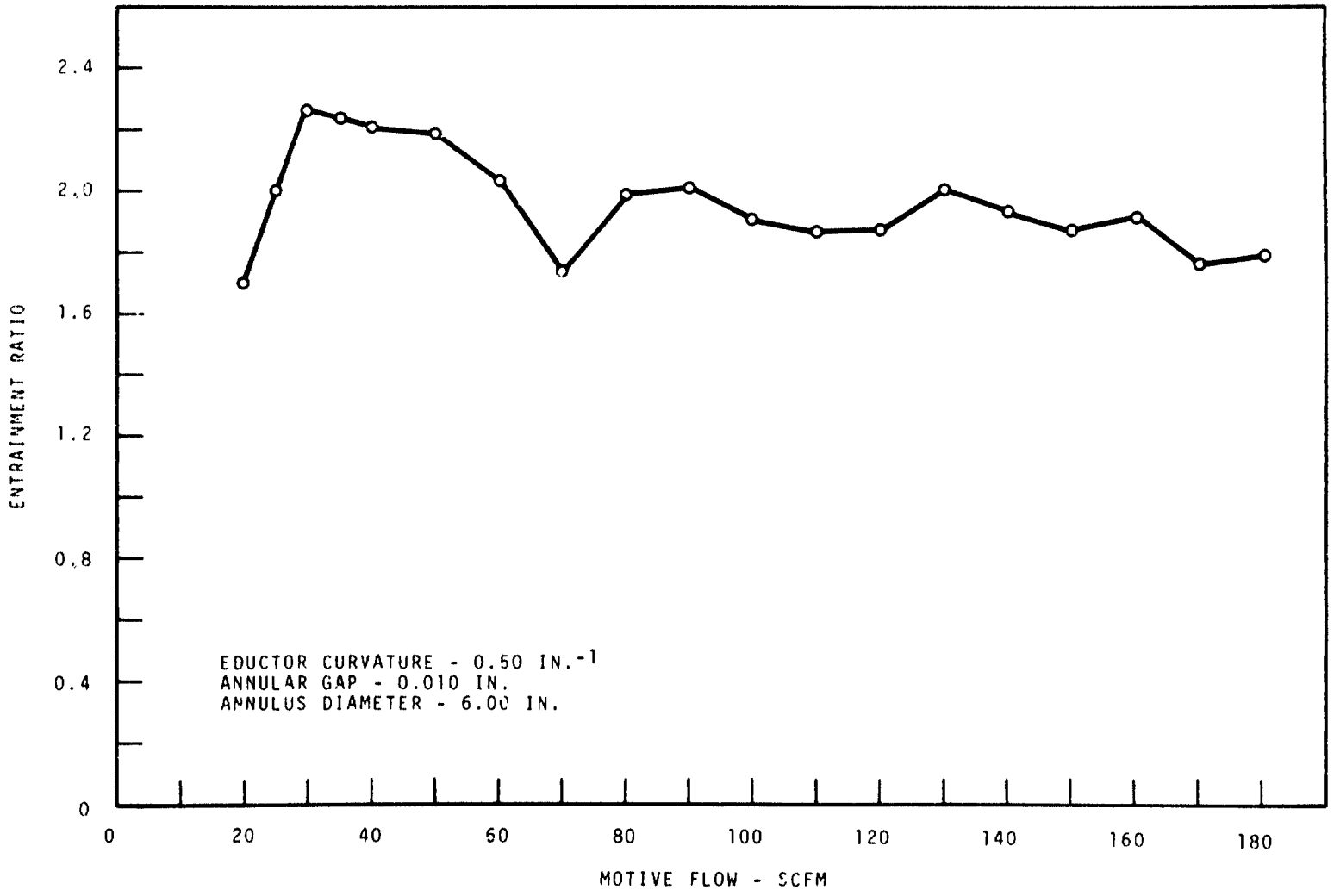

FIGURE 31. Entrainment Ratio Versus Motive Flow, Run E-2

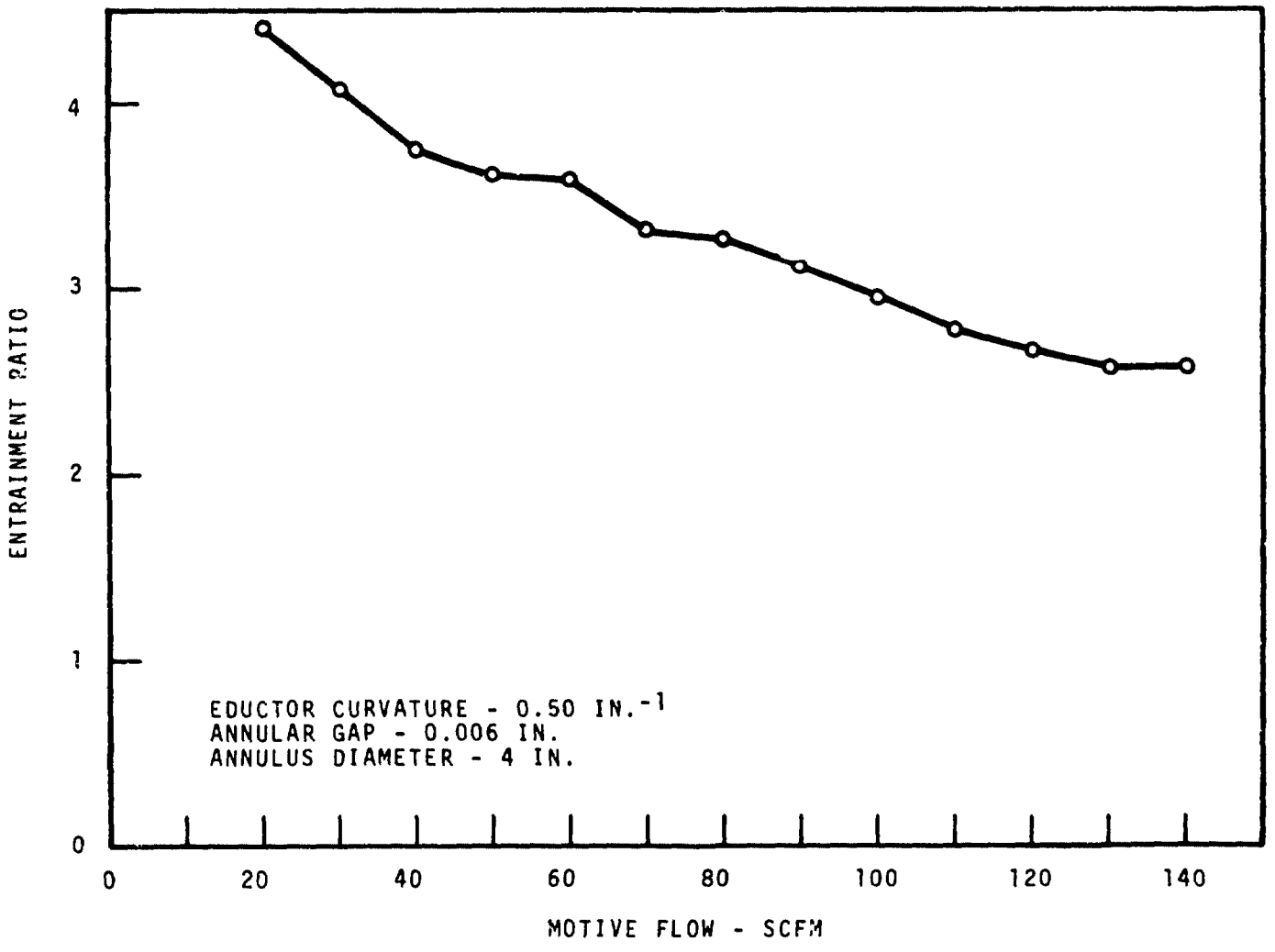

FIGURE 32. Entrainment Ratio Versus Motive Flow, Run E-3

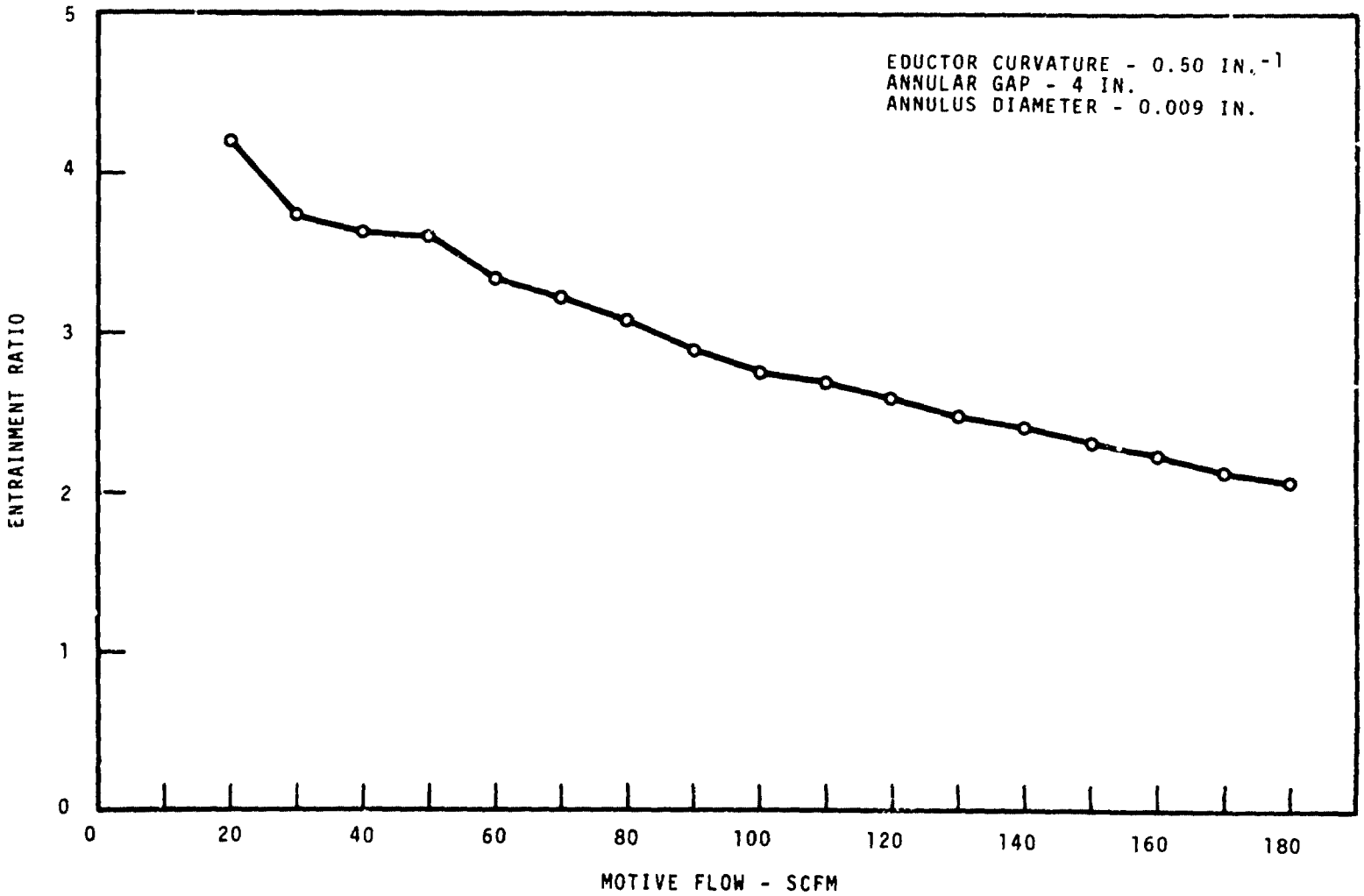

FIGURE 33. Entrainment Ratio Versus Motive Flow, Run E-4

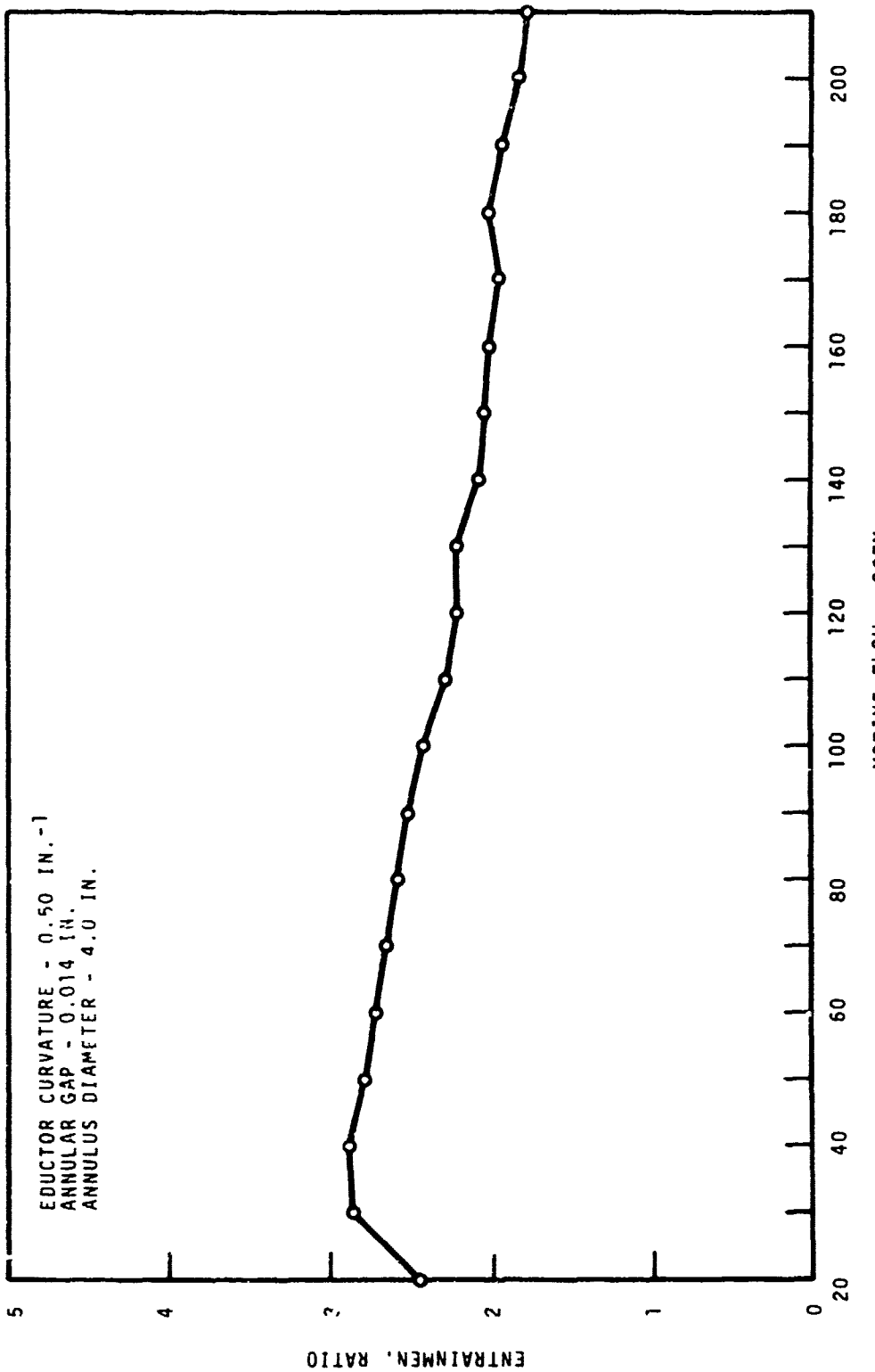

FIGURE 34. Entrainment Ratio Versus Motive Flow, Run E-5

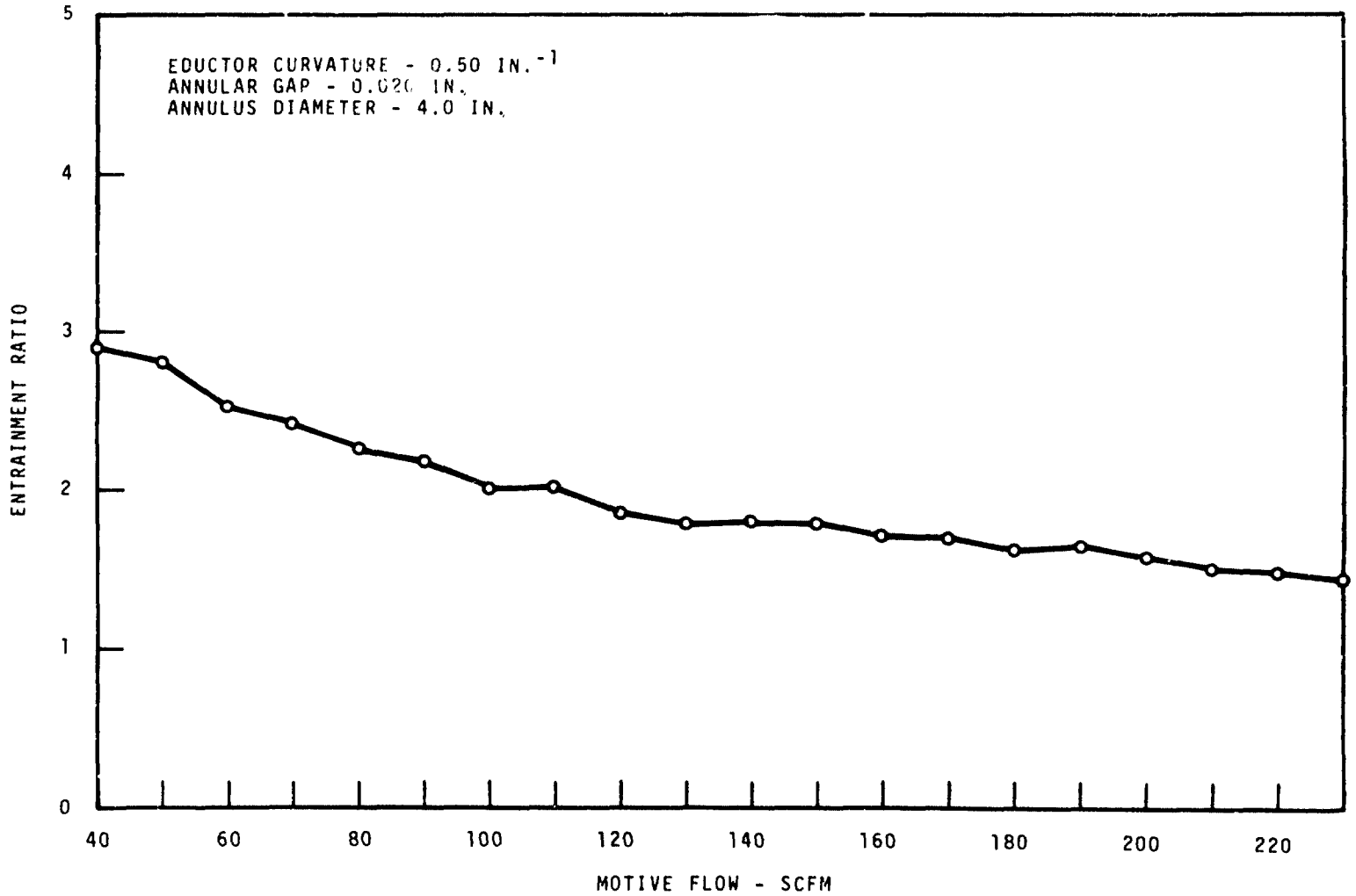

FIGURE 35. Entrainment Ratio Versus Motive Flow, Run E-6

entrainment ratio is of special interest. Figure 36 presents the entrainment ratio versus developed pressure or back pressure for a family of motive flow conditions in an eductor with a curvature of 0.50 $in.^{-1}$, an annulus diameter of 4.0 in. and an annulus gap of 0.006 in. Figures 37 and 38 show similar data for the same eductor when the annular gap is increased to 0.014 in. and 0.020 in. with motive flows of 190 scfm and 228 scfm, respectively. From this, it is shown that a reduction in performance is experienced when the annular gap is increased from 0.014 in. to 0.020 in.

Material Transport

The experimental apparatus was further modified for experiments involving the pneumatic conveying of crushed rock materials. The modifications included: A collection chamber for the conveyed material which would allow the measurement of the volume of mixed motive and entrained air, an inclined feed table and instrumentation to measure the pressure drop through the conveying duct. The eductor section was fitted with a metal insert which provided an inlet geometry of 0.50 $in.^{-1}$ curvature and 4.0 in. diameter annulus. The crushed rock material used for the experiments was a 3/8 in. minus having a bulk density of 81.5 lb/ft^3.

Figure 39 shows the material conveying rate as a function of the motive air flow. Included is the motive air pressure supplied to the eductor, and the calculated horsepower to compress the air at that flow condition. It should be noted that during the tests using 50 scfm motive flow, the velocity of the conveying air in the duct was insufficient to maintain fluidized transport while conveying at the rates measured. For the higher motive flow used in the experiments, the velocity in the conveying duct when no material was being processed was 6820 ft/min. During the conveying operations, while processing crushed rock at a rate of 4 tons per hour, the velocity of the conveying gases was reduced to an average of 4600 ft/min. At this conveying rate, the pressure drop through twenty feet of conveying ductwork averaged two inches of water.

Most of the data gathered to support the development of the mathematical model was taken in the inlet region of the eductor. These data

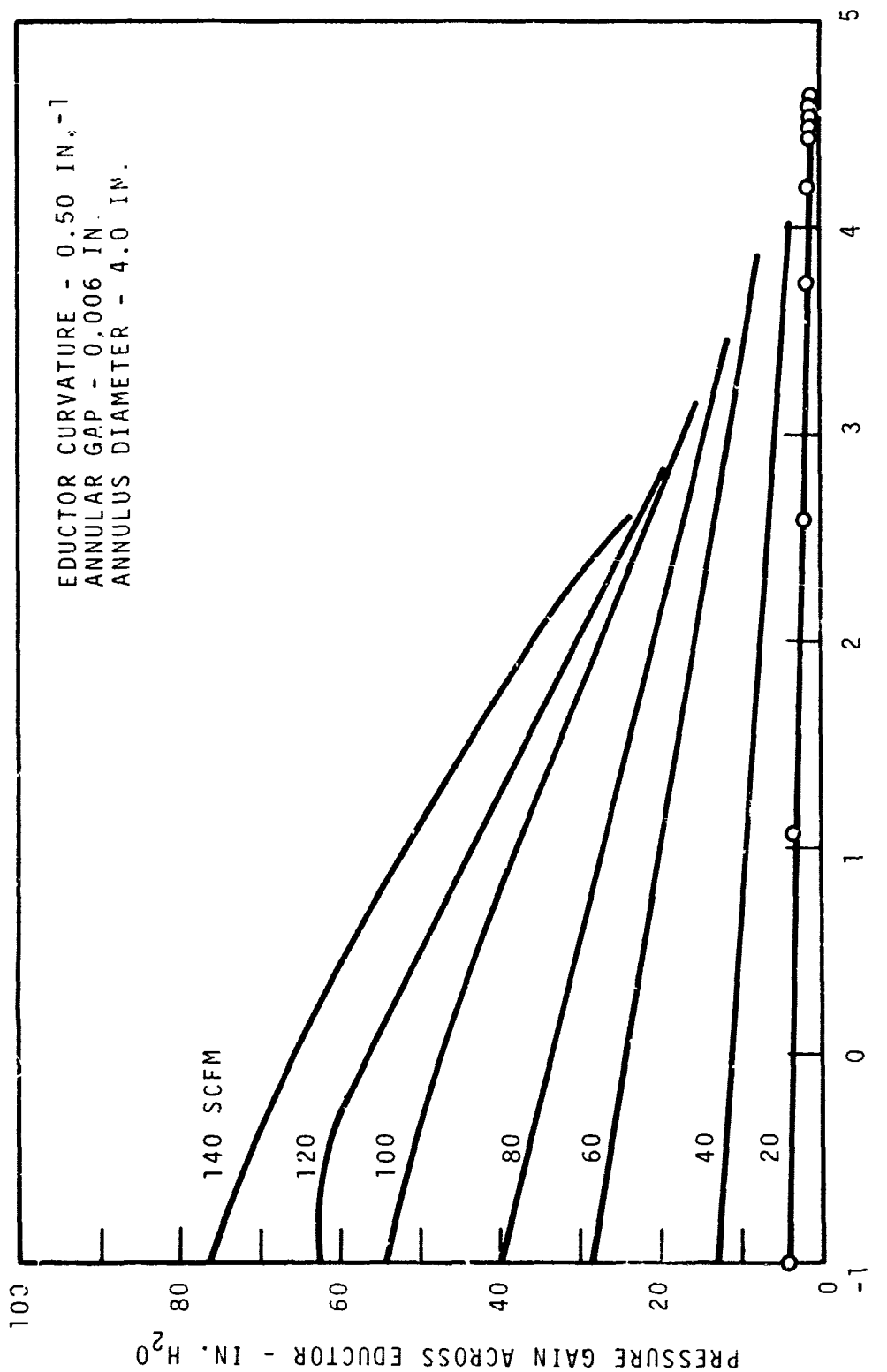

FIGURE 36. Pressure Gain Across Eductor Versus Entrainment Ratio, Run P-8

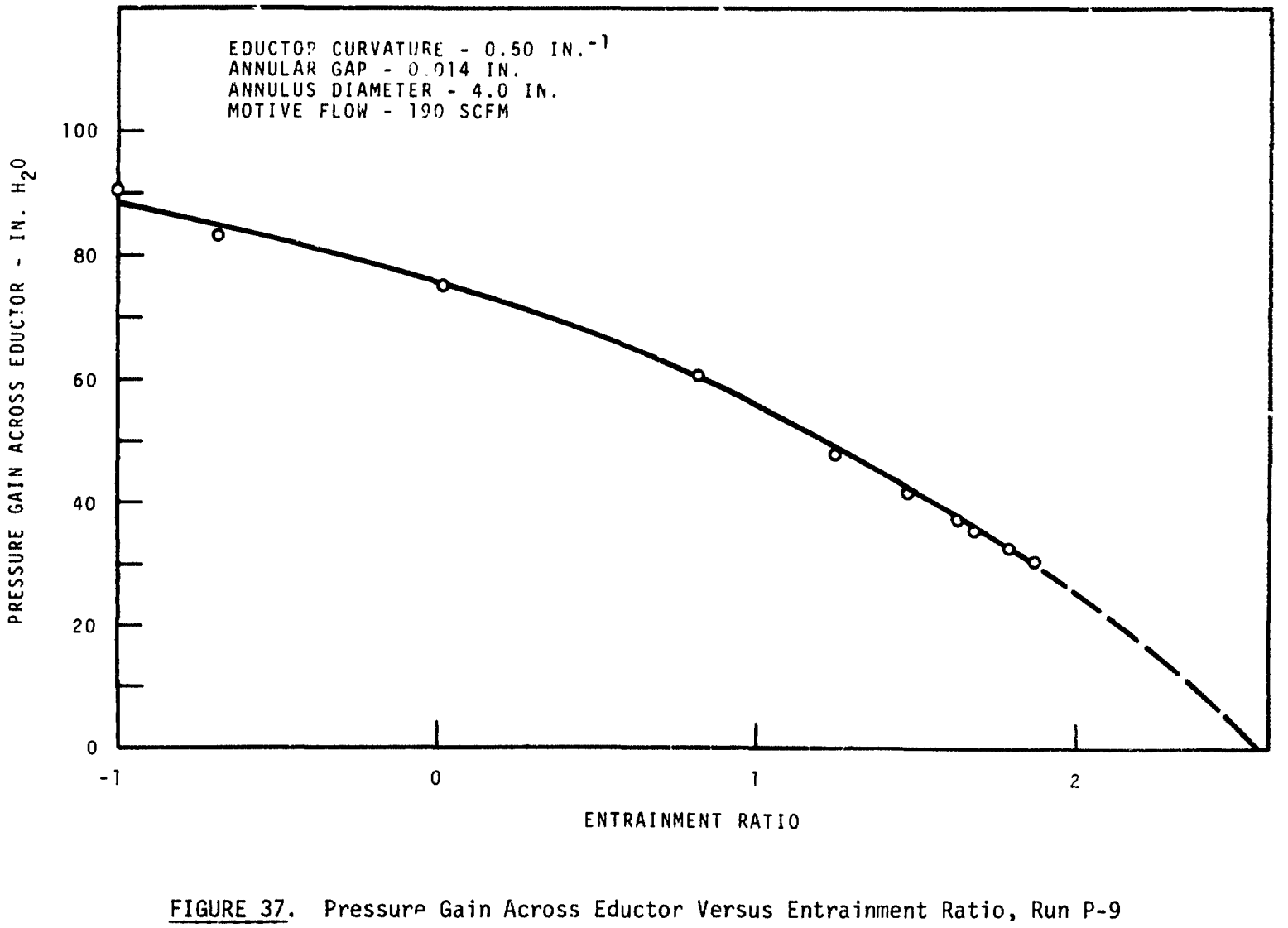

FIGURE 37. Pressure Gain Across Eductor Versus Entrainment Ratio, Run P-9

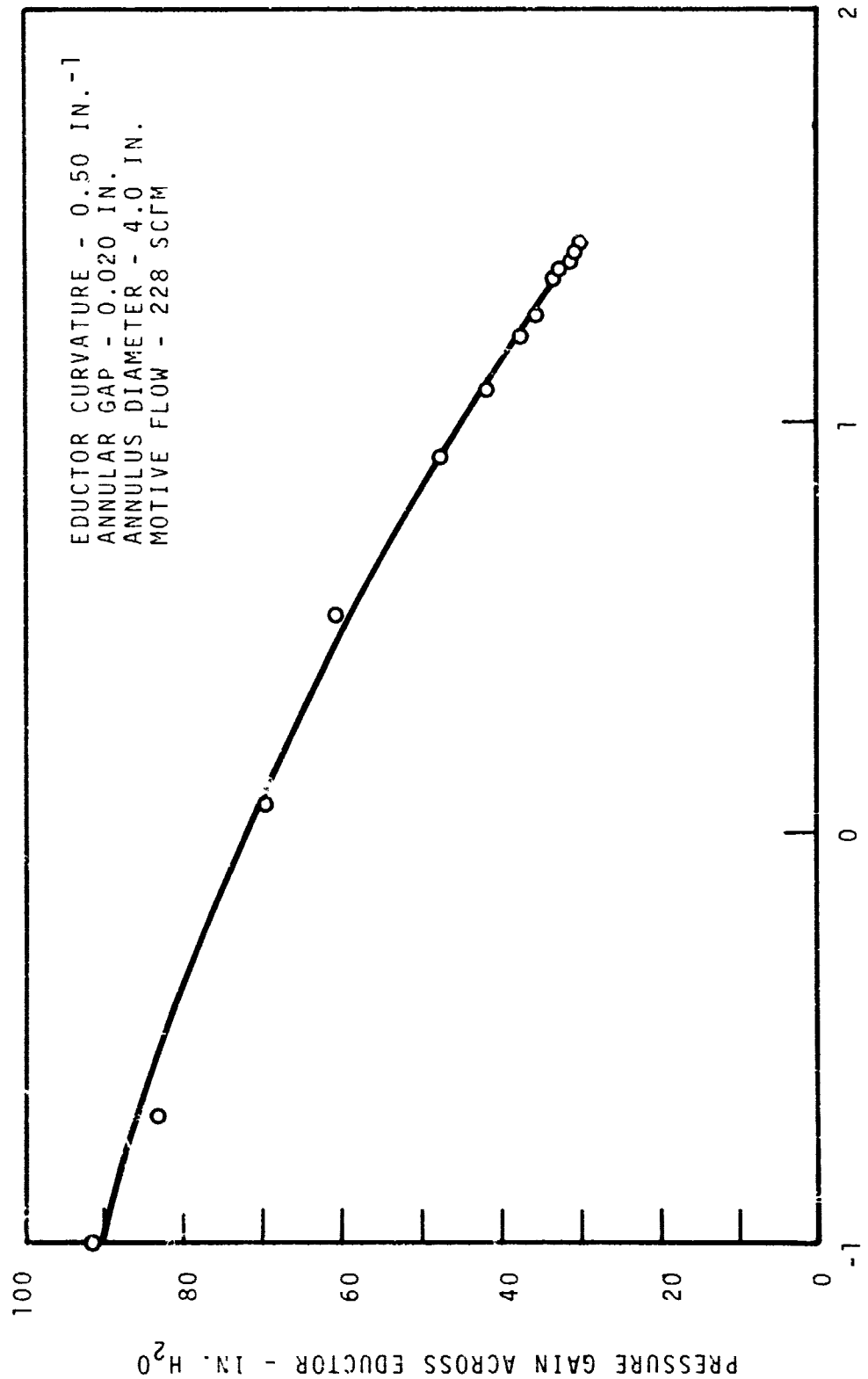

FIGURE 38. Pressure Gain Across Eductor Versus Entrainment Ratio, Run P-10

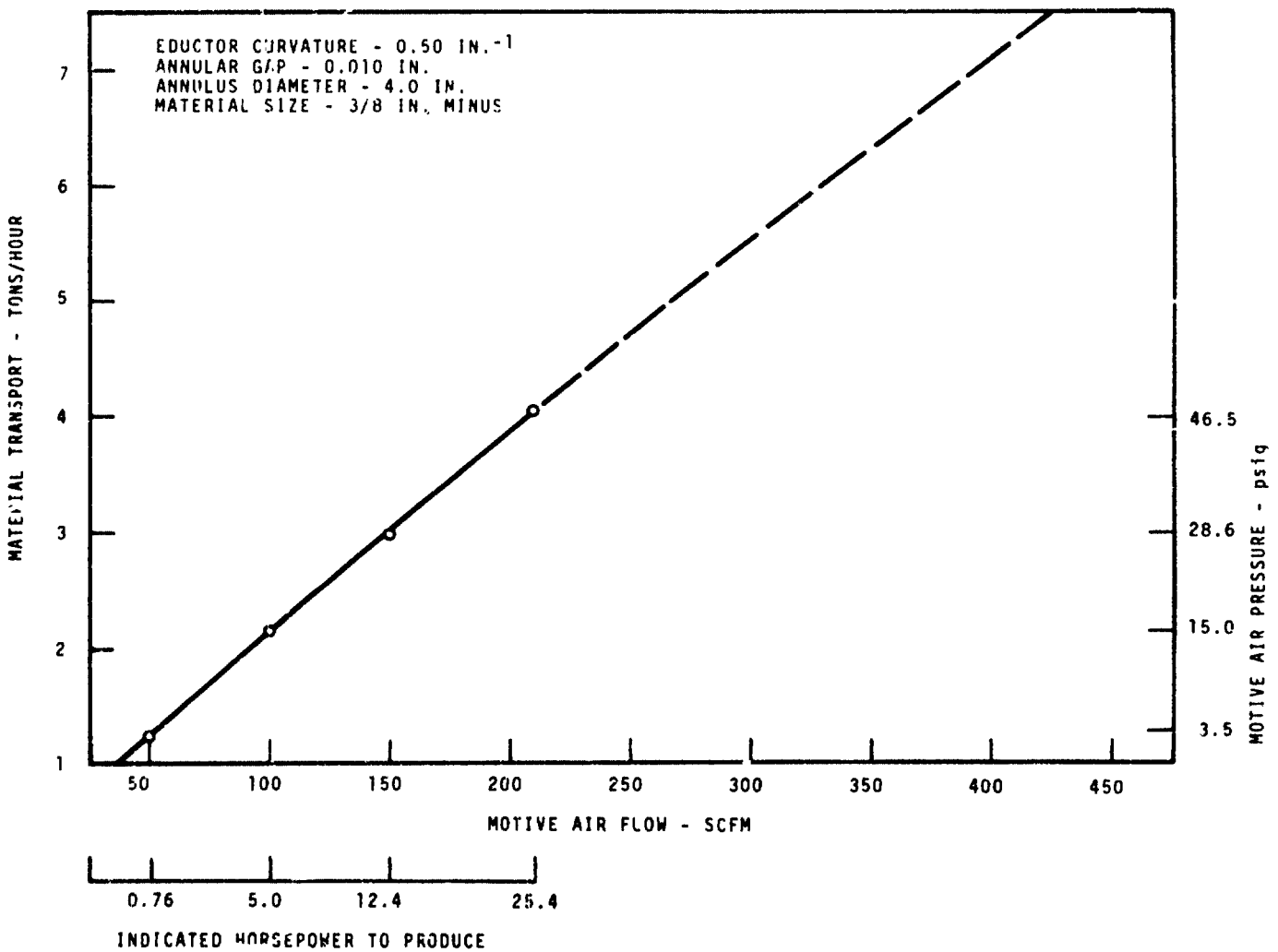

FIGURE 39. Material Transport Rate Versus Motive Flow

are presented in Figures 40 through 47. These physical measurements may be used in evaluating mathematical models designed to predict the performance of Coanda eductors.

COMPARISON OF MODEL PREDICTIONS WITH EXPERIMENTAL RESULTS

As noted earlier in this report, the lack of an eddy viscosity model has prevented the satisfactory prediction of flow fields in Coanda eductors. The comparison presented here is designed to elucidate the differences between the computed and experimental results.

VELOCITY AND PRESSURE PROFILES FOR CASE I

For this case, the primary air flow was 39.5 scfm, the inlet slit width was 0.006 in., the slit diameter was 6 in., the radius of curvature of the entrainment section was 3 in., and the entrainment ratio was 2.62.

The axial velocity profile measured at the entry to the constant cross section mixing section is compared to that predicted in Figure 48. It is apparent that the wall jet does not diffuse as rapidly as predicted by the theory. This discrepancy stems from the relatively high viscosity used in the SYMJET solution to this problem. When lower viscosities were tried, the jet detached from the curved surface a short distance downstream from the inlet.

The centerline pressure distribution computed from the model is compared to that measured experimentally in Figure 49. In the inlet region, reasonable agreement between the measured and predicted profiles is shown. However, after the maximum in pressure is reached, the numerical model predicts a much greater drop in pressure than actually occurs. This discrepancy is apparently caused by inaccuracies in the centerline velocity profile. It is plausible that the predicted pressure distribution could actually be obtained if the fluid possessed the viscosity assumed in the model.

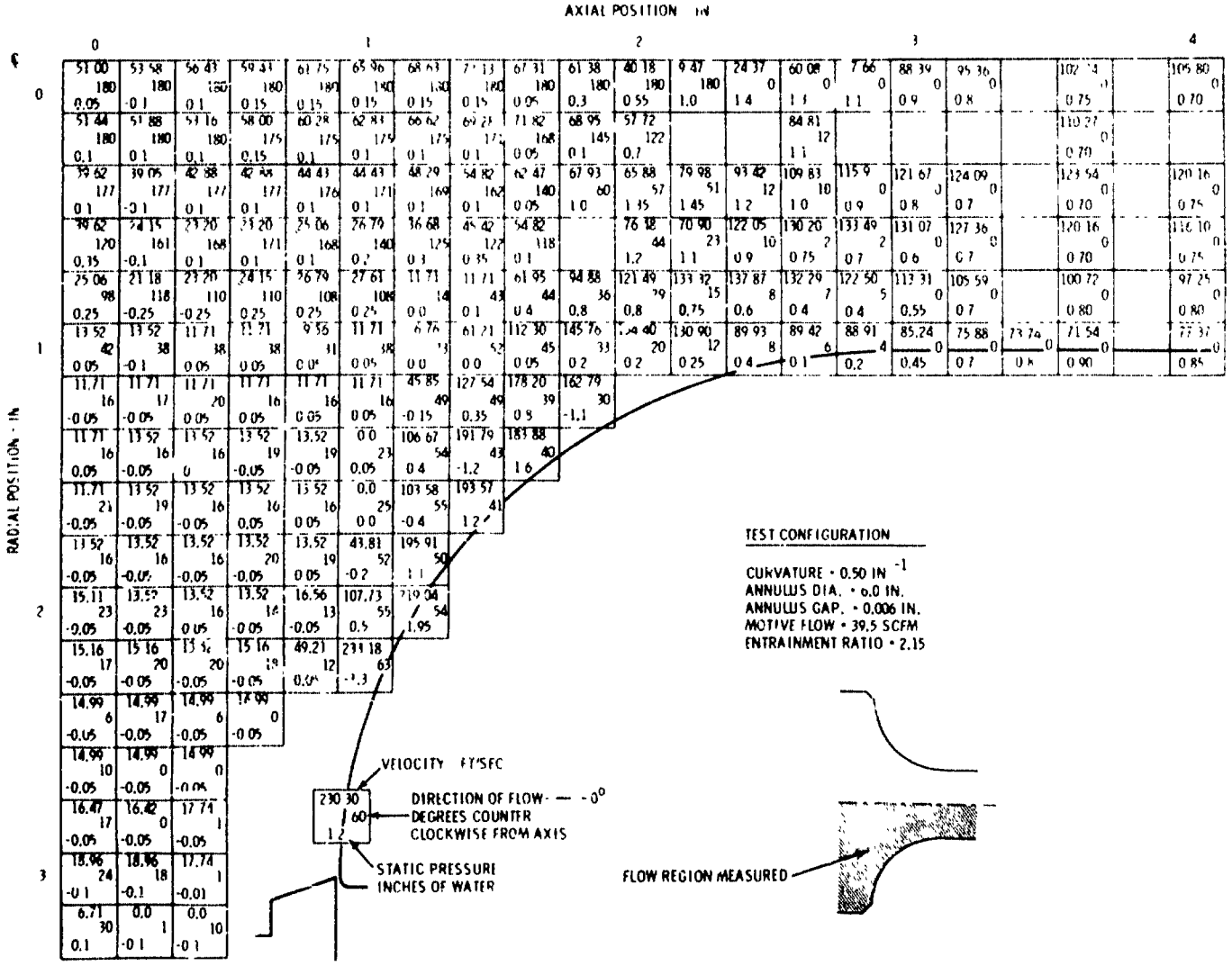

FIGURE 40. Velocity, Direction and Static Pressure Data, Case No. 1

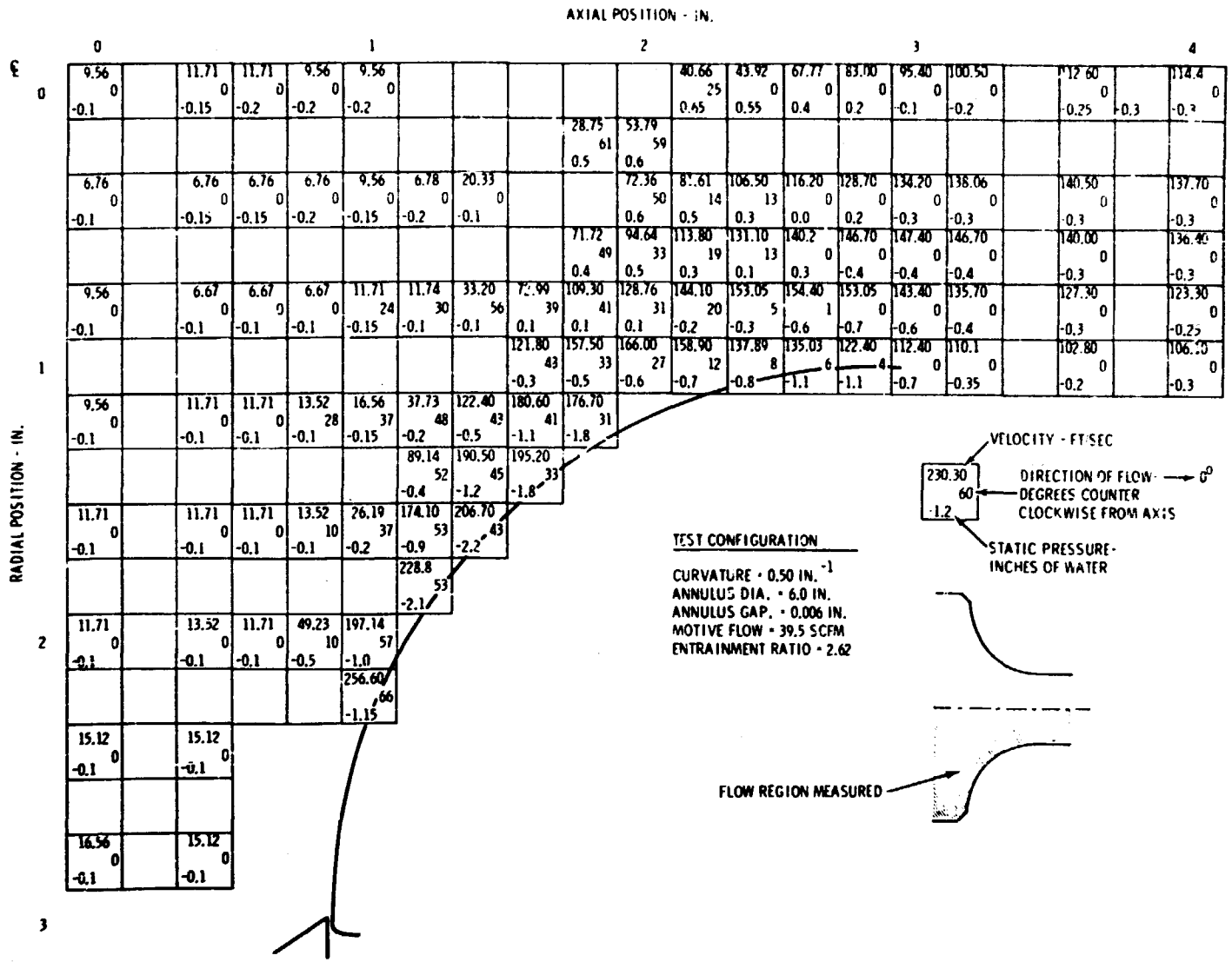

FIGURE 41. Velocity, Direction and Static Pressure Data, Case No. 2

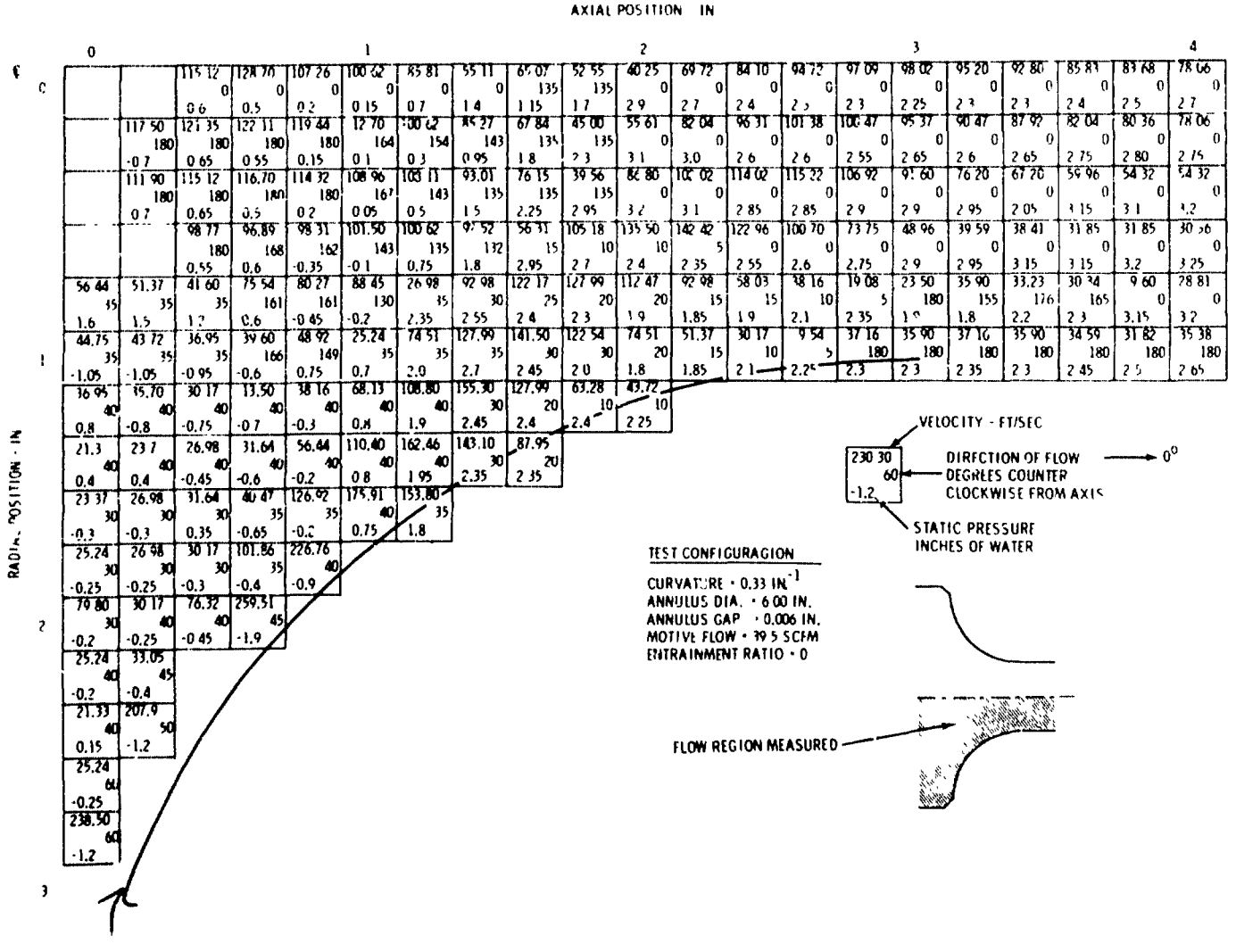

FIGURE 42. Velocity, Direction and Static Pressure Data, Case No. 3

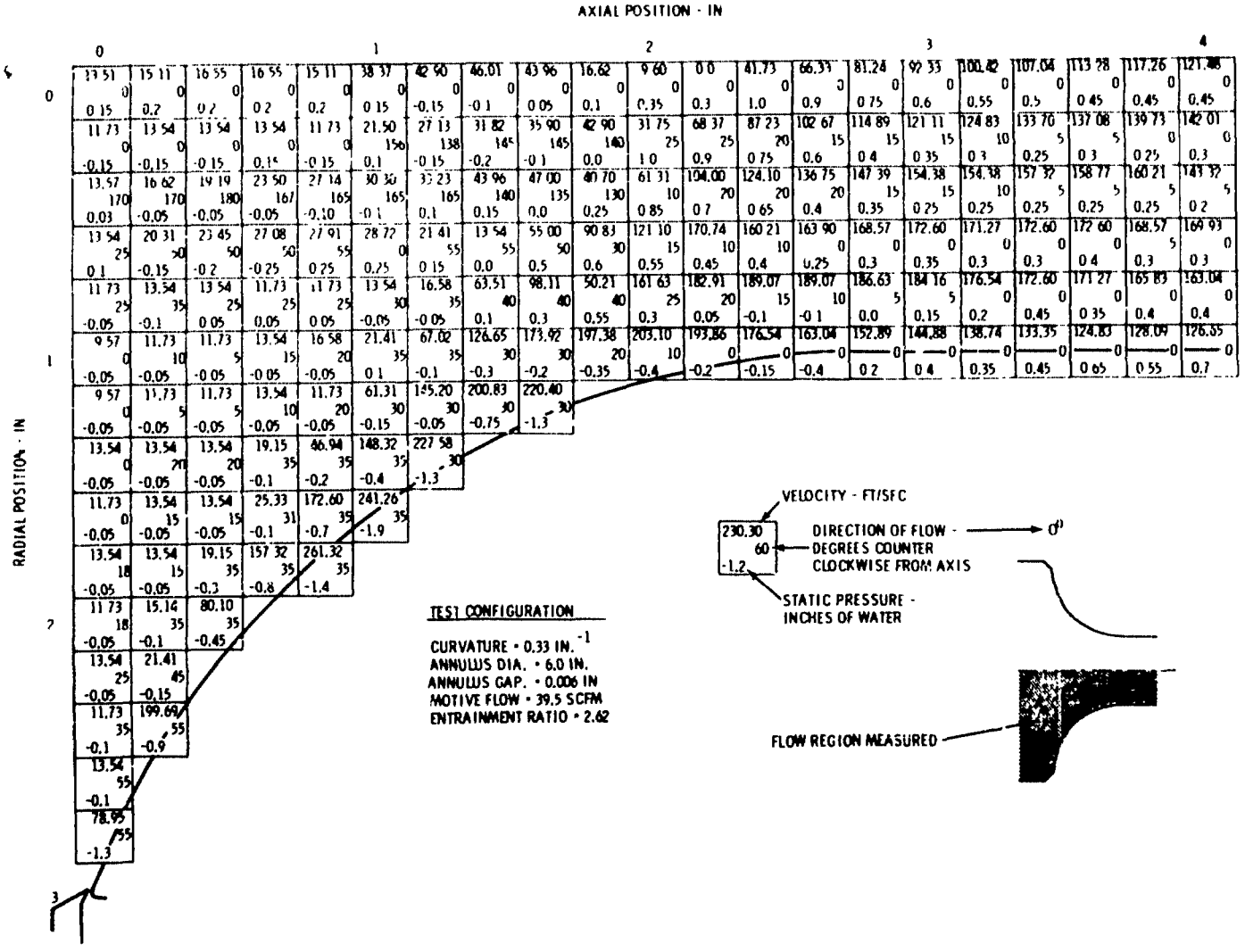

FIGURE 43. Velocity, Direction and Static Pressure Data, Case No. 4

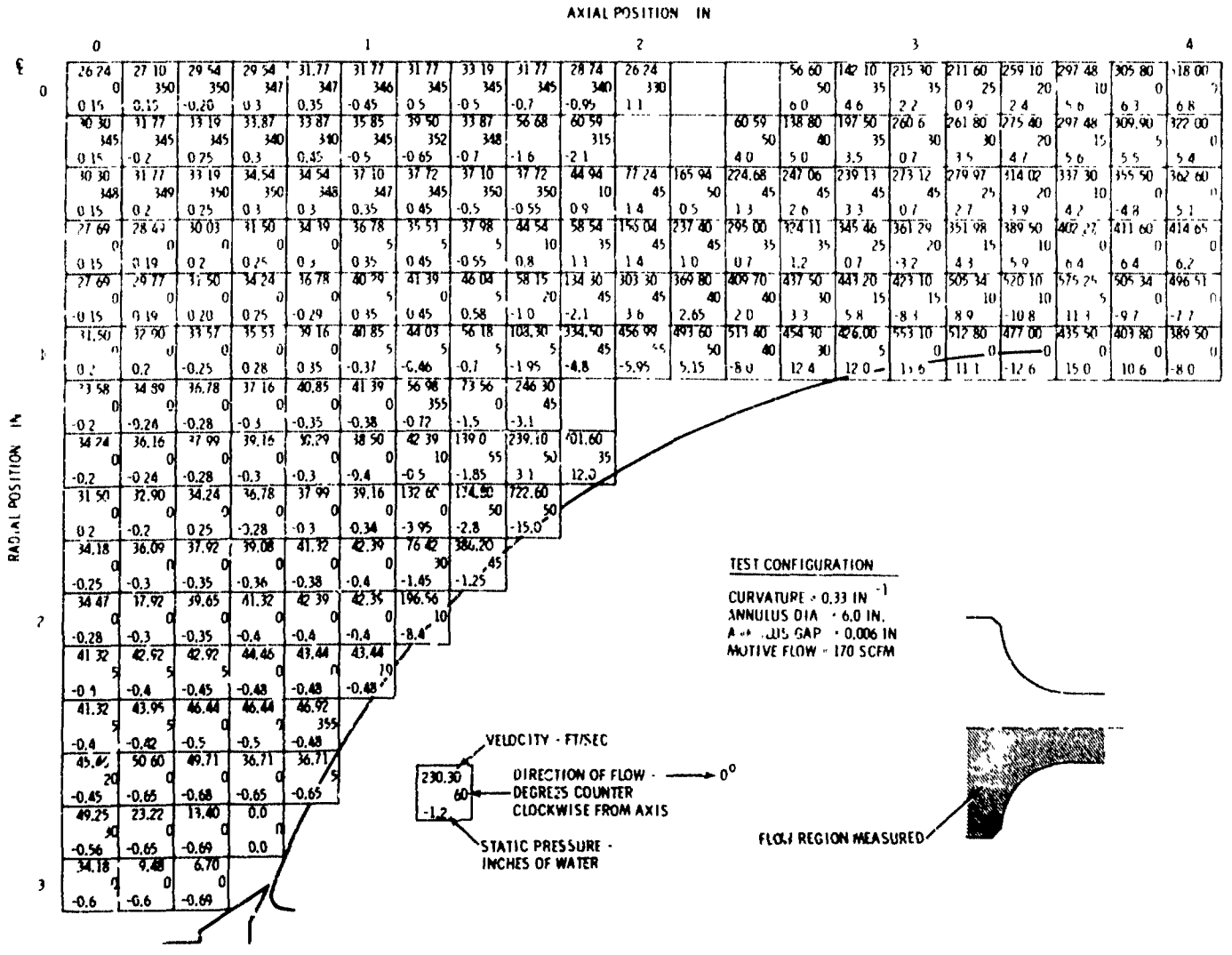

FIGURE 44. Velocity, Direction and Static Pressure Data, Case No. 5

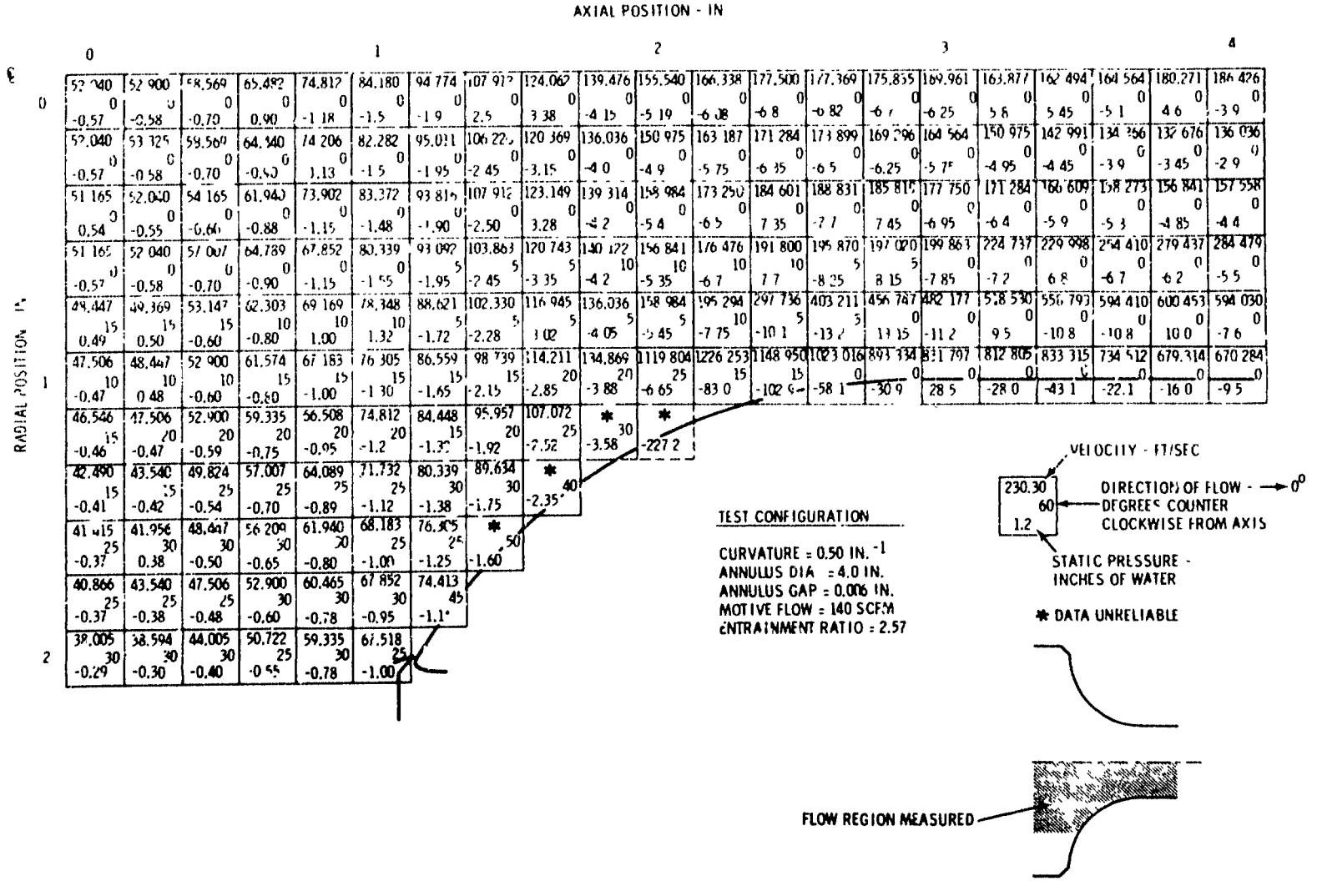

FIGURE 45. Velocity, Direction and Static Pressure Data, Case No. 6

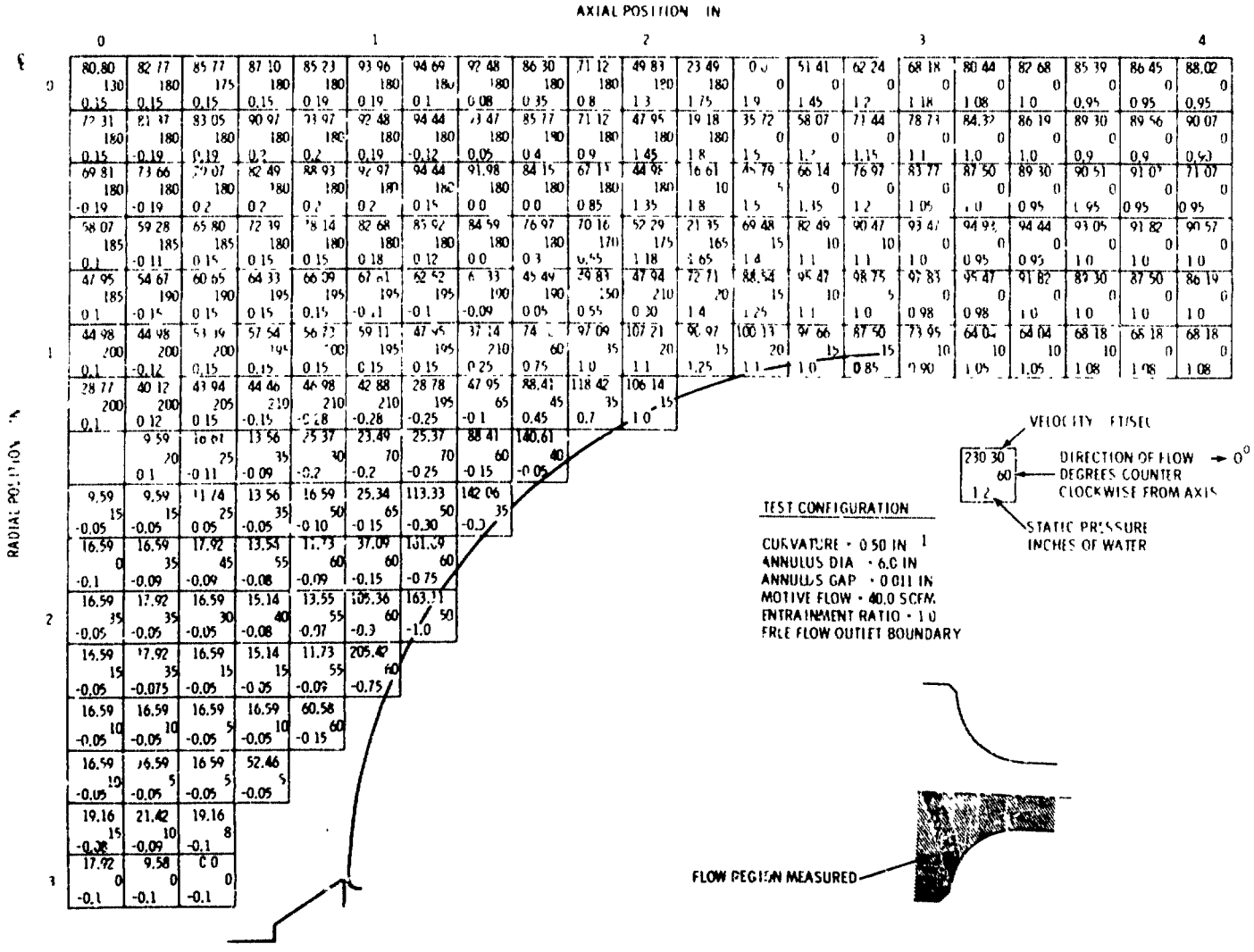

FIGURE 46. Velocity, Direction and Static Pressure Data, Case No. 7

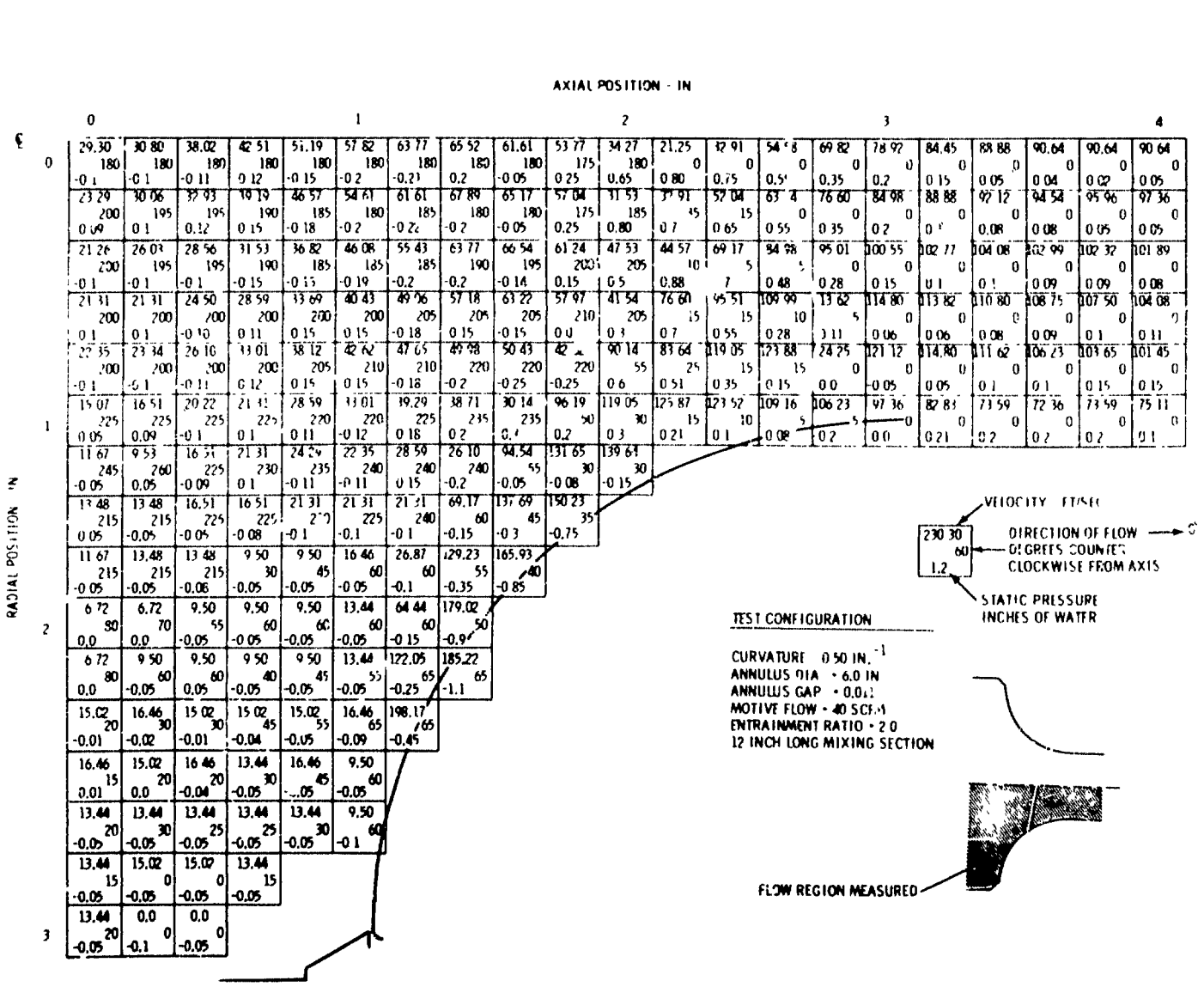

FIGURE 47. Velocity, Direction and Static Pressure Data, Case No. 8

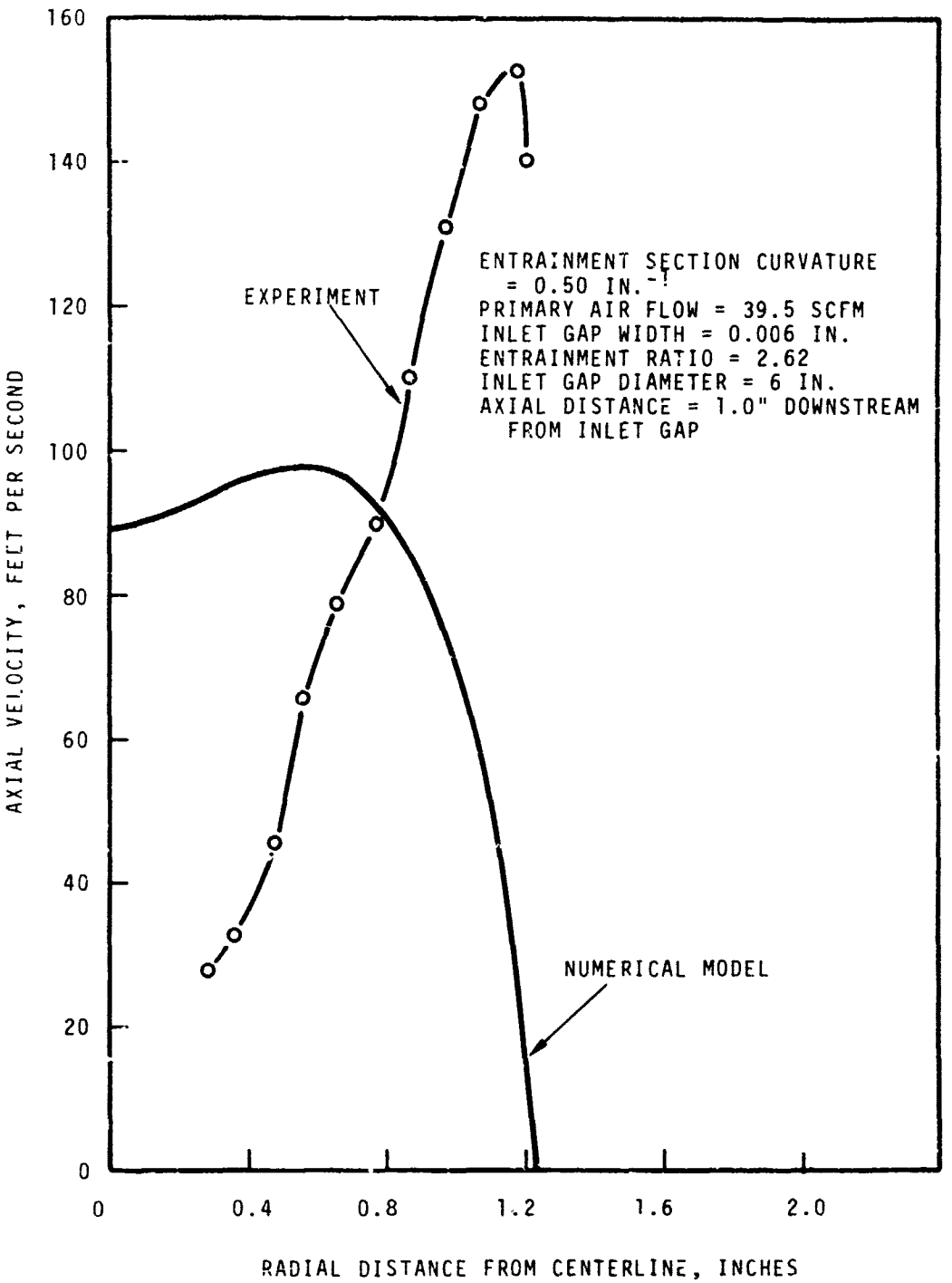

FIGURE 4E Comparisor of Measured and Predicted Axial Velocity Profiles

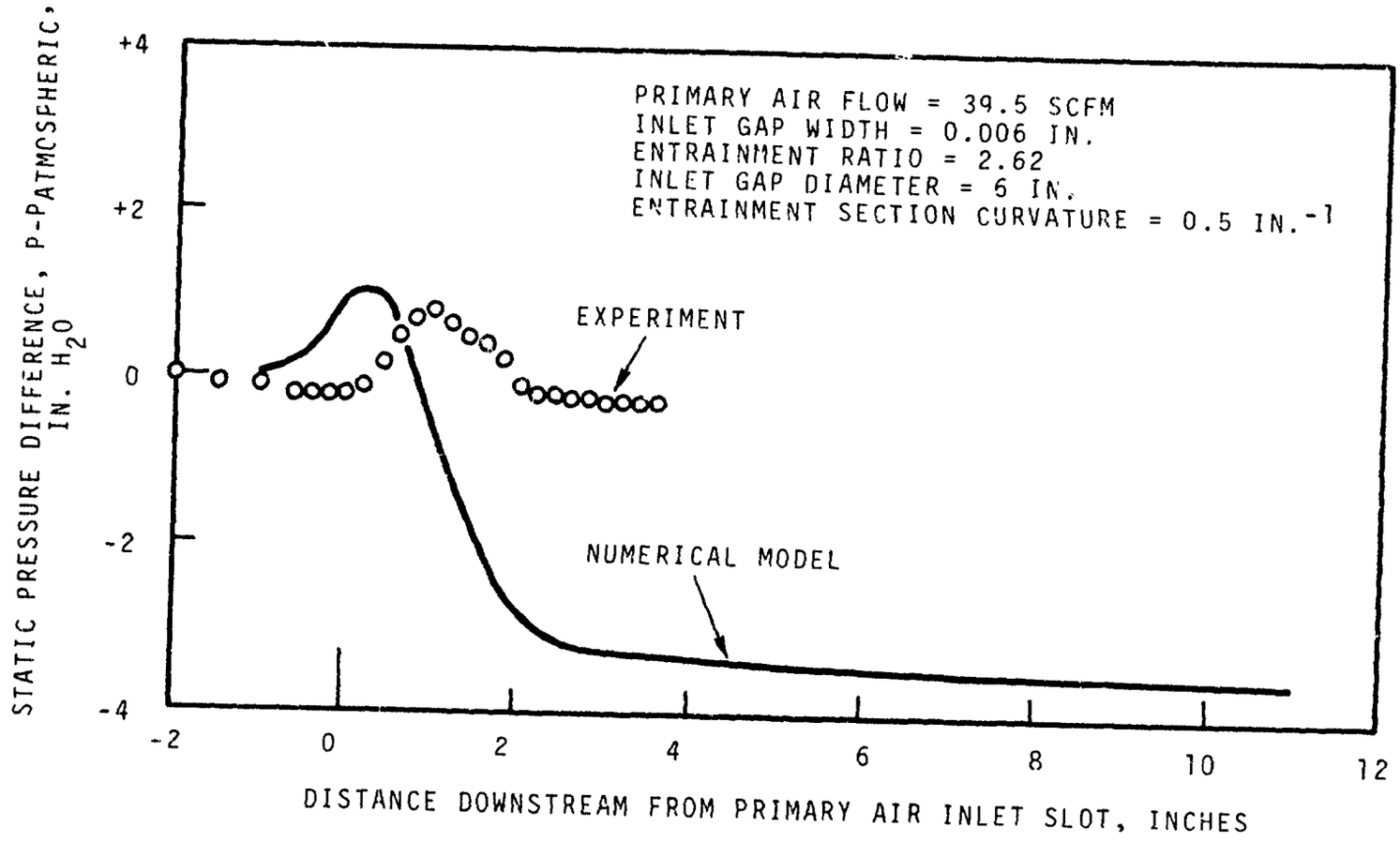

FIGURE 49. Centerline Pressure Distribution

VELOCITY AND PRESSURE PROFILES FOR CASE II

Experimental and theoretical profiles are worth comparing for this case because this geometry was found experimentally to be optimum among the cases studied experimentally. The primary air flow was 140 scfm, the inlet slit width was 0.006 in., the slit diameter was 4 in., the radius of curvature of the entrainment section was 3 in., and the entrainment ratio was 2.57.

The axial velocity profile measured at the entry to the constant cross section mixing section is compared to the predicted profile in Figure 50. As before, the theoretical profile is much flatter than the measured profile. It is thus apparent that the viscous flattening occurs for this case also.

Experimental and theoretical pressure profiles are compared in Figure 51. As was observed for Case I, reasonable agreement is observed near the inlet, but the curves diverge after the maximum in pressure is passed. This discrepancy is apparently caused by inaccuracies in the centerline velocity profiles which are attributable to the high values of viscosity used.

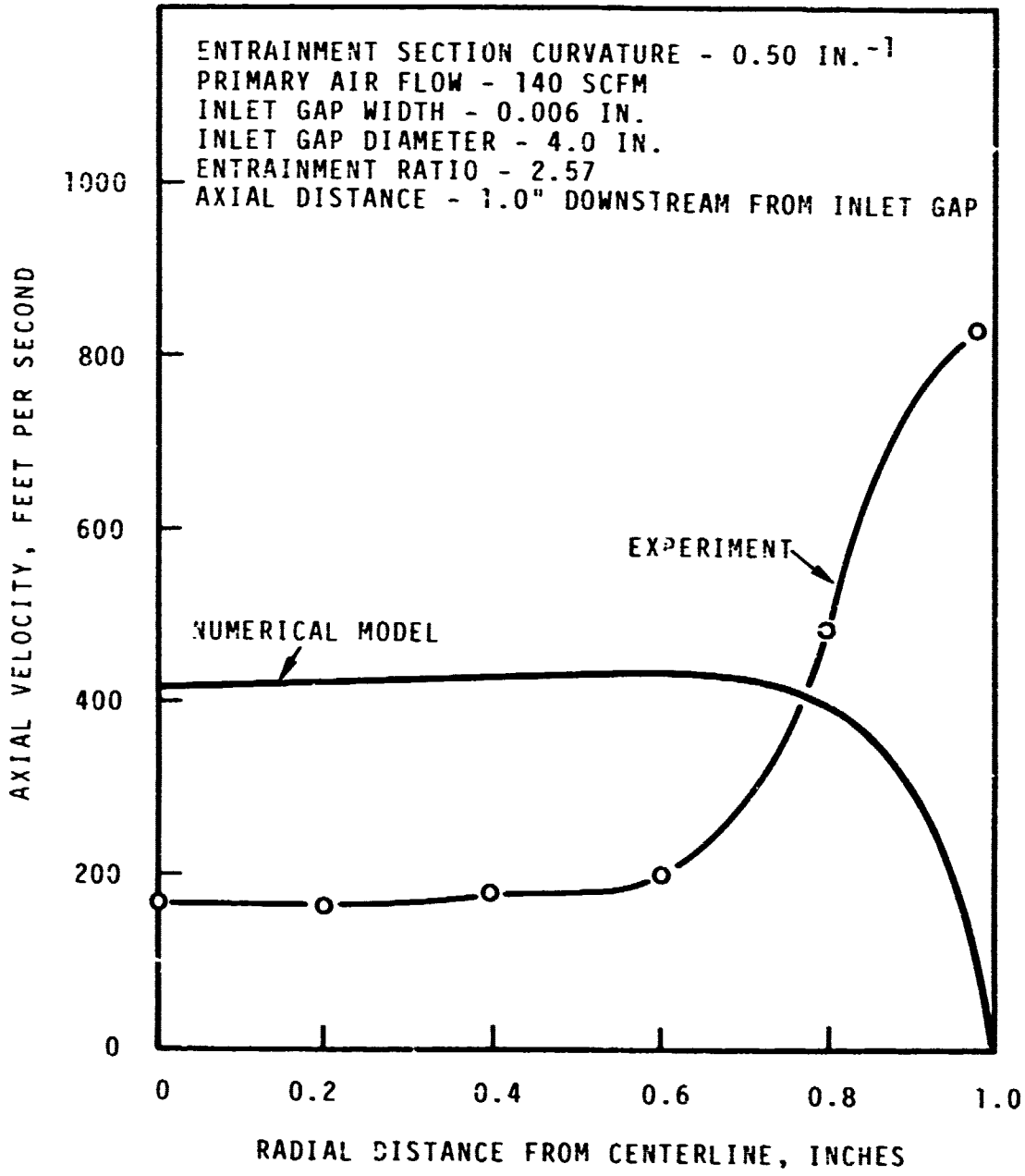

FIGURE 50. Comparison of Measured and Predicted Axial Velocity Profiles

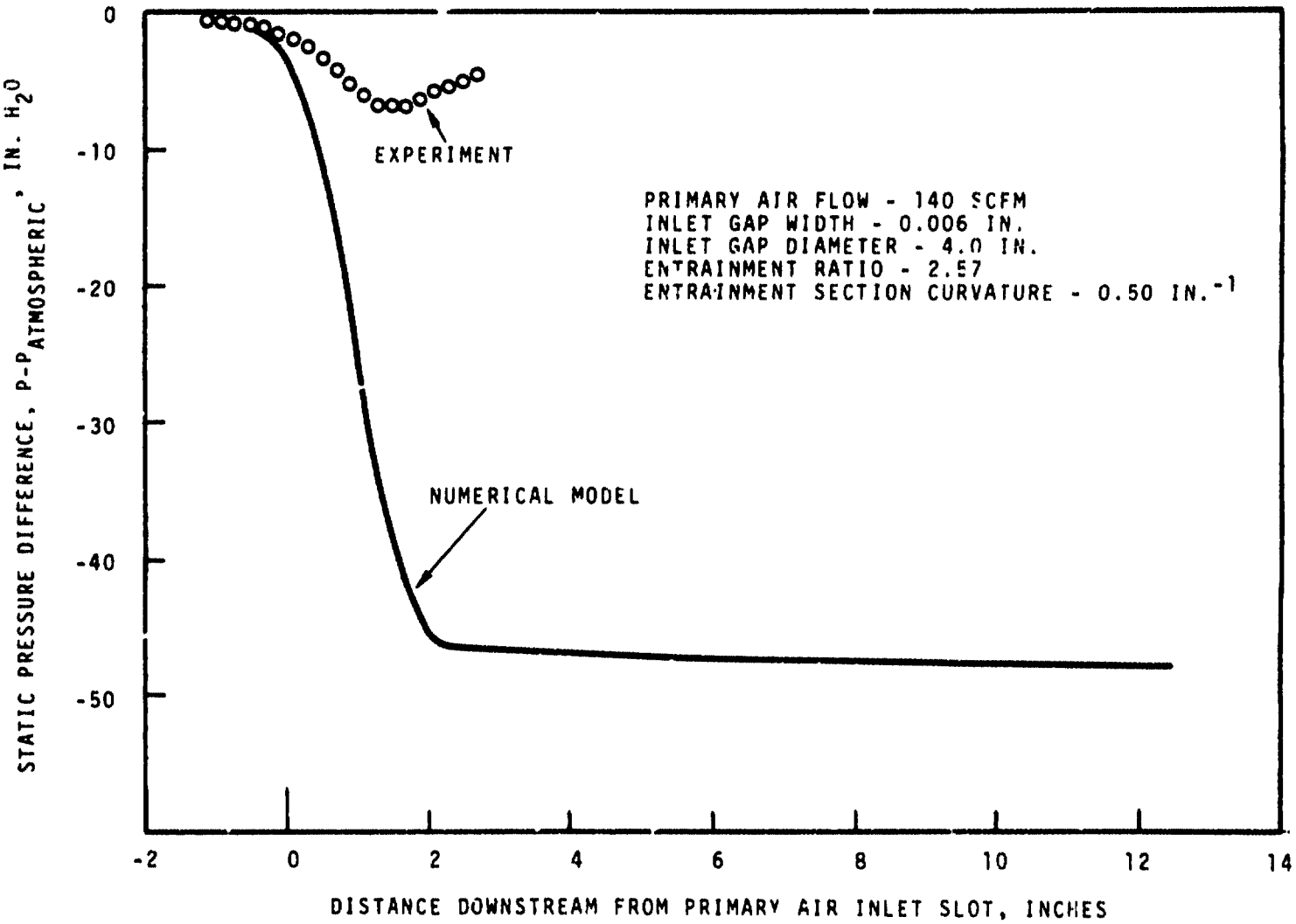

FIGURE 51. Centerline Pressure Distribution

REFERENCES

1. C. Bourque and B. G. Newman. "Reattachment of Two-Dimensional, Incompressible Jet to an Adjacent Flat Plate," The Aeronautical Quarterly, Vol. XI, pp. 201-232, August 1960.

2. K. Sridhar and P.K.C. Tu. "Experimental Investigation of Curvature Effects on Turbulent Wall Jets," The Aeronautical Journal of the Royal Aeronautical Society, Vol. 73, pp. 977-981, November 1969.

3. M. B. Glauert. "The Wall Jet," Journal of Fluid Mechanics, Vol. 1, pp. 625-643, 1956.

4. A. Klinkenberg and H. H. Mooy. "Dimensionless Groups in Fluid Friction, Heat and Material Transfer," Chemical Engineering Progress, Vol. 44, No. 1, pp. 17-36, January 1948.

5. J. G. Knudsen and D. L. Katz. Fluid Dynamics and Heat Transfer, McGraw-Hill Book Company, Inc., 1958, pp. 132-133.

6. K. E. Torrance and J. A. Rockett. "Numerical Study of Natural Convection in an Enclosure with Localized Heating from Below-Creeping Flow to the Orset of Laminar Instability," Journal of Fluid Mechanics, Vol. 36, No. 1, pp. 33-54, 1969.

7. A. K. Runchal and M. Wolfshtein. "Numerical Integration Procedure for the Steady-State Navier-Stokes Equations," Journal of Mechanical Engineering Science, Vol. 11, No. 5, pp. 445-453, 1969.

8. D. S. Trent. "A Numerical Model for Predicting Heat Dispension in Thermal Plumes Issuing from Large, Vertical Outfalls in Shallow Coastal Waters," Doctoral Dissertation, Corvallis, Oregon. (To be published.)

9. M. M. Gibson and D. B. Spalding. "A Two-Equation Model of Turbulence Applied to the Prediction of Heat and Mass Transfer in Wall Boundary Layers," Am. Soc. of Mech. Engrs., Paper 72-HT-15, Presented at AICHE-ASME Heat Transfer Conference, Denver, Colorado. August 6-9, 1972.

10. K. H. Ng and D. B. Spalding. "Turbulence Model for Boundary Layers Near Walls," The Physics of Fluids, 15, pp. 20-30, January 1972.

11. J. Rotta. "Paper 1, Statistical Theory of Non-Homogenous Turbulence," Imperial College of Science and Technology, Dept. of Mechanical Engineering, Translation TWF/TN/39, March 1968.

12. J. Rotta. "Paper 2, Statistical Theory of Non-Homogenous Turbulence," Imperial College of Science and Technology, Dept. of Mechanical Engineering, Translation TWF/TN/38, February 1968.

13. P. Bradshaw and D. H. Ferriss. "Applications of a General Method of Calculating Turbulent Shear Layers," Paper 71-WA/FE-8, ASME Winter Annual Meeting, Wash., D.C., November 28 - December 2, 1971.

APPENDIX A

PROJECT ORGANIZATION ACCORDING TO FUNCTION

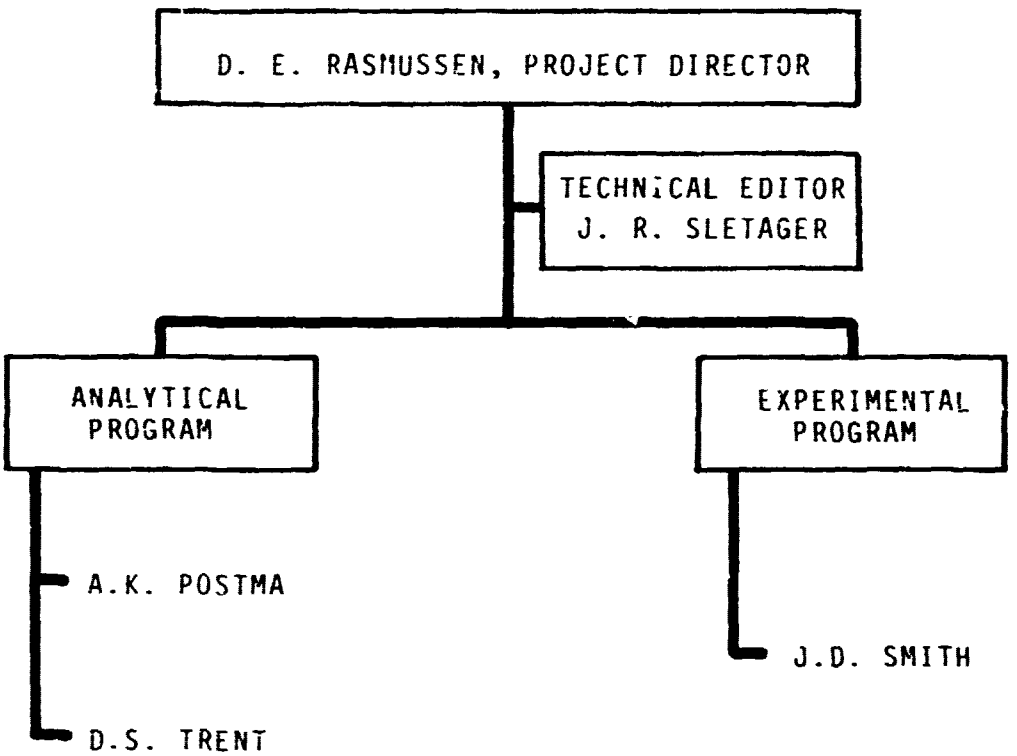

APPENDIX B

BIBLIOGRAPHY OF LITERATURE RELATED TO COANDA EDUCTORS

BIBLIOGRAPHY

Abbott, D.E. and Kline, S.J., "Experimental Investigation of Subsonic Turbulent Flow Over Single and Double Backward Facing Steps", Journal of Basic Engineering, pp. 317-325, Sept. 1962.

Anderson, D.C., Jr., "An Experimental Investigation of Compressible Jet Wall Attachment at Low Reynolds Numbers", 1969, University Microfilm 69-18608.

Bangert, L.H., "The Turbulent Wall Jet with an Initial Boundary Layer", AIAA Paper No. 71-612, June 1971.

Beeken, B.B., "A Theoretical and Experimental Study of a Coanda Curved Wall Attachment Device", ASME, Winter Annual Meeting and Energy Systems Exposition, N.Y., N.Y., Dec. 1-5, 1968, Paper 68-WA/FE-27.

Binion, T.W., Jr., "Investigation of the Recirculation Region of a Flow Field Caused by a Jet in Ground Effect with Crossflow", AEDC-TR-70-192, Arnold Engineering Development Center, Air Force Systems Command, Arnold Air Force Station, Tenn., Sept. 1970.

Bourque, C. and Newman, B.G., "Reattachment of a Two-Dimensional, Incompressible Jet to an Adjacent Flat Plate", The Aeronautical Quarterly, Vol. XI, pp. 201-232, August 1960.

Bourque, C. and Hguyen, H., "The Effect of Back Pressure on the Position of Reattachment of a Jet to an Adjacent Flat Plate", Fourth Cranfield Fluidics Conference, 17th-20th March 1970, Coventry, Paper X2.

Brown, F.T., "A Combined Analytical and Experimental Approach to the Development of Fluid-Jet Amplifiers", Journal of Basic Engineering, pp. 175-184, June 1964.

Burkett, R.J., Chalmers-Dixon, P., Morris, P.J. and Pyle, D.L., "On the Flow of Fluidized Solids Through Orifices", Chemical Engineering Science, Vol. 26, No. 3, pp. 405-418, March 1971.

Chavez, S.P. and Richards, C.G., "A Numerical Study of the Coanda Effect", ASME, Fluidics Conference, Atlanta, GA., June 22-23, 1970, Paper 70-Flcs-12.

Chu, Wen-Hwa, "Generalized Finite-Element Method for Compressible Viscous Flow", AIAA Technical Notes, pp. 2275-2276, Nov. 1971.

Davies, G.S., Mitra, A.K. and Roy, A.N., "Momentum Transfer Studies in Ejectors", I&EC Process Design and Development, Vol. 6, No. 3, pp. 293-299, July 1967.

DeFrate, L.A. and Hoerl, A.E., "Optimum Design of Ejectors Using Digital Computers", Computer Techniques, Chemical Engineering Progress Symposium Series, Vol. 55, No. 21, pp. 43-51.

BIBLIOGRAPHY (contd)

de Vries, G. and Norrie, D.H., "The Application of the Finite-Element Technique to Potential Flow Problems", ASME, Journal of Applied Mechanics, pp. 1-5, June 1970.

Edelman, G.M. and Shapiro, A.H., "Tables for Numerical Solution of Problems in the Mechanics and Thermodynamics of Steady One-Dimensional Gas Flow Without Discontinuities", Design Data, Journal of Applied Mechanics, pp. A-344 - A-351.

Erian, F.F., "Influence of Pressure Gradient on Turbulent Flows with Asymmetric Mean Velocity", Journal of Applied Mechanics, pp. 901-904, Dec. 1969.

Esch, R.E., "Numerical Solution of Transient Viscous Flow Problems", SER, pp. 28-34, Winter 1964.

Exley, J.T. and Brighton, J.A., "Flow Separation and Reattachment in Confined Jet Mixing", ASME, Applied Mechanics and Fluids Engineering Conference, Evanston, Ill., June 16-18, 1969, Paper 69-FE-29.

Felsing, G.W. and Moller, P.S., "Coanda Flow Over a Circular Cylinder with Injection Normal to the Surface:, AIAA Journal, Vol. 7, No. 5, pp. 842-846, May 1969.

Foa, J.V., "A Pressure Exchanger for Marine Propulsion", Rensselaer Polytechnic Institute, Technical Report Abstract 700095, pp. 346-352.

Gartshore, I.S. and Newman, B.G., "The Turbulent Wall Jet in an Arbitrary Pressure Gradient", The Aeronautical Quarterly, pp. 25-56, Feb. 1969.

Glauert, M.B., "The Wall Jet", Journal of Fluid Mechanics, Vol. 1, pp. 625-643, 1956.

Goradia, S.H. and Colwell, G.T., "Parametric Study of a Two-Dimensional Turbulent Wall Jet in a Moving Stream with Arbitrary Pressure Gradient", AIAA Journal, Vol. 9, No. 11, pp. 2156-2165, Nov. 1971.

Hoge, H.J., Eichacker, S.S. and Fiske, D.L., "Studies of Jet Compression - I, Apparatus and Methods. Results with Air at Room Temperature", Journal of Basic Engineering, pp. 426-432, Sept. 1959.

Hubbartt, J.E. and Bangert, L.H., "Turbulent Boundary Layer Control by a Wall Jet", AIAA Paper No. 70-107, Jan. 1970.

Johnson, L.D., "Experimental Investigation of Turbulent Jet Attachment to a Convex Wall", Naval Postgraduate School, Monterey, Calif., Sept. 1968, University Microfilm AD 847 579.

Kacker, S.C. and Whitelaw, J.H., "The Turbulence Characteristics of Two-Dimensional Wall-Jet and Wall-Wake Flows", ASME, Winter Annual Meeting, N.Y., N.Y., Nov. 29 - Dec. 3, 1970, Paper 70-WA/APM-35.

Kastner, L.J. and Spooner, J.R., "An Investigation of the Performance and Design of the Air Ejector Employing Low-Pressure Air as the Driving Fluid", pp. 149-159.

Keenan, J.H. and Neumann, E.P., "A Simple Air Ejector", Journal of Applied Mechanics, pp. A-75 - A-81, June 1942.

Keenan, J.H., Neumann, E.P. and Lustwerk, F., "An Investigation of Ejector Design by Analysis and Experiment", Journal of Applied Mechanics, pp. 299-309, Sept. 1950.

Keller, J.B., "Teapot Effect", Journal of Applied Physics, Vol. 28, No. 8, pp. 859-864, August 1957.

Kesler, K.L., "Turbulent Jet Attachment to Convex Walls", Naval Postgraduate School, Monterey, Calif., June 1963, University Microfilm AD 838-963.

Kind, R.J., "Calculation of the Normal-Stress Distribution in a Curved Wall Jet", The Aeronautical Journal of the Royal Aeronautical Society, Vol. 75, pp. 343-348, May 1971.

Korbacher, G.K., "The Coanda Effect Deflection Surfaces Detached from the Jet Nozzle", Canadian Aeronautics and Space Journal, pp. 1-6, Jan. 1962.

Mal'onee, R.C. II and Jacoby, S.L.S., "Plane, Turbulent Compressible Wall Jet With and Without Parallel Free Stream", ASME, Fluids Engineering Conference, Symposium on Unsteady Flow, Philadelphia, PA., May 6-9, 1968, Paper 68-FE-40.

Manian, V.S., McDonald, T.W. and Besant, R.W., "Heat Transfer Measurements in Cylindrical Wall Jets", Int. J. Heat Mass Transfer, Vol. 12, pp. 673-679, Pergamon Press, Great Britian, 1969.

McRee, D.I. and Edwards, J.A., "A Simplified Two-Dimensional Jet Reattachment Model", ASME, Winter Annual Meeting, N.Y., N.Y., Nov. 29-Dec. 3, 1970, Paper 70-WA/Flcs-8.

Mehus, T., "An Experimental Investigation into the Shape of Thrust Augmenting Surfaces in Conjunction with Coanda-Deflected Jet Sheets (Part II)", Institute for Aerospace Studies, University of Toronoto, Jan. 1965.

Metral, Albert and Zerner, Frederic, "The Coanda Effect", a facsimile report reproduced by the USAEC, AEC-TR-3386.

BIBLIOGRAPHY (contd)

Miller, E.B., "The Visualization of Turbulent Flows by Means of Flow Birefringence", Wyle Laboratories Research Staff Report WR 67-12, July 1967.

Newman, B.G., "The Deflexion of Plane Jets by Adjacent Boundaries - Coanda Effect", Boundary Layer and Flow Control, pp. 232-264, Pergamon Press, London.

Olson, R.E., "Spreading Rates of Compressible Two-Dimensional Reattaching Jets Upstream of Reattachment", pp. 139-165.

Panitz, T. and Wasan, D.T., "Flow Attachment to Solid Surfaces: The Coanda Effect", AIChE Journal, Vol. 18, No. 1, pp. 51-57, Jan. 1972.

Paranjpe, S.C. and Sridhar, K., "Effects of an Initial Gap on the Turbulent Jet Flow Over a Curved Wall", The Aeronautical Journal of the Royal Aeronautical Society, Vol. 72, pp. 63-67, Jan. 1968.

Pearson, C.E., "A Computational Method for Viscous Flow Problems", J. Fluid Mech., Vol. 21, Part 4, pp. 611-622, 1965.

Perry, C.C., "Two-Dimensional Jet Attachment", 1967, University Microfilm 67-15672.

Plotkin, A., "The Flow of a Laminar, Incompressible Jet Along a Parabola", Journal of Applied Mechanics, ASME Paper No. 71-APM-MM, 1971.

Reba, Imants, "Applications of the Coanda Effect", Scientific America, Vol. 214, pp. 84-93, 1966.

Reiner, Markus, "The Teapot Effect ... A Problem", Physics Today, pp. 16-20, Sept. 1956.

Rockwell, D.O. and Fiske, P.M., "Jet Reattachment to Walls of Various Shapes", Journal of Basic Engineering, pp. 1-6.

Sarpkaya, Turgut, "FLUERICS, 25. The Deflection of Plane Turbulent Jets by Convex Walls, Part - 1", U.S. Army Materiel Command, Harry Diamond Laboratories, Washington, D.C., Nov. 1968.

Sarpkaya, T., "The Performance Characteristics of Geometrically Similar Bistable Amplifiers", Journal of Basic Engineering, Paper No. 68-WA/FE-18, pp. 1-6.

Sarpkaya, T. and Richardson, D.C., "Turbulent Jet Over an Inclined Wall", Journal of Basic Engineering, pp. 287-293, June 1970.

Sato, Masayosi and Matsuoka, Kenji, "Separation Point of Two-Dimensional Tangential Jet Along Circular-Cylindrical Wall", Osaka Prefecture, University Bulletin, Series A - Engineering and Natural Sciences, Vol. 16, No. 2, pp. 205-212, 1967.

Savkar, S.D., "An Experimental Study of Switching in a Bistable Fluid Amplifier", University Microfilms Limited, High Wycomb, England, 1970.

Schneider, J. and Boccio, J., "Calculation of Turbulent Boundary Layers with Heat Transfer and Pressure Gradient Utilizing a Compressibility Transformation, Part III - Computer Program Manual", NASA Contractor Report NASA CR-1925, Jan. 1972.

Shapiro, A.H. and Hawthorne, W.R., "The Mechanics and Thermodynamics of Steady One-Dimensional Gas Flow", Journal of Applied Mechanics, pp. A-317 - A-336, Dec. 1947.

Sheeran, W.J. and Dosanjh, D.S., "Observations on Jet Flows from a Two-dimensional, Underexpanded, Sonic Nozzle", AIAA Journal, Vol. 6, No. 3, pp. 540-542, March 1968.

Sparrow, E.M. and Yu, H.S., "Local Non-Similarity Thermal Boundary-Layer Solutions", Journal of Heat Transfer, pp. 328-334, Nov. 1971.

Squire, L.C., "A Law of the Wall for Compressible Turbulent Boundary Layers with Air Injection", J. Fluid Mech., Vol. 37, Part 3, pp. 449-456, 1969.

Sridhar, K. and Tu, P.K.C., "Experimental Investigation of Curvature Effects on Turbulent Wall Jets", The Aeronautical Journal of the Royal Aeronautical Society, Vol. 73, pp. 977-981, Nov. 1969.

Torda, T.P., Ghia, K.N. and Victory, E.L., "Analysis of Entrainment and Flow Augmentation for Coanda-Type Nozzles", Symposium on the Coanda Effect and Some Special Applications of Aero-Hydrodynamics, Bucharest, Rumania, June 1967, pp. 533-587.

Wei, M.H.Y. and Corsiglia, V.R., "An Analysis of Coanda Jet Flows", NASA SP-228, Analytic Methods in Aircraft Aerodynamics - A Symposium Held at Ames Research Center - Moffett Field, CA., Oct. 28-30, 1969, pp. 197-213.

Wille, R. and Fernholz, H., "Report on the First European Mechanics Colloquium on the Coanda Effect", J. Fluid Mech., Vol. 23, Part 4, pp. 801-819, 1965.

Wygnanski, I.J. and Champagne, F.H., "The Laminar Wall-Jet Over a Curved Surface", J. Fluid Mech., Vol. 31, Part 3, pp. 459-465, 1968.